EFFECT OF TEMPERATURE AND CARBONACEOUS ENVIRONMENT ON THE FATIGUE BEHAVIOUR OF AISI 316L AUSTENITIC STAINLESS STEEL

Desmond Edem Fiawoyife

A dissertation submitted to the Faculty of Engineering and the Built Environment, University of the Witwatersrand, in fulfilment of the requirements for the degree of Master of Science in Engineering

JOHANNESBURG, 2012

DECLARATION

I, **Desmond Edem Fiawoyife,** declare that this dissertation is my own unaided work except where otherwise acknowledged. It is submitted for the degree of Master of Science in Engineering at the University of the Witwatersrand, Johannesburg. It is not been submitted before for any degree or examination to any other university.

Signature:…….

Date:…….

ABSTRACT

Austenitic stainless steels are widely used in the chemical, petrochemical and food-processing industries due to their excellent corrosion resistance and good mechanical properties. However, due to their inherent austenitic structure, they have relatively low hardness, as well as poor wear resistance and short fatigue life. Thermochemical surface treatments are used to improve the wear resistance, hardness and fatigue life. Austenitic stainless steels are difficult to carburise due to the tenacious Cr_2O_3 layer on the surface, although plasma and gas carburising have proven to be very effective. However, this investigation sought to understand the effect of high carburising temperature on the mechanical properties of AISI 316L steel, without the removal of the tenacious Cr_2O_3 surface layer.

Pack carburising with 60% $BaCO_3$, 30% activated carbon and 10% sodium chloride was done on AISI 316L austenitic stainless steel at 450ºC, 550ºC, 650ºC, 700ºC and 750ºC for 24 hours. Tensile, impact, hardness testing and fatigue tests were done and optical microscopy, SEM and XRD were used to characterise the specimens.

The ultimate tensile strength (UTS) of the as-received samples was 647±4MPa. The values for samples carburised at 450ºC and 550ºC were 651±5.5MPa and 651±3.6MPa with no significant differences. Samples tested at 650ºC, 700ºC and 750ºC showed decreasing tensile strength (638±3.5-603±2.5MPa). The hardnesses of treated samples at 450ºC and 550ºC were similar to the as-received, ranging between 248$HV_{0.5}$ and 254$HV_{0.5}$. Hardnesses of samples carburised at 650°C, 700°C and 750°C decreased from the surface to the core, with limited carbide precipitation within the core, which had similar values to the as-received.

The number of cycles to failure of the as-received sample was 59298±2520 and was similar to the carburised samples at 450-650ºC (ranging from 61455±15076-51819±5257).

A significant reduction in fatigue strength was observed for samples carburised at 700ºC (25387±595) and 750ºC (7146±318), which was due to the effect of carbon intake of the samples.

The elongation for as-received material was 48.5±0.4%, and the reduction in area was 76.6±0.97%. These values decreased with increasing carburising temperatures from 450°C to 750°C. The decrease in ductility was attributed to uptake of carbon, causing surface hardening and minor carbide precipitation in the core. X-ray diffraction of the carburised samples showed a shift in γ peaks compared to the as-received samples, which was attributed to the carbon intake. Samples carburised at 450°C and 650°C had austenite grains, twin boundaries and slip lines within the grains. The frequency of the defects increased with increasing carburising temperature. The twins were more predominant at the surface and less so towards the core of the steel. The hardness increase was more effected by the carbon increase. There was limited carbide precipitation and a very thin observable carburised case.

The results showed that this type of pack carburising of austenitic stainless steel is not suitable for improving the properties of AISI 316L steel.

DEDICATION

I would like to dedicate this work to God and to the memory of my late grandfather, Clement Kodzo Adjiwu. Though you are gone, your memory still remains with me.

ACKNOWLEDGEMENTS

I would like to thank the following people and organisations, without which the work would have been fruitless and impossible:

- My supervisors, Prof. L.A. Cornish, Prof. C. Polese, Prof. S. Kwofie and Dr L.H. Chown for their continued and unwavering support. Especially Prof. Cornish and Dr Chown, for their commitment and incisive support in both my personal and professional development. Their lucid criticism, kindness and advice have been enormously helpful.

- The financial assistance from the South African Department of Science and Technology and the National Research Foundation (NRF) through the DST/NRF Centre of Excellence in Strong Materials (CoE-SM) is gratefully acknowledged.

- Mr Chris Fletcher, and especially Mr Jacobus Jonck, all of Advanced Materials Division, Mintek for their assistance and valuable contribution with the analysis and the fatigue experimentation.

- Mr Richard Couperthwaite and the Microscopy Unit of Advanced Materials Division (AMD), Mintek for the valuable contribution of the SEM and EDX analysis of the carburised samples and the fractured surfaces.

- Technicians at the workshop of the School of Chemical and Metallurgical Engineering for the fabrication and machining of the carburising case and the impact and tensile specimens.

- Research colleagues and graduate students under the DST/NRF Centre of Excellence in Strong Materials for all your support and kind hearted words. This research will not have been possible without your inputs and sense of humour.

TABLE OF CONTENTS

LIST OF FIGURES

LIST OF TABLES

CHAPTER ONE

INTRODUCTION

"Begin, be bold and venture to be wise"

— Quintus Horatius Flaccus

1. INTRODUCTION

Austenitic stainless steels are commonly used for structural applications, mainly because of the combination of excellent corrosion resistance and good mechanical properties [1927Bai, 1937Jen, 1949Zap]. On the other hand, low hardness and wear resistance, and short fatigue life are the major limitations to their use [1979Ill, 2002Bel, 2004Tok]. Surface engineering processes have been used to improve these properties [1988Bud, 2001Dav]. Fatigue failure accounts for 80-90% of mechanical failure of engineering structures and components [1958Tho, 1962Ald, 1979Ill]. It is a process of progressive localised permanent structural change occurring in a material subjected to conditions that produce fluctuating (alternating or cyclic or repeated) stresses and strains at some point or points and that may culminate in cracks or complete fracture after a sufficient number of cycles [1903Ewi, 1953Man, 1958Tho, 1962Ave].

The many engineering applications of stainless steels and the need to enhance the surface properties to improve their wear, surface hardness and fatigue life has generated much research interest. For instance, studies premised on low temperature carburised austenitic stainless steels had shown appreciable increased in surface hardness, wear and fatigue life. This is attributed to the surface hardness, formation of expanded austenite (S-phase) and high compressive residual stresses [1951Hen] induced in the steel matrix as a result of the carburising temperature and the interstitial carbon that diffused into the steel matrix [1999Sun1, 2002Bel, 2004Tok, 2006Aki].

Austenitic stainless steels are very difficult to case harden by pack carburising due to the presence of a self-healing and tenacious Cr_2O_3 layer on the surface [2008Ces]. The appropriate case hardening technique is plasma processing which improves surface hardness by five to seven times that of the as-received material [1999Ren, 2000Lia, 2000Few, 2006Min]. The plasma processes avoids the pre-removal step of the passive Cr_2O_3 layer by chemical or mechanical means [2006Min, 2010Pin].

Hitherto, little or no work has been done in studying the mechanical and fatigue behaviour of relatively high temperature carburising heat treatment of austenitic stainless

steels. At relatively high carburising temperatures (above 450ºC), the catastrophic processes of metal dusting and sensitisation (intergranular corrosion) are bound to occur, hence the study of mechanical and fatigue behaviour at these temperatures is hindered [2001Mat, 2003Gra, 2006Ter, 2009Lo]. Carbides, such as $M_{23}C_7$ and M_7C, are formed at the grain boundaries at these temperatures, and decrease the chromium content, hence decreasing the corrosion resistance of stainless steels [1948Uhl, 1959Hat, 1970Cih].

Structural components such as implants made from AISI 316L austenitic stainless steel fail under cyclic loading due to poor surface hardness and defects [1979Ill, 1983War]. The poor surface hardness and irregularities nucleate micro cracks which then escalate into macrocracks, resulting in fatigue failure. Thermo-chemical surface treatments are used to induce compressive residual stresses [1951Hen], surface hardness and expanded austenite or "S-phase" which contributed to improved mechanical properties; wear resistance, surface hardness and fatigue properties of the steel [1981Sly, 1988Bud, 2001Dav]. The choice of AISI 316L stainless steel for this research was influenced by availability and affordability, as well as its numerous structural applications and good mechanical properties.

It is therefore expected that fatigue behaviour and mechanical properties of AISI 316L will be enhanced through the surface treatment method of pack carburising. This research advanced and contributed to knowledge by investigating the relationship between the relatively high carburising temperatures (450ºC-750ºC), carbon content and its microstructural effects on the mechanical properties of AISI 316L austenitic stainless steel. The fatigue behaviour in relation to the surface treatment at these temperatures was established. In the light of available literature, the following objectives were identified for this project:

- To explore the possibility of relatively high temperature carburising of AISI 316L austenitic stainless steel,
- To investigate the effect of high carburising temperatures on the fatigue behaviour and mechanical properties of AISI 316L austenitic stainless steel,

- To study the effect of different treatment parameters (temperature and time) and optimise them,
- To conduct systematic characterisation on the high temperature carburised AISI 316L austenitic stainless steel by analysing the morphological effects.

In order to achieve the stated objectives, this dissertation is structured into six chapters with Chapter 1 introducing the general scope and the research objectives. Chapter 2 gives the literature review, outlining previous work done on the fatigue behaviour of surface treated AISI 316L austenitic stainless steels with emphasis on the mechanical properties and applications. The experimental procedure and methodological approaches are given in Chapter 3. Results from the experiments are given in Chapter 4, with the discussion in Chapter 5. Chapter 6 gives the conclusion and some recommendations.

CHAPTER TWO

LITERATURE SURVEY

"No matter how busy you may think you are, you must find time for reading, or surrender yourself to self-chosen ignorance"

— Atwood H. Townsend

2. LITERATURE SURVEY

2.1. INTRODUCTION

Stainless steels are low-carbon steels containing a high percentage of chromium, at least 10.5 wt% [1927Bai, 1937Jen, 1949Zap]. This addition of chromium gives the steel its unique corrosion-resistance properties, denoted as stainless or rustproof. The chromium content allows the formation of a passivating layer of chromium oxide on the steel surface. This protective film is also self-healing in the presence of small traces of oxygen if damaged mechanically or chemically [1927Bai, 1937Jen, 1949Zap]. This passivating and self-healing film is impervious, transparent, adherent and corrosion resistant.

In this literature survey, a review on the progress made on the development of stainless steels and surface enhancement techniques and its effect on the mechanical behaviour and properties, with much emphasis on the austenitic stainless steel, is outlined. The review focuses mainly on the following:

- A brief overview of the history and development of the ferrous alloys and the various microstructures of stainless steels,
- Surface enhancement techniques of austenitic stainless steels,
- Effects of surface enhancement on the mechanical properties of austenitic stainless steels.

2.2. STAINLESS STEELS: HISTORY AND DEVELOPMENT

2.2.1. Introduction

Ferrous alloys (predominantly iron) have been known and used for several millennia. Steel was the first technologically important ferrous metal to replace bronze around 1200 BC [1909For, 1920Cam, 1936Boy, 1939Ast]. Steel is a mostly iron, with carbon in the range of 0.2-2.1 wt%. Carbon is an important alloying element for iron [1909For, 1920Cam, 1936Boy]. The dominance of steels is due to the endless variety of microstructures and properties that can be generated by solid state transformations and processing, as well as the flexibility in its chemistry [1927Bai]. Steels also have a

combination of good mechanical properties and low cost. They are used in a wide range of applications, due to variation in carbon content, cold working and various heat treatment processes and also the option of alloying with other elements to impart a particular property [1937Jen].

2.2.2. Microstructure of steels

There are five main constituents of steels making up their microstructure:

- Ferrite,
- Austenite,
- Cementite,
- Pearlite, and
- Martensite.

The Fe-C phase diagram in Figure 2.1 showed the main constituents and the respective treatment temperatures.

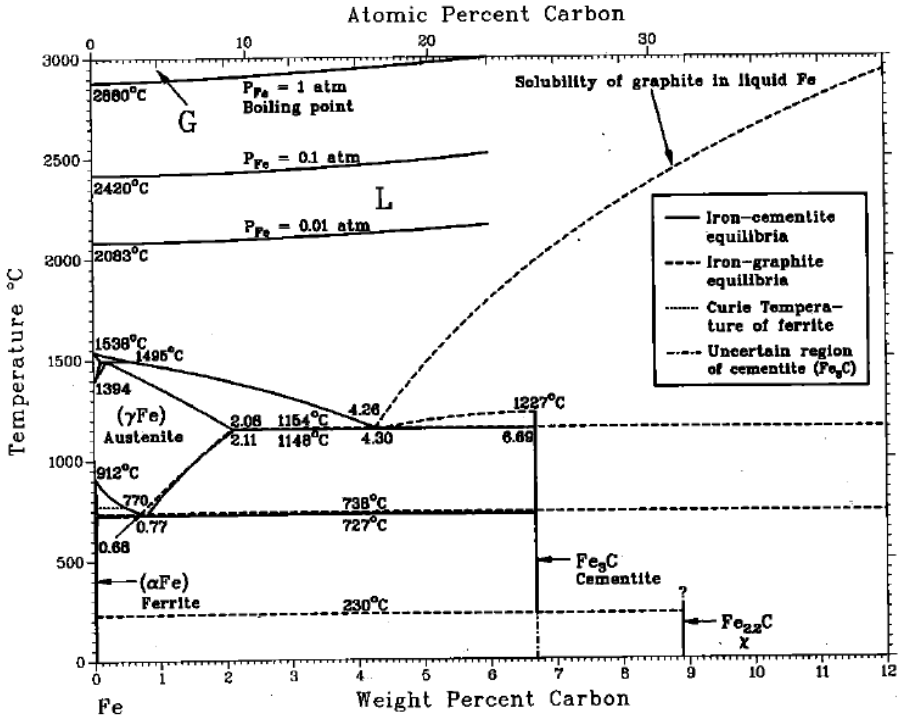

Figure 2.1. Fe-C equilibrium diagram [1986Mas].

2.2.2.1. Ferrite

Ferrite is a body-centred cubic (bcc) crystal structure and it is the structure for pure iron (Fe) at room temperature. It is often known as α-iron, or α-ferrite, at room temperature and δ-ferrite at high temperature. It is relatively soft and ductile, and these characteristics are imparted to the steels. Carbon solubility in ferrite at room temperature is very low, thus less than 0.01%. This structure gives steel and cast iron their magnetic properties. It is an example of a ferromagnetic material.

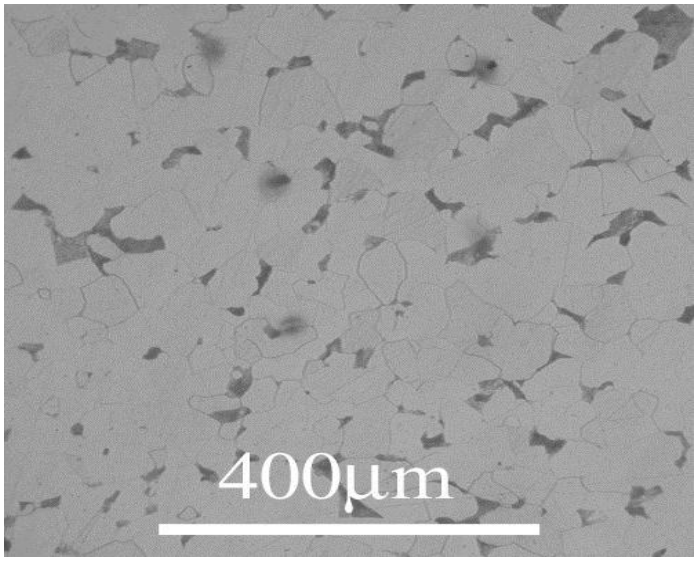

Figure 2.2. 0.1% carbon steel (mild steel) showing ferrite (light) and pearlite (dark) [URLCar].

2.2.2.2. Austenite

Austenite is face-centred cubic (fcc) crystal structure and a non-magnetic solid solution of iron. It exists above the critical eutectoid temperature. It is often referred to as γ-iron. This structure occurs during cooling of ferrous metals from elevated temperatures. Retained austenite is austenite that did not convert to martensite during cooling (quenching); the cooling did not reach the martensite finish, M_f temperature [1984Van], or was constrained by the volume increase of martensite.

2.2.2.3. Cementite

Cementite is one of the constituents of steel that is very hard and brittle. It is a compound of iron and carbon, iron-carbide (Fe_3C), and possesses an orthorhombic crystal structure.

Pure Fe_3C has a Vickers hardness value of about 800HV and up to 1400HV for highly alloyed ones [1984Van]. Cementite in steel results in increased hardness and decreased ductility and toughness.

2.2.2.4. Pearlite

When eutectoid steel is cooled from an austenitizing temperature of about 850°C to 750°C and held at this temperature, no transformation will take place. If the temperature is lowered to 650°C, pearlite will start to form after approximately 1s and the transformation will be completed in 10s, as shown in the curve II in Figure 2.3a [1984The]. Lowering the temperature of the formation of pearlite will result in finer lamellae, making the whole structure harder. The formation of pearlite is initiated at the austenite grain boundaries, or at some disarray in the austenite grains [1962Hil]. Pearlite is a lamellar structure of alternate layers of cementite and ferrite, which is formed by the eutectoid reaction $\gamma = \alpha + Fe_3C$. It combines the ductility of the ferrite (α) and the hardness and strength of the cementite (Fe_3C) and acts like a composite material [1984The]. This is important for a wide range of the properties of steel. The lamellar structure also acts as a barrier to inhibit crack propagation, as in composites, which gives pearlite good toughness.

2.2.2.5. Martensite

When there is a rapid cooling from the upper critical temperature to M_s line in Figure 2.3 curve V, austenite will start to transform to ferrite on reaching the line M_s. As cooling continues below M_s, there is little carbon migration while the austenite is transforming. The carbon atoms remain in solid solution in the α-iron. Since the space available for carbon atoms is less in α-iron than in γ-iron, the carbon atoms locally distort the lattice. Stresses induced due to martensite formation result in increased hardness of the steel. It is a needle or lath-like structure of iron and carbon as shown in Figure 2.4. [1971Mar]. Tempering is done to enhance the toughness of martensite, and allows some decomposition of the martensite.

Corrosion (usually rusting in the case of iron) is the major limitation to structural components made from steels. Corrosion is the degradation of materials properties due to

interactions with their environments, and is primarily associated with metallic materials [1948Uhl]. Corrosion results in material loss and its economic impact are felt heavily in an industrial economy. Reports from the historic congressional study on corrosion cost by the National Association of Corrosion Engineers (NACE) in 2002 [2002NAC, 2006Sha] indicated that the direct cost of corrosion on a country's gross national product (GNP) was approximately 3.1% annually. This figure amounted to over $276 billion per year, with the highest segments of the corrosion cost associated with utilities, transportation and infrastructure. Table 2.1 shows the cost of corrosion in the United States [2002Nac].

Stainless steels are a type of steel designed with properties and characteristics different from plain carbon steels. The excellent corrosion resistance promoted their use in the chemical processing and power-generating environments on which technological society is based [1949Zap, 1979Pic]. The classification of stainless steels as part of ferrous metals and alloys is shown in Figure 2.5.

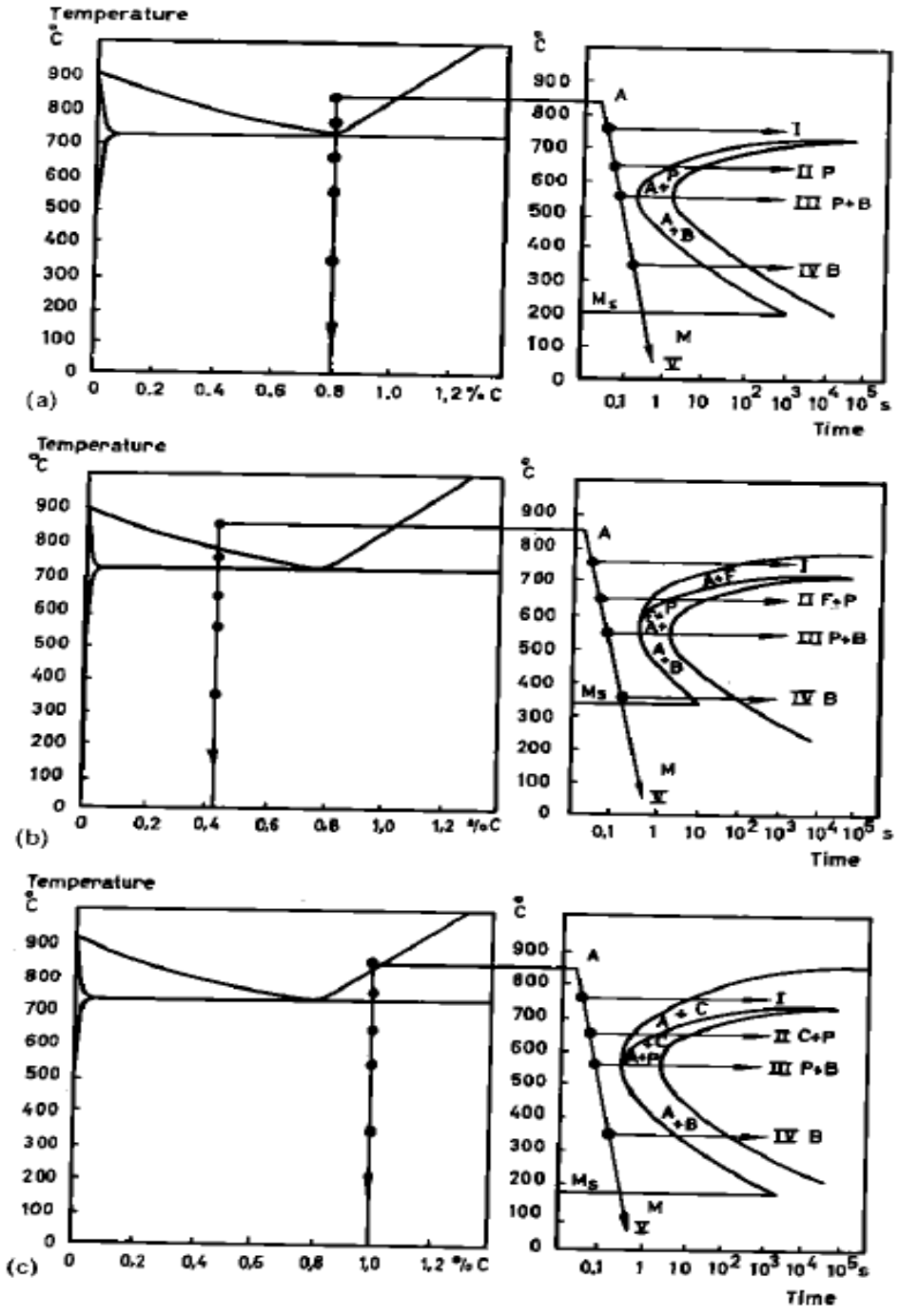

Figure 2.3. Structural transformations of steel containing (a) 0.8%C, (b) 0.45% C, and (c) 1.0% C: A=austenite, B=banite, C=cementite, F=ferrite, P=pearlite, M=martensite, M_s=start of martensite formation [1984The].

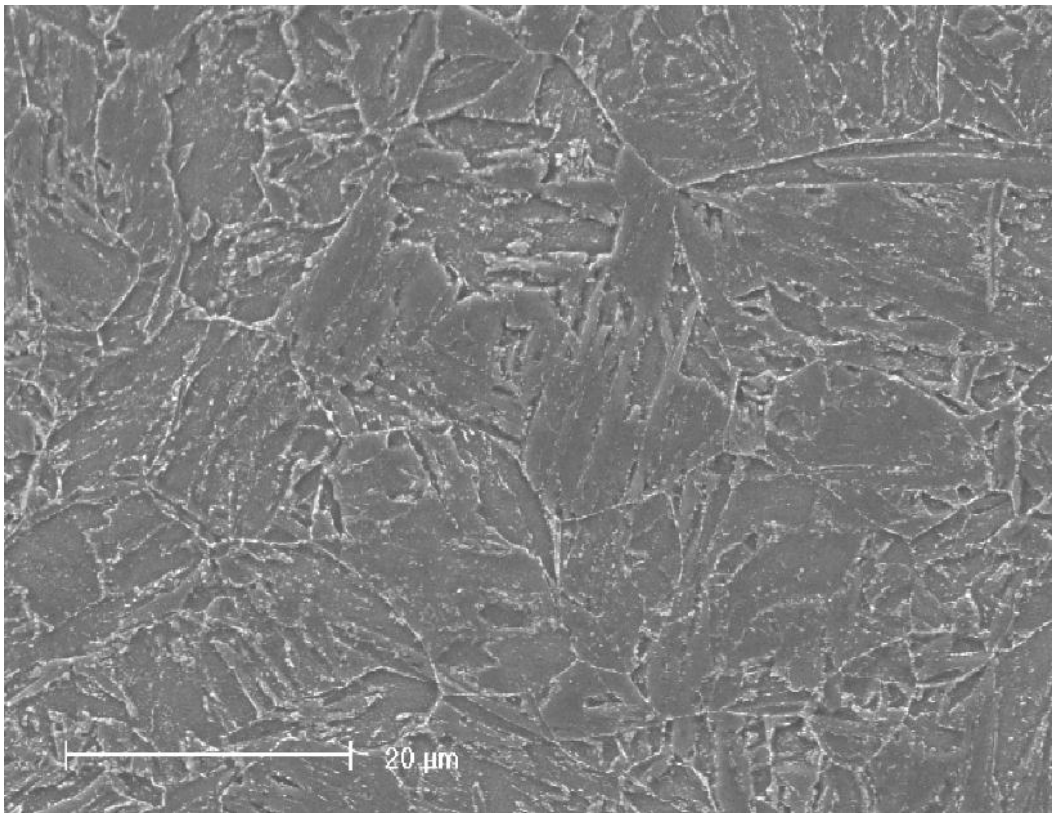

Figure 2.4. SEM image of a martensitic microstructure [URLMic].

Table 2.1. Corrosion cost in the United States [2002NAC].

Sector	Cost ($\$x10^9$)	Percentage (%)
Utilities	47.9	34.7
Transportation	29.7	21.5
Government	20.1	14.6
Infrastructure	22.6	16.4
Production and Manufacturing	17.6	12.8
Total	**137.9**	**100**

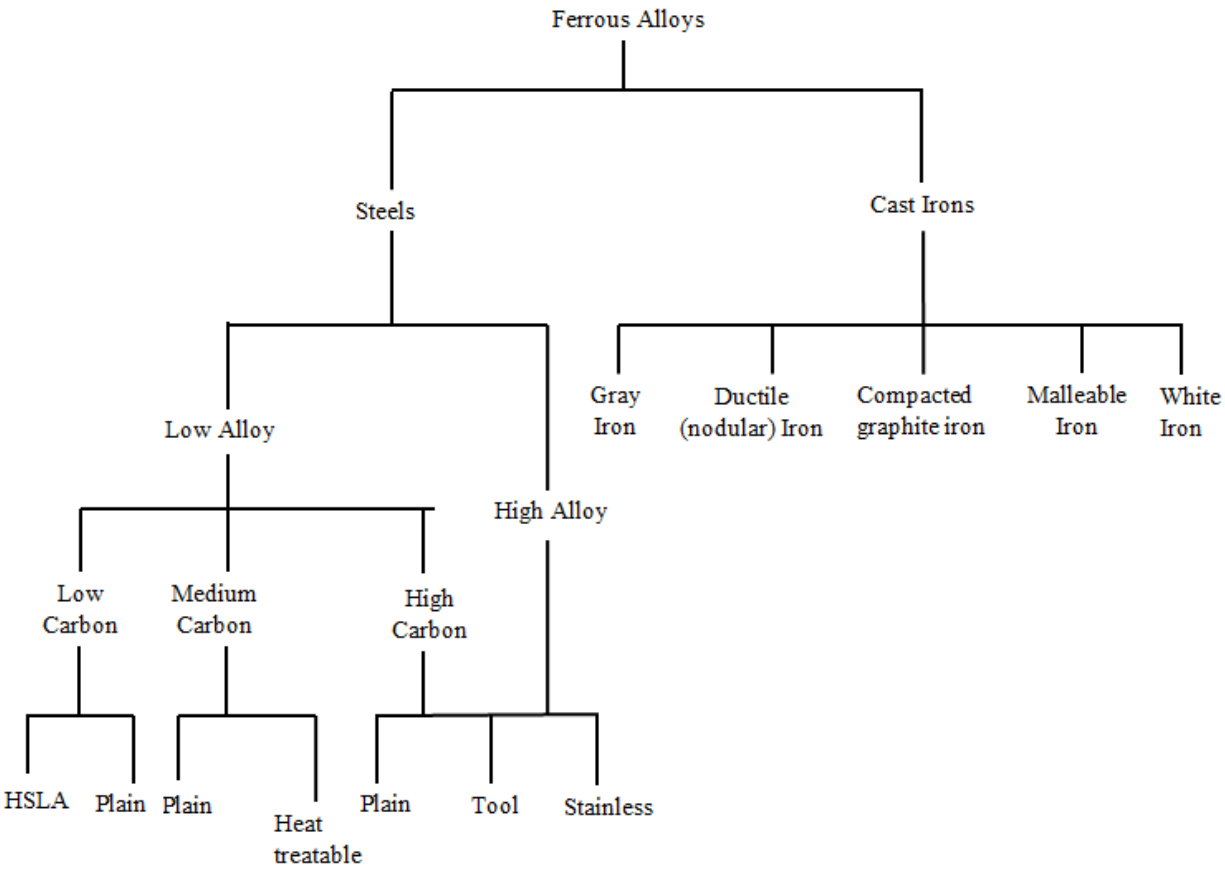

Figure 2.5. Classification scheme for various ferrous alloys [2007Cal].

2.2.3. History and development of stainless steels

The French engineer, Pierre Berthier, detected in 1821 that the addition of chromium to iron alloys (ferrous alloys) improved their corrosion resistance to acids and also enhanced stiffness [1911Mon]. In 1909, the microstructures of Fe-Cr-Ni and Fe-Cr alloys were independently studied by Albert Portevin and Léon Guillet in France. In 1911, the German metallurgist, Monnartz explained the passivation mechanism and determined the minimum percentage of chromium required to impart a rustless ability to steels [1911Mon]. It was observed that this alloy did not corrode or rust when exposed to atmospheric conditions. The new alloy was referred to as *rostfreistahl* in Germany, *rustless or rustproof iron* in Great Britain, and *acier inoxydable* in France [2000Car]. It was later denoted the modern designation as stainless steel in the United States and the United Kingdom, which continues today. The first casting of stainless steel was performed at Sheffield in the United Kingdom in 1913 [1936Boy, 2000Car].

In order to improve machinability, formability (weldability) and work hardening, major alloying elements such as nickel, cobalt, titanium and molybdenum are added to achieve the desired properties [1948Uhl, 1949Zap, 1979Pic]. These alloying elements also contribute to the enhancement of the corrosion resistant property of stainless steel [1948Uhl, 1949Zap, 1979Pic]. Since the inception of these alloys, production and development for structural applications have received a major boost. However, corrosion resistance was achieved at the expense of other mechanical properties: hardness, wear resistance, tensile strength, toughness and fatigue strength [1979Pic].

Factors such as corrosion and oxidation resistance in the operating environment, mechanical and physical properties, and fabrication characteristics in both hot and cold working conditions and welding necessitated the development of the various classes of stainless steel [1979Pic, 2000Car, 2004Tok]. These classes are also influenced by the chemical composition, microstructure and their phases [1979Pic].

2.3. CLASSIFICATION OF STAINLESS STEELS

There are more than 60 commercial grades of stainless steels [2000Car] and according to the International Stainless Steel Forum (ISSF) held in Brussels in March, 2011. The global annual production for 2010 was estimated at 30.7 million metric tons (mmt) [URLIs1].

The different grades are based on modification and/or addition of alloying elements, resulting in changes in chemical composition, crystallography and microstructure. These invariably affect the mechanical properties and applications [1949Zap], and have been grouped into:

- Austenitic stainless steels,
- Ferritic stainless steels,
- Martensitic stainless steels,
- Duplex or austenoferritic stainless steels, and
- Precipitation-hardened (P-H) stainless steels.

The stability of these phases is dictated by the alloying elements as grouped into α-forming and γ-forming elements [1984Pic, 2000Car]. Chromium and nickel are the

dominant alloying elements heading each group and the overall respective compositions are therefore known as the chromium and nickel equivalences. These have been empirically determined using the most common ferrite-forming and austenite-forming elements and is given below [1949Sch, 1979Pic]:

The Cr and Ni equivalence (wt %) are respectively given as:

%Cr+2.0%Si+1.5%Mo+5%V+5.5%Al+1.75%Nb+1.5%Ti+0.75%W and

%Ni+%Co+0.5%Mn+30%C+0.3%Cu+25%N

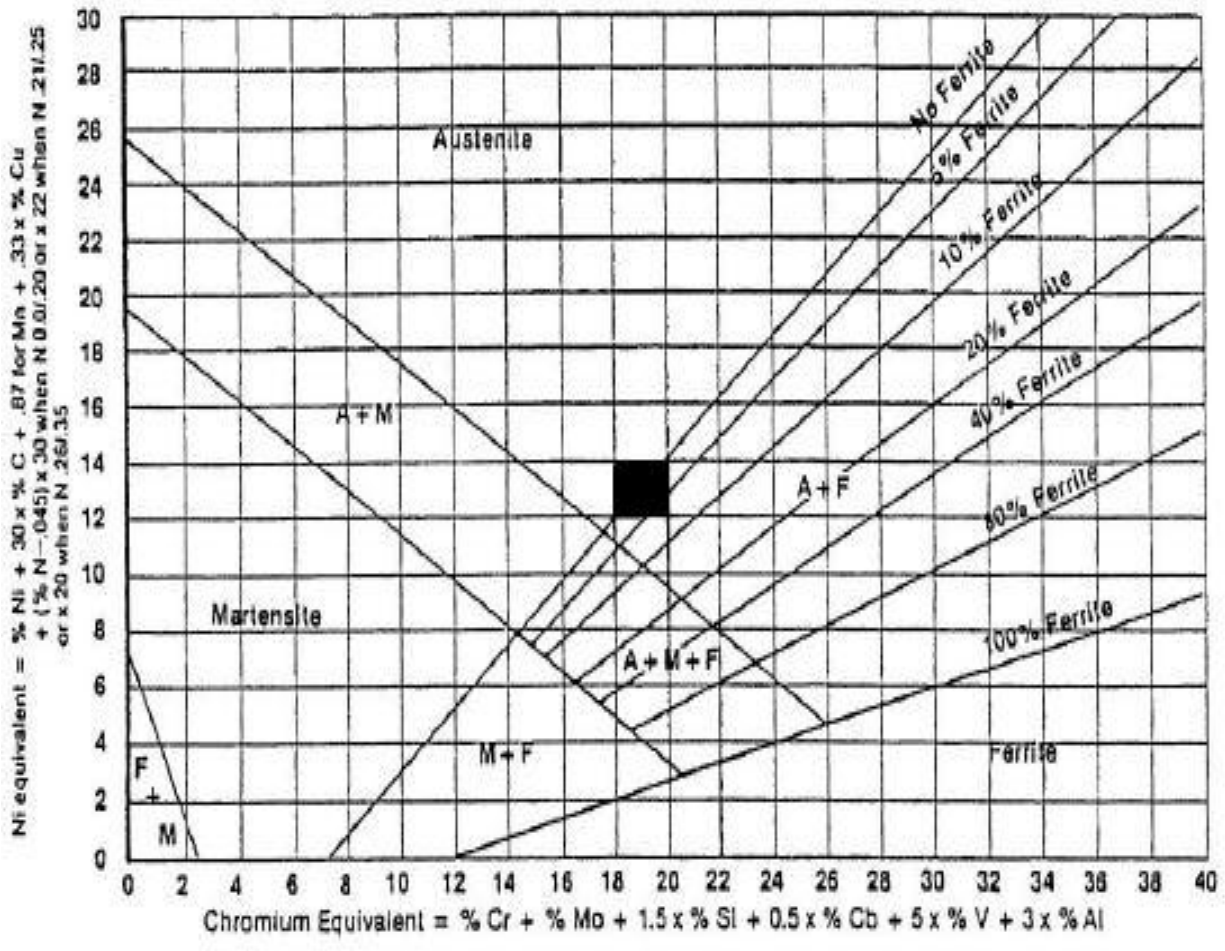

Figure 2.6. Schaeffler diagram based on Cr and Ni equivalence [1949Sch, 2000Car].

Plots of the Cr and Ni equivalences give the Schaeffler diagram, shown in Figure 2.6, [1949Sch], which is used as an estimate for expected phases for a given alloy composition. For example, martensitic and ferritic structures are obtained with high

chromium equivalence and the austenite phase is stabilized at high nickel equivalence. The Cr and Ni equivalence is also used to assess the phase formation in weldments. Hence, the weld metal chemistry can be modified to ensure better results and prevent hot cracking in the welds [1979Pic, 2000Car].

Secondary phases such as carbides, nitrides and intermetallic phases are also found in Fe-Ni-Cr systems in minute quantities. These phases also affect the corrosion properties and mechanical properties of stainless steels [1948Uhl]. Table 2.1 summarises the stainless steel classes and the range of the major alloying elements.

Table 2.2. Classification of stainless steels by microstructure [1949Zap].

Types of stainless steels	Typical Composition (wt%)
Martensitic	12-18 Cr; < 1.2 C
Ferritic	17-30 Cr; < 0.2
Austenitic	18-25 Cr; 8-10 Ni; ≤ 0.03 C
Duplex	18-26 Cr; 4-7 Ni; 2-3 Mo
Precipitation-hardening (P-H)	12-30 Cr with alloyed with Al, Ti, Mo

The summary of the classes of stainless steels and their respective mechanical properties, designations and metallurgical characteristics are further described.

2.3.1. Martensitic stainless steels

Martensitic stainless steels alloys are designated as AISI 400 series and are typically iron-chromium-carbon (Fe-Cr-C) alloys with 12-18 Cr and 0.07-0.4 C (wt%), according to the American Iron and Steel Institute (AISI). In most cases, carbon does not exceed 1.2 wt%, according to AISI. High carbon content expands the gamma loop in the Fe-Cr phase diagram. When the steel is heated the crystal structure transforms to austenite (stable at 1050ºC [2006Bha]), and then the steel is hardened when quenched [1984Pic, 1999Bed,

2000Car]. Due to the distorted body-centred tetragonal (bct) crystal lattice in the hardened condition, they are called the martensitic stainless steels [1949Zap].

Martensitic stainless steels exhibit the following characteristics:

- Mainly martensite crystal structure,
- Ferromagnetic,
- Hardened by heat treatment,
- Poor welding characteristics,
- Less corrosion resistant compared to the other grades, and
- High strength and moderate toughness in the hardened-and-tempered condition.

Tempering is a controlled reheating of the workpiece to a temperature below its lower eutectic critical temperature, which allows a portion of the martensite to decompose into ferrite and carbides. It is done to ensure good mechanical properties such as strength, toughness and ductility. Precise control of time and temperature during the tempering process is critical to achieve the desired balance of physical properties [1968Col].
Alloying elements such as Mo, W, V and Nb are added to martensitic stainless steels to cause secondary hardening, which increases the tempering resistance and strength as well as decreasing toughness and resistance to stress corrosion [1967Slu, 1968Col]. Elements such as Ni, Co, Mn and Cu are also used to increase toughness, since N and C reduce toughness significantly when used excessively. Precipitation of intermetallic phases can also provide hardening and strengthening mechanisms independent of the carbon content. This can be achieved by the addition of Ti, Al, Cu, and Mo [1967Slu, 1999Bed].

In summary, martensitic stainless steels are used because of their high strength and hardness, which is achieved at the expense of corrosion resistance. Major applications include cutting tools, shafts, valves, bearings, engines, gears, wear resistant parts in aerospace applications, hydroelectric power generation, chemical and petrochemical industries [1979Pic, 1984Pic, 1999Bed].

2.3.2. Ferritic stainless steels

Ferritic stainless steels are ferritic alloys up to the melting point, as indicated by their names. They are also designated as AISI 400 series, containing 17-30 wt% Cr and a low carbon content, which is less than 0.2 wt% according to American Iron and Steel Institute (AISI). Small amounts of austenite form at high temperatures depending on the amount of alloying elements such as N and C [1979Pic, 1984Pic, 1999Bed]. The ferritic structure is stronger than the austenitic, and the absence of Ni reduces the cost over the austenitic alloys. This modification reduces corrosion resistance, formability and toughness [1979Pic, 1984Pic, 1999Bed, 2007Osh].

Ferritic stainless steels exhibit the following characteristics:

- Due to high chromium content, they exhibit a body-centred cubic ferrite crystal structure,
- Cannot be hardened by heat treatment, but through cold working, hence are always used in the annealed condition,
- Poor weldability,
- Ferromagnetic and with sufficient Cr and Mo, and
- Retain their microstructures up to the melting temperatures.

Alloying elements such as Ni, Co, Mo, Ti, and Al precipitate β-phase intermetallic compounds, carbides ($M_{23}C_6$ and M_7C_3) and nitrides (M_2N) [1948Uhl, 2009Lo], which reduce the toughness of ferritic stainless steels. These alloys show ductile-to-brittle-transition-temperatures (DBTT) and generally have low toughness as a result of the alloy additions. Molybdenum additions increase the corrosion resistance. Stabilization of ferritic alloys with Nb and Ti is done to prevent intergranular corrosion or sensitisation, which is due to chromium carbide precipitation at the grain boundaries and depleting the nearby matrix of beneficial Cr [1979Pic, 1984Pic]. Although these alloys have low ductility, they have superior yield and ultimate tensile strength compared to the austenitic steels. The stacking fault energy is higher, hence there is a low work hardening rate, reducing the flow stresses during forming processes [1979Pic, 1984Pic, 1999Bed].

Ferritic stainless steels have high resistance to stress corrosion cracking and hence are extensively used in applications involving chemical plants. Austenitic stainless steels are increasingly being replaced by ferritic stainless steels since they are cheaper. Efforts are been made to improve their weldability and toughness, so as to increase the range of applications [1979Pic, 1984Pic, 1999Bed, 2007Osh].

2.3.3. Duplex stainless steels

Duplex stainless steels are made up of a composite structure consisting of the ferrite and austenite phases. They have improved mechanical properties due to the combined effect of the properties inherent in the ferritic and austenitic alloys [1984Pic]. They are composed of about 18 to 30 wt% Cr and relatively low nickel contents (4 to 7 wt%), according to AISI specifications. The low nickel contents in these steels provide cost reduction as compared to the austenitic stainless steels [1984Pic].

Duplex stainless steels have the following characteristics:

- Generally magnetic and non-austenitic,
- High resistance to stress-corrosion cracking,
- High weldability,
- Excellent pitting resistance, and
- High yield and tensile strengths as compared to austenitic and ferritic stainless steels.

When the volume fraction of each phase is altered, mechanical and physical properties can be altered. Strength is increased by the presence of ferrite and the reduction of the austenite grain size and also during deformation, a process that cause austenite to transform to martensite [1999Bed, 199Vor].

Due to the good mechanical properties, they are mostly used in severe corrosion environments and industries such as chemical plants, petrochemical, oil, pulp, nuclear, textile and pharmaceutical and structures in coastal areas since they have high resistance to chloride ion attack [1979Pic, 1984Pic, 1996Ame, 1999Bed, 1999Vor]. One of the most common grades is the Type 2205.

2.3.4. Precipitation-hardening stainless steels

Precipitation-hardening stainless steels are not defined by the bulk microstructure, but through the strengthening mechanism [1948Zap, 1967Slu]. The starting microstructures of these alloys are mostly austenite or martensite. The austenitic alloys are thermally treated to transform austenite into martensite, before precipitation hardening can be accomplished [1961Asm, 1967Slu, 1979Str]. The alloys require low C content, approximately 16 to 19 wt% Cr and austenite-forming elements such as Ni and Mn so as to reduce the formation of δ-ferrite [1979Pic, 1984Pic]. Molybdenum and vanadium are added for tempering resistance and Ti, Al, Cu and Co to induce the precipitation hardening effects [1967Slu, 1979Pic].

These alloys find their use in areas that require high strength, moderate corrosion resistance, and good fabricability. Typical applications include shafting, aircraft components, high-temper springs, and fasteners [1979Pic, 1984Pic, 1999Bed].

2.3.5. Austenitic stainless steels

Austenitic stainless steels are low carbon steels based on iron-chromium-nickel alloys which contain 18 wt%-25 wt% Cr, 8 wt%-20 wt% Ni and with at least 0.15 wt% C, to prevent carbide precipitation at the grain boundaries [1948Uhl, 1979Pic]. Austenitic stainless steels constitute the largest stainless steel family in terms of number of alloys and usage. They account for about 70-80% of the total world volume production of stainless steel, according to AISI. These alloys were discovered around 1910 through the addition of nickel to chromium-bearing iron alloys [1949Zap, 1979Pic].

For austenitic stainless steel, high chromium and nickel contents suppress the transformation of austenite to a mixture of ferrite and cementite, hence keeping the materials fully austenite on cooling [1949Zap]. The nickel maintains the austenite phase on cooling and the chromium slows down the transformation, so that a fully austenitic structure can be achieved with about 8% Ni. Addition of nickel to 18 wt% Cr steels enlarges the gamma loop considerably in the Fe-Cr equilibrium diagram, as shown in Figure 2.7 [1949Zap, 1960Pry, 1986Mas, 2006Bha]. When nickel is increased in the 18

wt% Cr steels, the amount of austenite at the solution-treatment temperature is increased. The austenite transforms to full or partial martensite when the nickel content in these steels is low. Increased Ni also decreases the temperature at which martensite starts forming (M_s). With about 8 wt% Ni, M_s drops below room temperature, hence stable austenite is retained after cooling from the solution-treatment temperature to room temperature.

Austenitic stainless steels exhibit the following characteristics:

- Non-magnetic,
- Better corrosion resistance compared to the other stainless steel classes,
- Easily welded,
- Hardened by cold working, but not heat treatment,
- Good ductility and toughness,
- Excellent surface finish, and
- Excellent corrosion resistance to several corrosive environments at both room and high temperatures.

Even though austenitic stainless steels are widely used in most structural applications in the aerospace, telecommunication, nuclear, petrochemical, biomedical and chemical industries, there are some limitations to their usage. The limitations such as low wear resistance, low resistance to stress corrosion cracking, low ultimate stress, short fatigue life and low hardness are drawbacks to the numerous applications, resulting in failure of those structures and components [1959Ehr, 1962Ver].

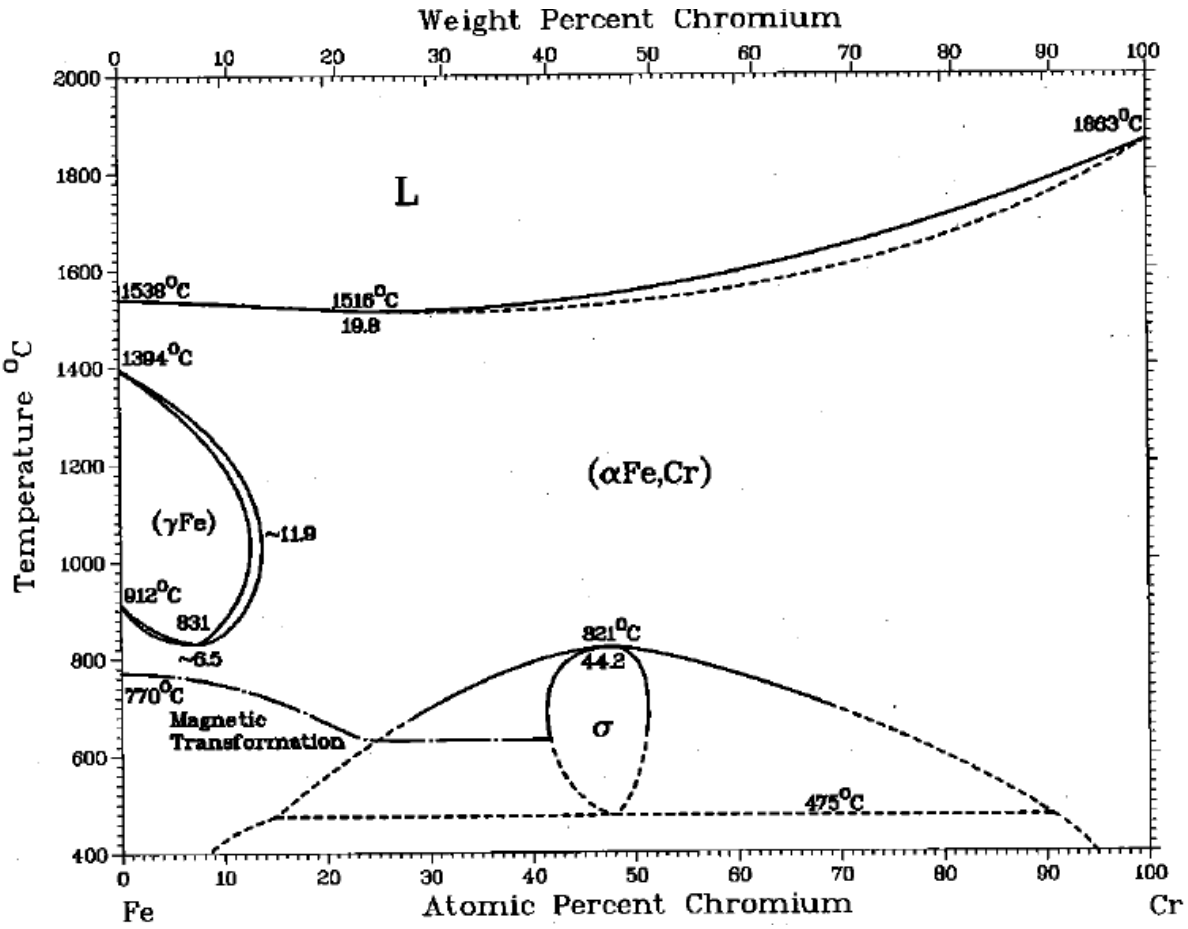

Figure 2.7. Fe-Cr equilibrium diagram [1986Mas].

Austenitic wrought stainless steels are classified according to AISI into three groups:

- AISI 200 series, i.e. alloys of iron-chromium-nickel-manganese,
- AISI 300 series, i.e. alloys of iron-chromium-nickel, and
- Nitrogen-strengthened alloys of the austenitic stainless group.

A general classification of the various types of stainless steels, possible alloying elements and their enhanced mechanical properties is shown in Figure 2.8 [1999Bed].

Being the subject of this research project, the mechanical properties, with emphasis on the fatigue properties and surface hardness, of austenitic stainless steels, and of AISI 316L in particular, are described later.

Austenitic alloys are used in the low carbon annealed form. AISI 316L, is the low carbon form of AISI 316. AISI 316L steel has a general composition of 0.03 max C, 17-18 Cr,

10-12 Ni, 2-3 Mo (wt%) and minor amounts of other alloying elements [1949Zap]. The low carbon content is to avoid the formation of chromium carbide precipitates that deplete chromium from the austenite matrix and cause a loss in corrosion resistance [1984Hal].

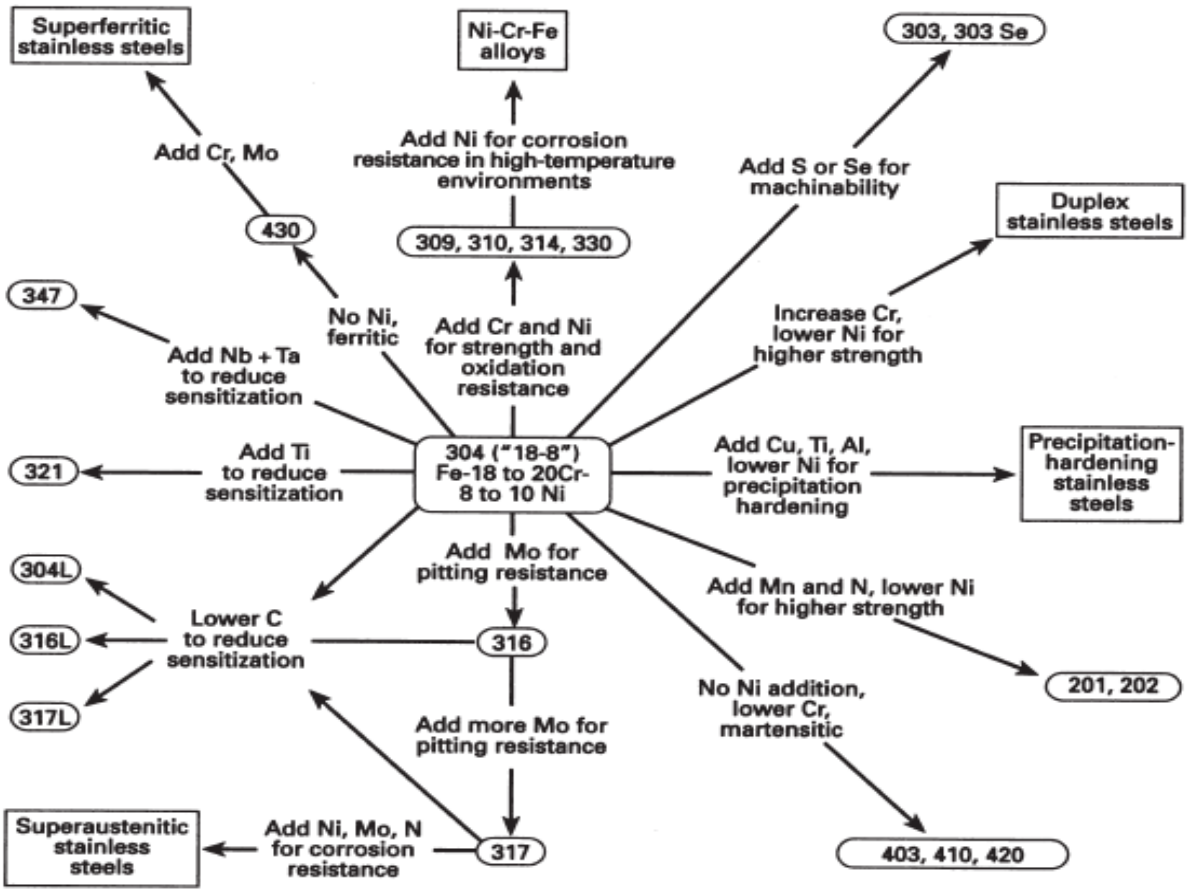

Figure 2.8. Composition and property linkages in the stainless steel family [1999Bed].

2.4. CORROSION PROPERTIES OF AISI 316L STAINLESS STEEL

Austenitic stainless steels outrank their ferritic and martensitic counterparts in terms of corrosion resistance, hence they are used in several industries and applications. The superior corrosion resistance is attributed to the synergistic effect of the chromium and other alloying elements such as nickel, molybdenum, titanium, niobium and manganese [1949Zap]. Chromium reacts with oxygen to produce an impervious, adherent and self-

healing oxide film on the surface of the steel, hence protecting the bulk material from attack from the corrosive environment. Molybdenum added to stainless steels improves localized corrosion resistance [1948Uhl, 1972Wei], whereas nickel increases resistance to stress corrosion, high temperature oxidation resistance and crevice corrosion in chloride containing environments such as seawater [1948Uhl, 1959Ehr].

The corrosion resistance of austenitic stainless steels is not only defined by the content and proportion of alloying elements, but also the way these elements are dispersed in the microstructure [1948Uhl, 2009Gal]. The precipitation of secondary phases and the rate at which these phases segregate is also a factor dictating the type of corrosion, either localized in the form of crevice, pitting, intergranular, or general corrosion [1948Uhl, 1966Oso, 1968Hor].

Polarisation is the change in equilibrium potential of an electrochemical reaction upon the application of a current. Polarisation reduces the driving force of the corrosion reaction and minimizes metal loss by changing the potential of either the anode or cathode, or both, so that the difference in potential between the cathode and anode is reduced to a minimum [1948Uhl]. The polarisation curve, a current-potential plot, thus the degree of potential change as a function of current applied for a metal surface whose corrosion rate is being determined. When the potential of the metal surface is polarised by the application of the current in a positive direction, it is said to be anodically polarised; a negative direction signifies that it is cathodically polarised. Alloying elements affect the polarisation curve of austenitic stainless steels as shown in Figure 2.9 [1948Uhl, 1986Sed, 2006Sha]. For instance, Cr is known to increase resistance to pitting by increasing the pitting potential in the noble direction. This reduces the passive current density. This is demonstrated in Fe-Cr-Ni alloys in sulphuric acid solution [1966Oso] and for Fe-Cr alloys in a chloride solution [1968Hor].

The solubility of carbon in austenite is reduced by the chromium content in austenitic stainless steel to about 0.05% as shown in Figure 2.10 [1979Sed]. Carbon of at least 0.05% will remain in solution in the austenite only if the material is solution treated or quenched. During heat treatment or slow cooling in the temperature range of 500ºC-

800ºC, precipitation of carbides takes place. Below 500ºC, low mobility of substitutional elements hinders the precipitation of carbides.

The precipitation of chromium carbides in austenitic stainless steels when heat treated or welded at temperature range of 500ºC-800ºC has become important [1933Bai, 1984Hal, 2003Was]. The $M_{23}C_7$ carbide is the predominant carbide responsible for the depletion of chromium in the area surrounding the precipitate [1948Uhl]. The Cr-depleted solid solution then cannot form a film, hence corrosion is very rapid in these regions [1933Bai, 1948Uhl, 1979Sed]. This type of corrosion is referred to as sensitisation, which can result to the localized intergranular corrosion [1948Uhl, 2006Sha], and can eventually lead to failure of the component under service [1933Bai, 1984Hal, 1986But]. The susceptibility of sensitised stainless steel to preferential intergranular attack has been cited as evidence of chromium depletion along grain boundaries, hence the theory proposed by Bain *et al*. [1933Bai], which is generally accepted as the main mechanism of intergranular corrosion [1948Uhl, 1984Hal, 1986But, 2003Was].

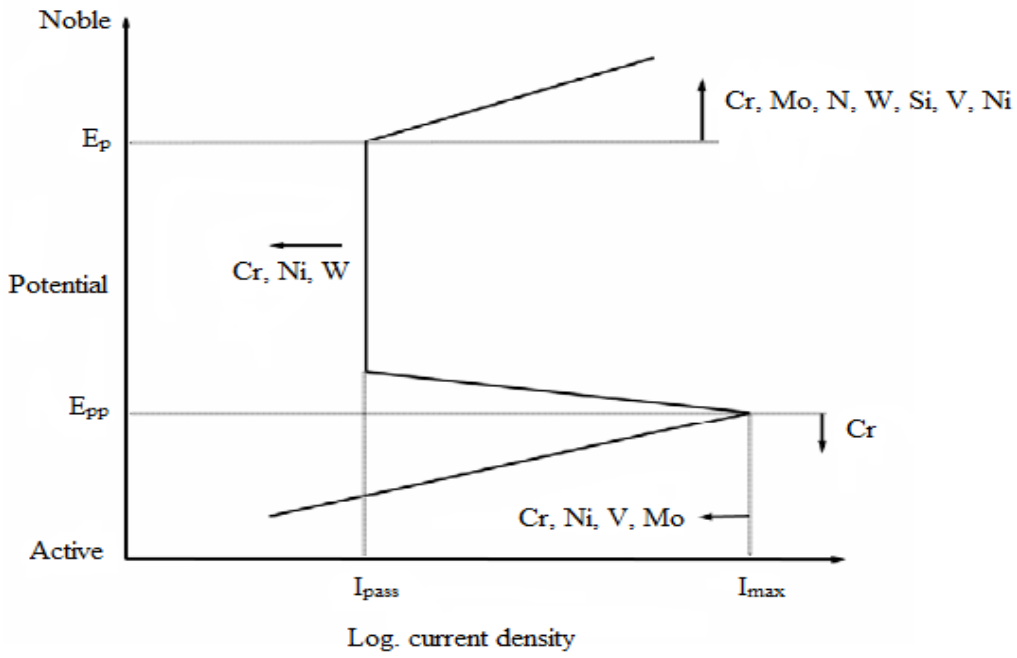

Figure 2.9. Effect of alloying elements on the polarisation curve of austenitic stainless steel [1986Sed].

In order to avoid sensitisation, carbon contents of austenitic stainless steels were reduced and kept low and other alloying elements such as Ti and Nb were added as stabilizers [1948Uhl]. This modification was achieved at the expense of mechanical properties, such as surface hardness, tensile strength, wear resistance and fatigue strength [2008Ces, 2009Ern, 2011Ern, 2011Li].

Crystallographic orientations of grains, and grain boundaries influence carbide precipitation in austenitic stainless steels [1948Uhl]. Grain boundaries are sometimes susceptible to carbide precipitation, unlike the coherent twin boundaries [1972Bar, 1998Tri, 2001Hon]. This is due to lower misfit and high number of atoms common to both grains of the coherent twin boundary which increase the energy of the boundary, making it difficult for carbides to precipitate. [1964Bra].

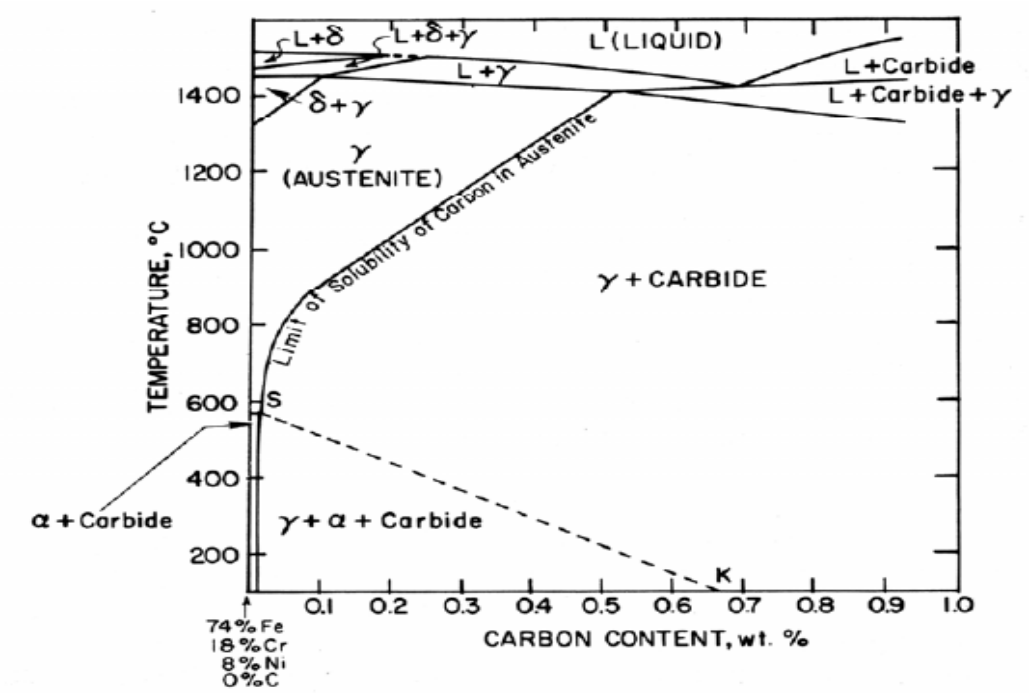

Figure 2.10. Solubility of carbon in austenitic stainless steel [1979Sed].

The presence of deformation slip bands and MnS inclusions in the microstructure decreases the corrosion resistance [1986Sed]. The MnS inclusions are favourable sites for pitting. Any discontinuity or weak point in the passive chromium oxide film is often at the precipitates, which is susceptible to corrosion as shown in Figure 2.11 [1972Sed].

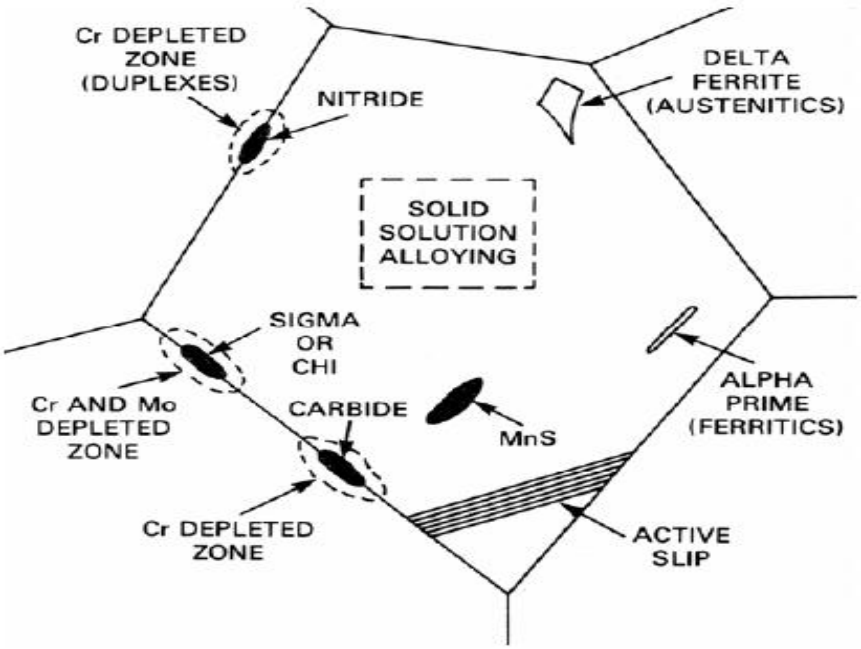

Figure 2.11. Metallurgical features detrimental to the corrosion resistance of austenitic stainless steels [1984Sed].

2.5. WEAR PROPERTIES OF AUSTENITIC STAINLESS STEELS

2.5.1. Friction and wear

Friction and wear are as a result of the sliding or rolling contact experienced by two mating surfaces under the application of a force. Energy dissipation is associated with the former, while the latter results in material loss [1953Arc, 1954Bow, 1991Bhu, 2008Sto]. The wear rate of a material is dependent on the frictional forces between the surfaces in contact. Suitable material selection and the use of solid or liquid lubricants suppressed the effect of friction, hence the wear rate of the mating surfaces was reduced [2008Sto]. In the use of materials such as polymers, ceramics or metals, it is difficult to avoid detrimental phenomena such as friction and wear once the surfaces are in contact during service [1968Lan].

Friction is the force resisting the relative motion of solid surfaces, fluid layers, and/or materials sliding against each other. The frictional force is the resistive force parallel to

the direction of motion [1954Bow]. The coefficient of friction (μ) is the degree of friction, a dimensionless scalar value which describes the ratio of the force of friction between two bodies and the force pressing them together [1954Bow, 1959God]. The two modes of friction are sliding or rolling friction. Sliding friction is the friction between two sliding surfaces which is due to adhesion between flat surfaces, ploughing by wear particles, hard asperities (protruding parts of the surface) and asperity deformation. Rolling friction is dependent on inconsistent slip during rolling. The mixed elastic and plastic deformations result in the energy losses [1953Arc, 1991Bhu, 2008Sto].

On the other hand, wear is a process of removal of material from surfaces in solid state contact, occurring when the surfaces are in sliding or rolling motion together [1961Rab, 1991Bhu]. The rate of material removal is generally slow, but steady and continuous. Figure 2.12 shows the five main categories of wear and the specific wear mechanisms that occur in each category [1991Bhu, 2008Sto].

2.5.2. Wear properties of AISI 316L stainless steel

The wear resistance of stainless steel is moderately low as shown in the material selection chart in Figure 2.13 [1999Ash]. The phenomenon of wear involves other material properties such as strength, hardness, toughness and thermal conductivity [1975Hal, 1987Lim]. The operating conditions such as contact geometry, load, sliding speed, asperities and temperature also influence the wear rate [1975Hal, 1978Bos], thus wear is a complex problem.

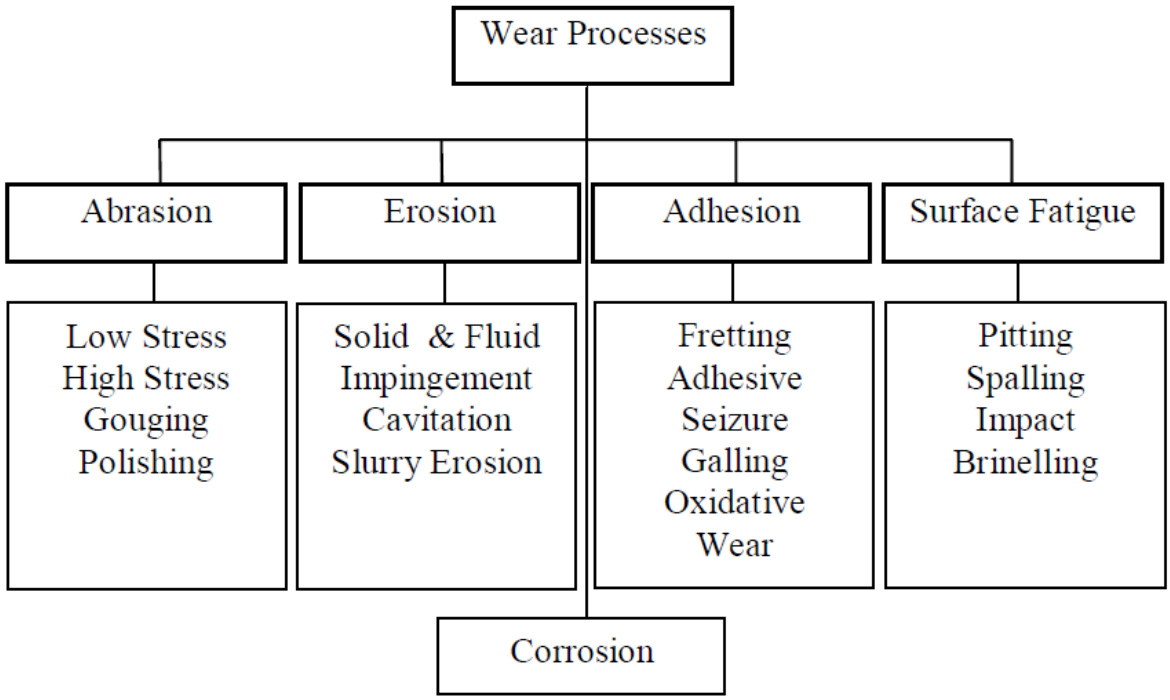

Figure 2.12. Types of wear mechanisms [1991Bhu, 2008Sto].

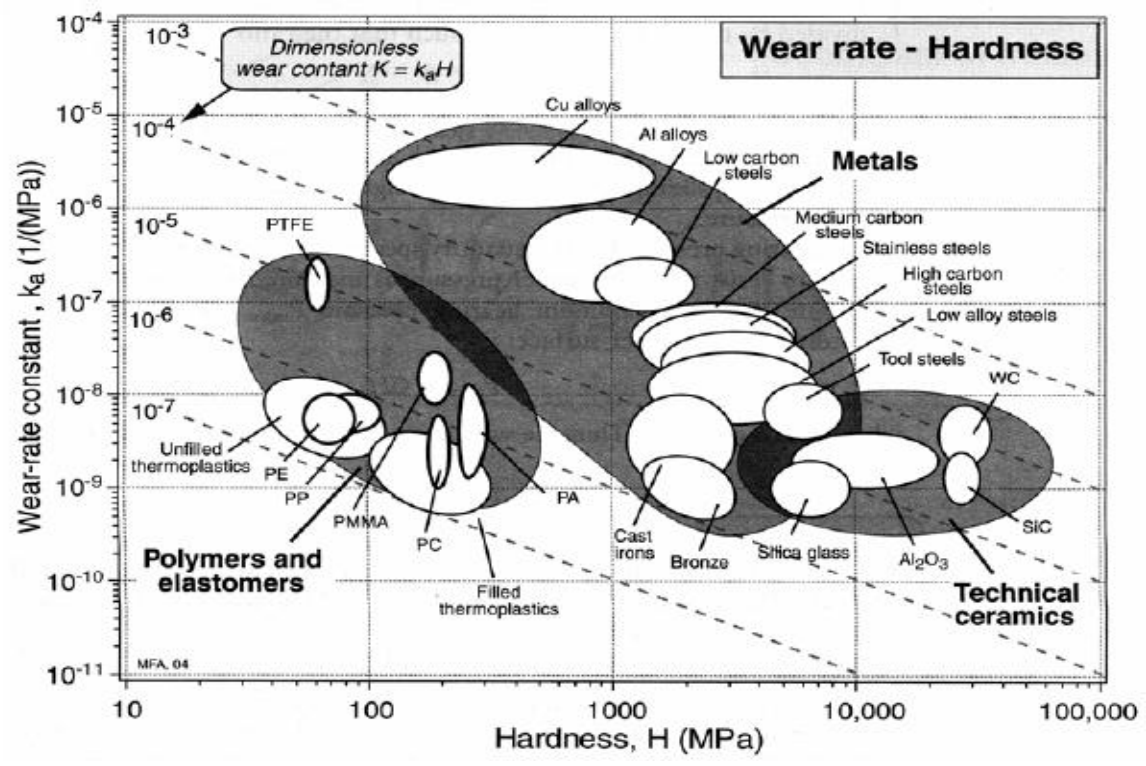

Figure 2.13. Material selection chart: Wear resistance [1999Ash].

In general, the poor wear resistance of austenitic stainless steels is associated with damage by galling and seizing [1980Hsu] at high loads and low sliding speeds. Wear of severe nature takes place by adhesion [1956Arc, 1983Qui]. In adhesive wear mode, junctions are formed between the sliding elements, at the interacting asperities, and are subsequently deformed until rupture occurs, producing very rough wear tracks [1980Sar]. Materials from one of the contacting surfaces are transferred to its counterpart through sliding, as shown in Figure 2.14 [2009Gal]. Plastic flow is not confined to the interacting asperities, but extends towards the subsurface. This result in the nucleation of cracks, which propagate parallel to the surface and are ultimately responsible for the detachment of plate-like wear debris particles of large size, through a mechanism called delamination wear.

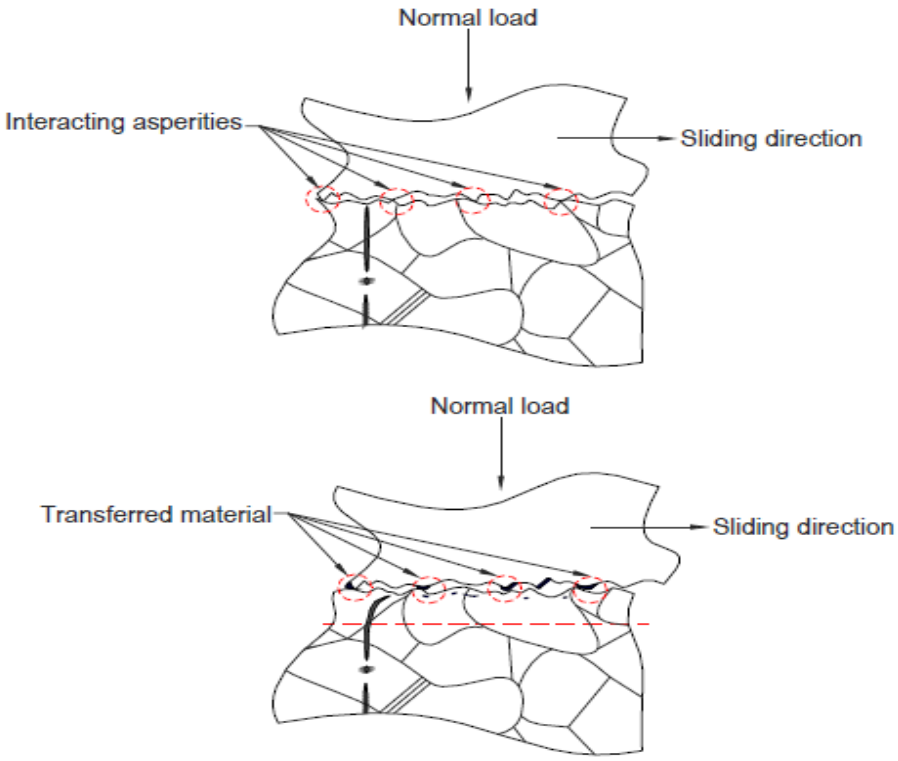

Figure 2.14. Transfer of material between interacting asperities and deformation of the subsurface [2009Gal].

At low temperatures, below M_s, the strain produced at the surface and subsurface of austenitic stainless steels sliders is sufficient to induce a martensitic transformation. The formation of martensite had significant effect on the wear [1977Dum, 1980Hsu,

1984Smi], and increased the hardness of the substrate, and consequently the wear resistance [1956Arc, 1977Dum]. On the other hand, the austenitic substrate, even after work hardening, was not strong enough to support the hard but brittle martensite surface layer. This led to a high rate of fracture and formation of abrasive debris particles [1980Hsu]. The resilience and toughness of the material are of significant importance. To rank the wear resistance property of the material, the ratio of hardness to elastic modulus is a more appropriate index than the mere hardness [1951Obe]. The best tribological performances have been reported for the combination of high surface hardness and relatively low elastic modulus, to reduce the tendency of plastic deformation and reduce the mismatch of properties. Deformation is found to be in the elastic range [2000Ley].

Reduced wear rates are associated with the formation of a flat and smooth protective oxide layer on the surface of austenitic stainless steel [1977Dum, 1986Smi], and the onset of a mechanism called oxidational wear [1983Qui]. The protective oxide on the surface of the steel is removed by abrasion or flaking, leaving fresh metal substrate exposed to the environment [1963Lan]. The abrasion mainly depends on the load, and the adhesion is a function of the temperature and the sliding speed. Under the right sliding conditions, a thin and tough oxide layer covers the surface uniformly, and provides good wear resistance [1977Dum].

The ductility and resilience of the oxide layer are important to accommodate the deformation of the substrate [1983Qui]. The elastic properties and hardness of the underlying material are critical to provide the necessary support to the oxide layer. Under stable oxidational wear conditions, the oxide layer grows up to a critical thickness, at which it becomes unstable, and can flake off.

In terms of the frictional force, coefficients in the range 0.4-0.7 have been reported for a wide range of sliding conditions [1985Hsu]. An average coefficient of friction of 0.5 is mostly used [1980Hsu, 1986Smi], in spite of some variations and fluctuations in the frictional force [1984Smi]. The fluctuating nature of the frictional force is associated with the interaction of surface asperities [1992Rab, 1999Sto], wear mode transitions, and formation, trapping and detachment of large wear debris particles [1982Bar].

Discontinuities in the plastic deformation at the subsurface, such as twinning and phase transformations, would also yield to fluctuations and variations in friction [1980Hsu].

Wear rate is considered to be inversely proportional to the hardness of the material [1989Gra]. Results on abrasive wear tend not to confirm this proportionality [1977Dum]. In materials of simple microstructure, there may be a direct relation between hardness and wear rate; this has been shown, for example, for commercially pure metals. This is not the case for materials of more complex microstructure (typified by most engineering alloys) [1989Gra]. In steels, the relation of wear to hardness is affected by the carbon content and the structural condition of the matrix as shown in Figure 2.15.

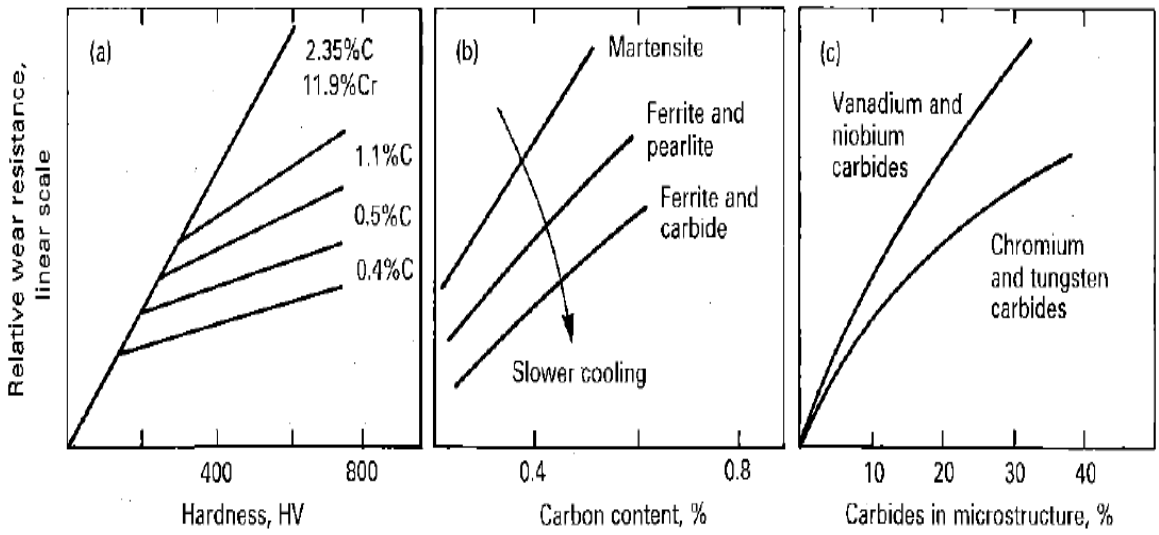

Figure 2.15. Relative wear resistance of steels against: a) Hardness; b) Carbon content; and c) Carbides [1989Gra].

This summary of the wear resistance properties of austenitic stainless steels was intended to introduce the basic principles of wear and friction. It is clear that the poor tribological performance of austenitic stainless steel is a cause for concern, and gives serious limitations for many applications, which demand excellent corrosion and wear resistance [1987Bel]. According to the US National Academy of Engineering (NAE) and the National Research Council (NRC), other materials are being developed as better alternatives for the austenitic stainless steels. Some of their properties are achieved at the expense of corrosion resistance, toughness and cost. Surface engineering offers an alternative way of improving the tribological properties of austenitic stainless steels at the

surface, with or without less adverse effects of the traditional properties of the material [1987Bel, 1999Sun, 2002Bel].

2.6. SURFACE TREATMENT OF AUSTENITIC STAINLESS STEELS

2.6.1. Introduction and fundamental concepts

Engineering components made from austenitic stainless steels and other materials degrade or catastrophically fail under service [2002ASM]. This is due to the surface-related phenomena such as wear, corrosion and fatigue which necessitated the interdisciplinary subject of surface engineering to improve surface properties of these components [1984Str, 1986Rob, 1987Bel].

The fundamental principles and origin of surface engineering were based on the traditional surface heat-treatment techniques such as quench hardening, nitriding and carburising [1987Bel, 1990Bel]. Surface engineering involves the application of conventional and new surface technologies to improve components and materials surface properties [1992Bel]. The innovative aspect of surface engineering is the design approach, and the increasing awareness of the importance of the surface properties and the surface conditions to the performance of the interacting surfaces [1991Rob, 1992Bel].

Surface engineering can be broadly classified into three main groups [1978Ell]:

- Coating of the substrate using methods such as physical vapour deposition (PVD), chemical vapour deposition (CVD), or thermal spraying,
- Modification of the structure of the substrate through induction hardening, flame hardening and shot peening, and
- Modification of the chemical composition and the substrate structure through techniques such as thermochemical processes, ion implantation, etc.

The choice of a particular type of treatment is mostly influenced by empirical experience rather than detailed or analytical study [1978Sma, 1986Rob, 1992Bel]. Figure 2.16 shows the various types of surface engineering techniques, with their approximate surface thickness [1990Bel].

Surface engineering treatments aid in the reduction of component size and weight, increase their life span and decrease energy losses associated with friction [2005Jam].

Thermochemical surface treatment of stainless steels is difficult to perform due to the presence of a tenacious Cr_2O_3 layer on the surface. This tenacious Cr_2O_3 layer serves as a passive layer and acts as a barrier that inhibits the diffusion of carbon or nitrogen atoms into the steel matrix. Plasma processing is the most ideal case hardening process for stainless steels. It also avoids pre-removal steps of the passive oxide layer by either chemical or mechanical means, e.g. sputtering. When the surface of a solid is bombarded with energetic particles, it becomes eroded, surface atoms are removed, and the morphology of the surface is modified; this is the phenomenon known as sputtering [2007Beh]. In stainless steels, sputtering is carried out at temperatures of about 400ºC for an hour, with high intensity pure hydrogen plasma [2006Min, 2010Pin]. A chemical means of pre-treatment of stainless steels in halogen-containing environment, e.g. fluorine, provides an effective activation of the surface. The passive and tenacious Cr_2O_3 layer is transformed to a fluorine-containing surface layer, which becomes permeable for the diffusion of carbon and nitrogen atoms into the steel matrix.

Some of the more conventional surface modification techniques are presented as follows.

- **Carburising** is heat treatment, which modifies the surfaces of steel. Carbon dissolves in higher amounts in austenite than in ferrite. Carbon has a small atomic size and occupies the interstitial sites, and austenite has larger interstitial sites than ferrite. Carburising is a diffusion-controlled process and high surface hardness and toughness are induced. There are three main methods: liquid (liquid bath of cyanide solutions), solid (pack carburising with carbon from graphite or charcoal) and gas carburising (carbon from hydrocarbons such as methane, propane and butane) [1977ASM, 1992Bro].

- **Nitriding** is another process that causes the diffusion of nitrogen into the interstitial sites of the stainless steel. It uses the same principles as that of carburisation [1977ASM, 1988Dea, 1992Bro].

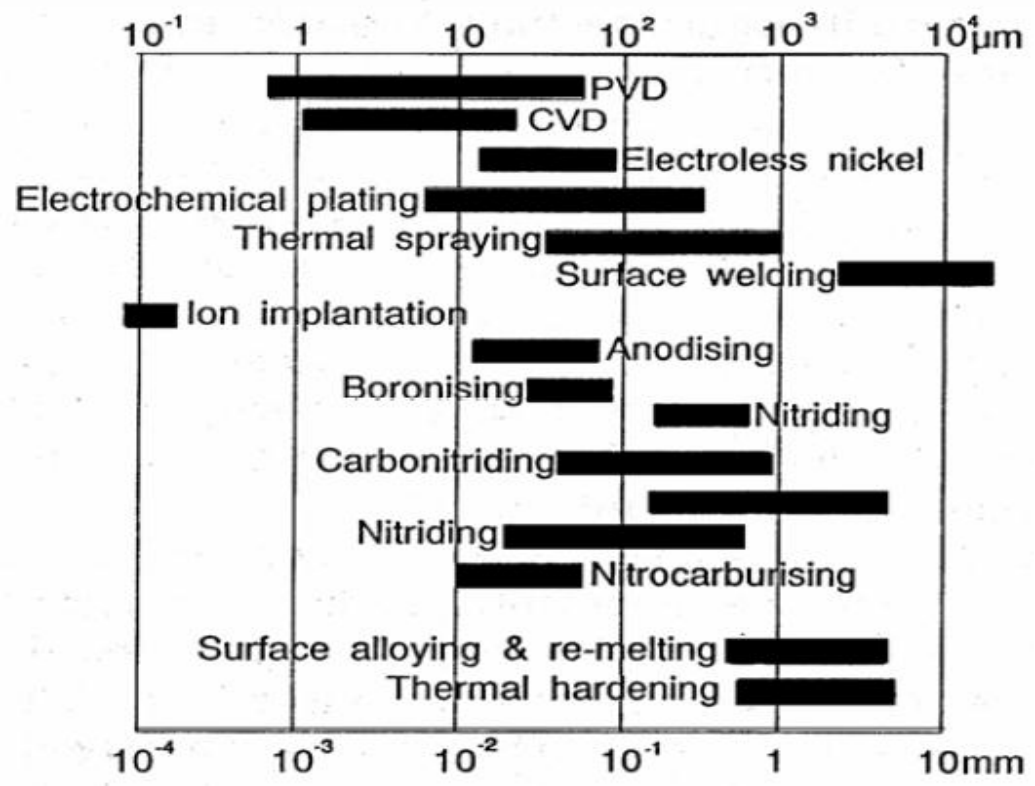

Figure 2.16. Surface engineering techniques and approximate surface thickness [1990Bel].

- **Ion implantation** is surface modification technique where carbon or nitrogen atoms are ionised in an implanter in the presence of electrons accelerated from a hot filament, producing ions in a plasma state with high energy. Positive ions of the carbon or nitrogen are extracted through a narrow slit and then accelerated in an electric field. The extracted ions are then directed on to the surface of the stainless steel in a vacuum. Due to the high energy of the ions, they collide easily with host atoms, displacing them from their lattice sites, resulting in the impinging ion coming to rest at some distance from the surface, hence enhancing the workpiece [1992Bro, 2006Sak, 2007Lia].

- **Laser hardening** is another surface modification technique that employs laser beams to heat the surface of the workpiece (e.g. stainless steel) for a short period. The heated layer is cooled rapidly by high thermal conductivity and the underlying colder metal, producing a hard surface layer. The heat affected zone is small, hence the

accumulation of distortion is minimal. There is good control of the hardening, due to the ability to control the laser beam [1992Bro, 1996Sta].

- **Physical vapour deposition** (PVD) belongs to the family of vacuum deposition, which is used to deposit thin films or coatings atom-by-atom in a vacuum onto the solid surface. The deposition of the coatings involves physical processes, such as high temperature vacuum evaporation or plasma sputter bombardment, rather than chemical reactions. The PVD techniques have been used to deposit TiN, ZrN and CrN on the surface of AISI 316L austenitic stainless steel. Excellent adherence of the film to the substrate, elevated compressive residual stresses and mechanical strength give rise to significant improvement of the fatigue performance of the base material [2001Ber, 2004Ber, 2004Puc].

For the purpose of this research, emphasis will be placed on the thermochemical or diffusion hardening processes in the next section.

2.6.2. Thermochemical and diffusion surface treatment

Thermochemical surface treatment (case hardening, surface hardening or cementation) is the process of hardening the surface of metals, often low carbon steels, by infusing elements into the surface of the metal, forming a thin layer of a harder alloy. The chemical composition of the substrate material is then modified, changing the microstructure of the metal, which in turn affects its properties. These changes are effected in the structure through heat treatment [1977Asm, 1988Dea].

The British standard EN 10052:1994 [1994BSI] defines thermochemical treatment *as "heat treatment carried out in a medium suitably chosen to produce a change in chemical composition of the base metal by exchange with the medium".* Diffusion treatment, on the other hand, "*is heat treatment or operation intended to cause the diffusion towards the interior of the ferrous product of elements previously introduced into the surface (for example, carburising, boriding or nitriding)"* [1994BSI].

From the definitions above, it can be established that thermochemical treatment is governed by two main factors: absorption reaction with the medium, and the diffusion in

the metal [1977ASM]. Various media such as solid, liquid, gas and plasma are employed for the thermochemical surface treatment of steels.

The transport of absorbed substances in the metal is achieved through the process of diffusion. The underlying principle is based on Fick's laws of diffusion [1949Col, 1954Dar]:

$J = -D\frac{\partial \emptyset}{\partial x}$ [Fick's first law] Equation 2.1

$\frac{\partial \emptyset}{\partial t} = D\frac{\partial^2 \emptyset}{\partial x^2}$ [Fick's second law] Equation 2.2

where:

J = "diffusion flux" [(amount of substance) per unit area per unit time],

D = diffusion coefficient or diffusivity in dimensions of [length^2.time^{-1}],

$\emptyset$ = concentration in dimensions of [(amount of substance). length^{-3}],

x = position [length],

t = time [seconds].

Transport of a substance in solution is driven by its concentration gradient, actually potential gradient, and the diffusion coefficient which depends on temperature, chemical composition and the structure of the substrate [1977ASM].

Generally, diffusion based surface treatments are slower compared to other surface deposition methods [1972Hur]. Thermochemical treatments produce case-core interfaces that are smooth. The case-core interfaces improve wear, fatigue and the load bearing capacity of components [1991Sun].

2.6.3. Low temperature thermochemical surface treatment of austenitic stainless steels

Surface engineering treatments are alternative methods employed in increasing surface hardness, which improves the wear resistance and fatigue properties of steels [1985Zha, 1988Dea]. Surface treatment of austenitic stainless steels is mostly considered a bad practice [1961ASM]. It causes problems such as formation of passive oxide films and the precipitation of chromium carbides [1999Sun1]. The passive oxide films hinder diffusion

of the hardening elements into the steel and they need to be removed by surface activation processes (e.g. sputter cleaning) prior to the surface treatment process [2000Par, 2004Som].

Surface treatments are conducted at high temperatures, around 900ºC-1000ºC for carburising and 500ºC-600ºC for nitriding [1973Ede, 1977ASM]. At these temperatures, the corrosion resistance is decreased due to the precipitation of chromium carbides and nitrides at the grain boundaries of the austenitic stainless steels [1933Bai, 1979Sed, 1984Hal]. However, low temperature thermochemical treatment with nitrogen and/or carbon had been devised to increase surface hardness without affecting or improving the corrosion resistance [1985Zha].

Hard, wear and corrosion resistant layers can be produced at the surface of austenitic stainless steels by means of this low temperature carburising or nitriding [2002Bel]. The corrosion resistance of austenitic stainless steels can be retained when the carburising and nitriding processes are conducted at temperatures approximately 450ºC and 550ºC respectively, as shown in Figure 2.17. The precipitation-free surface layer induced by carburising and nitriding is referred to as expanded austenite (EA) or 'S-phase' [1999Sun2, 2001Li, 2002Bel, 2006Chr].

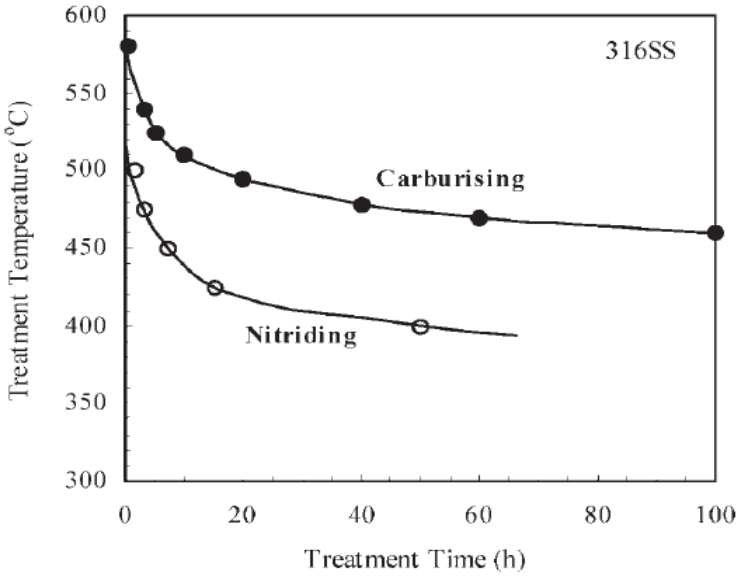

Figure 2.17. Threshold temperature-time curves for the formation of expanded austenite in AISI 316 using plasma carburising and plasma nitriding [2002Bel].

2.6.3.1. Metallurgy of expanded austenite (EA)

Expanded austenite (EA) or the "S-phase" is obtained by the dissolution of a high amount of interstitial carbon or nitrogen into austenite at low temperatures of about 550ºC for carbon and 450ºC for nitrogen [2002Bel]. This occurs through a local paraequilibrium (same ratio of alloying elements to iron in either phases or equal chemical potential of carbon [2004Hil]) [2002Bel, 2006Chr]. The thickness of the expanded austenite is in the order of 20 µm for nitriding and 50 µm for carburising [1999Sun], with about 20-30 at.% N and 5-12 at.% C [2006Chr].

Although there was controversy with the crystal structure of expanded austenite (EA) [1999Mar, 2002Mel], it has been accepted that the S-phase is a part of the substrate with an fcc crystal structure [1999Li, 1999Sun3, 2001Sun, 2000Few], with some distortions which are attributed to the high content of interstitial elements (carbon or nitrogen) in solution [1999Li, 2004Chr].

Expanded austenite is thermodynamically metastable, hence is decomposed to stable austenite, carbides and/or nitride phases when heated [1999Li, 2003Li]. As shown in Figure 2.17, the EA produced from nitriding decays faster compared to that produced from carbon. For prolonged service times, operating temperatures in the order of 200ºC for nitrogen and 300ºC for carbon should be considered [2002Bel]. The metastability (para-equilibrium) of expanded austenite (EA) is attributed to the higher diffusion rates of the carbon and nitrogen compared to the substitutional chromium and nickel elements at the low treatment temperatures [2003Sun, 2006Mic]. The precipitation of carbides and nitrides are suppressed at these conditions [2003Sun, 2006Mic]. The formation of EA is dependent on alloying elements. For example, chemical reactivity and high affinity of chromium to carbon and nitrogen increased the rate of EA formation [2000Par, 2001Li, 2003Sun, 2006Chr]. The interstitial carbon and nitrogen atoms occupy the octahedral sites of the fcc lattice and are surrounded by the substitutional chromium atoms [2000Par]. Molybdenum also slows the precipitation of carbides, allowing for higher treatment temperature, which can lead to increased thickness of EA [2005Sun], and also expands the octahedral interstices in the fcc lattice [2007Tsu].

2.6.3.2. Properties of expanded austenite (EA)

Tensile properties of surface treated austenitic stainless steels have shown improvement compared to the untreated samples. Thermal cycling is one of the factors that contribute to the enhanced mechanical properties [2004Tok, 2006Mic]. Surface treatments resulted in decreased in yield strength and ductility, with minor increases in ultimate tensile strength and the elastic modulus. The improvements in mechanical properties were attributed to the presence of high compressive residual stresses on the surface layer, and strain ageing produced during the surface treatment process [2002Tha, 2004Tok, 2006Mic].

Austenitic stainless steels suffer severe metallic wear due to the formation of strong adhesion junctions between the contact surfaces and severe surface/subsurface plastic deformation [1980Hsu, 1984Whi]. The EA was effective in improving dry sliding wear resistance by inhibiting surface plastic deformation and abrasion. Adhesion between the contact surfaces was also eliminated hence the wear of the carburised surfaces occurs in a mild micro-abrasive mode [2002Sun, 2007Qu], which is in contrast with the severe adhesive and abrasive wear experienced by the untreated austenitic steel surfaces [1980Hsu, 1984Whi]. However, subsurface cracks and deformation occurred. This led to catastrophic failures under heavy loads [2002Sun]. Carbon EA layers were thicker and tougher than the nitrogen EA, hence can withstand subsurface crack propagation, compared to their nitrogen EA counterparts [2002Sun].

Corrosion resistance of low temperature carburising or nitriding of austenitic stainless steels is dependent on the testing conditions. In NaCl solutions, EA remains passive under a wider range of potentials compared to the untreated austenitic stainless steel. Carbon EA shows some advantage over nitrogen EA [1977ASM, 2003Tha]. For repassivation, passive films heal slower on EA than on austenitic stainless steels [2003Tha, 2006Don]. Higher initial current densities have been measured on EA layers with the absence of pitting potential, which is not the case for the untreated austenitic stainless steels [1999Sun, 2002Tha, 2002Aok].

The fatigue life of austenitic stainless steels is increased due to the presence of high compressive residual stresses on the expanded austenite layer. An improvement of about 25% of the fatigue life and changed failure mode has been reported [2002Tha]. The hard expanded austenite layer suppressed the alternating slip deformation at the surface [2004Tok, 2006Mic]. For low temperature carburising of austenitic stainless steels, a minor increase in the notch sensitivity is reported by Ceschini *et al.* [2008Ces].

2.6.4. High temperature thermochemical surface treatment of austenitic stainless steel

Welding and heat treatment in temperature ranges of 450-800ºC is detrimental to stainless steels, and these temperatures are considered relatively high [1969Sta, 1984Mar]. Sensitisation is a detrimental phenomenon which leads to chromium-carbide precipitation at the grain boundaries. Growth and high concentration of chromium in $M_{23}C_6$ particles decreases the chromium content in regions that are adjacent to these chromium-rich precipitates. This is attributed to the slower diffusing rate of chromium than carbon atoms in the matrix, and the less time for chromium to diffuse to the carbides at the grain boundaries. This resulted in the chromium content in the regions near grain boundaries to be lowered below 13%, a critical value for required stainless corrosion behaviour. Chromium diffusion from the bulk of the grains increases the concentration above the critical limit at prolonged treatment time. The depleted zones become weak and are easily broken in aggressive environments [1984Cih, 1996Sed], making sensitised stainless steels prone to intergranular corrosion (IGC) and intergranular stress corrosion cracking (IGSCC) [1969Sta, 1984Cih, 1985Bog].

The localised corrosion resistance is improved by molybdenum additions to stainless steel [1966Lew, 1972Wei], but Mo can also favour the formation of intermetallic phases and other types of carbides in the steel [1966Lew, 1972Wei]. Long exposure of AISI 316L stainless steels to elevated temperature can result in the formation of other intermetallic phases such as sigma, chi and Laves phases [1972Wei, 1983Lai, 1984Hal]. Substitutional elements in the austenite matrix are responsible for nucleation and growth, and the formation of intermetallic phases is hindered by the slower diffusion rate of these substitutional elements. This can lead to the depletion in the chromium and molybdenum

as carbides are formed, which are detrimental to the steel [2006Ayd]. For instance, sigma phase, FeCr, generally expanded as $(FeNi)_x(CrMo)_y$, adversely affects the mechanical properties and localised corrosion resistance [2000Sch]. It nucleates mainly on the grain boundaries and is found in 316L stainless steels after 100h at 800ºC [1972Wei].

Intergranular corrosion in stainless steel is accelerated by potential differences between the grain boundaries and the grains [1948Uhl, 1984Mar]. The availability of anodic sites at the grain boundary triggers the intergranular attack by passivating the sample. The chromium-depleted zones set up a passive-active cell of appreciable potential difference, with grains exhibiting passive behaviour, resulting in large cathodic areas relative to the small anodic areas at the grain boundaries which exhibit the active behaviour [1948Uhl]. With decreasing potential, the protective passive film over chromium-depleted (sensitised) areas is more easily dissolved than that on the undepleted (non-sensitised) surface [2006Ayd].

2.7. FATIGUE PROPERTIES OF AUSTENITIC STAINLESS STEELS

2.7.1. Introduction to fatigue properties of materials

Fatigue is a process of progressive localised permanent structural change occurring in a material subjected to conditions that produces fluctuating (alternating or cyclic or repeated) stresses and strains at some point or points and that may culminate in cracks or complete fracture after a sufficient number of cycles [1903Ewi, 1953Man, 1954Cof, 1958Tho, 1962Ave]. The simultaneous action of cyclic stress, tensile stress, and plastic strain is responsible for fatigue failures [2002ASM]. The cyclic stress and strain starts the crack; the tensile stress produces crack growth (propagation). The conditions for fatigue loading are shown in Figure 2.18. For a fluctuating load, the mean stress is greater than the stress range; with a pulsating or repeated load the mean stress is equal to half the stress range; and with an alternating load, the mean stress is zero. In all instance stated, the stress amplitude is half the stress range.

Prediction of fatigue failures has been considered in terms of S-N curves (Figure 2.19), the Goodman [1899Goo] (Figure 2.20) and the Soderberg [1939Sod] diagrams (Figure

2.21) [2000Tim]. These diagrams are based on constant amplitude tests, but such conditions seldom apply in practice, and the stress amplitude and any component of the mean stress may vary.

The Goodman and Soderberg diagrams [1899Goo, 1939Sod] are used to investigate the relationship between stress amplitude, mean stress and fatigue limit. For instance, if the mean stress is at zero, thus perfect alternation, then the fatigue limit will be a maximum before failure.

In the Goodman diagram [1899Goo] (Figure 2.20), the fatigue limit is zero when the mean stress is equal to the tensile strength of the material, since the material will fail at this value before any cyclical loading can commence. Therefore, if the point representing the stress amplitude and mean stress for any given set of conditions lies within the area bounded by the axes and the 'Goodman line' and the shaded area, then the materials will not fail according to the Goodman relation.

In the Soderberg diagram [1939Sod] (Figure 2.21), the fatigue limit is zero when the mean stress is equal to the yield stress of the material. The point representing the stress amplitude and mean stress for the material must lie within the area bounded by the axes and the 'Soderberg line' if failure by fatigue is to be avoided.

Studies on fatigue are intended to produce endurance and fatigue data for materials. The information ascertained from crack initiation and growth stages can be used to evaluate the damage mechanism of the material [1953Hea]. Experimental data can be presented as strain-endurance plots, for total, elastic or plastic strain range versus the number of cycles to failure, or as load-controlled plots [1983War]. This is illustrated schematically in Figure 2.22.

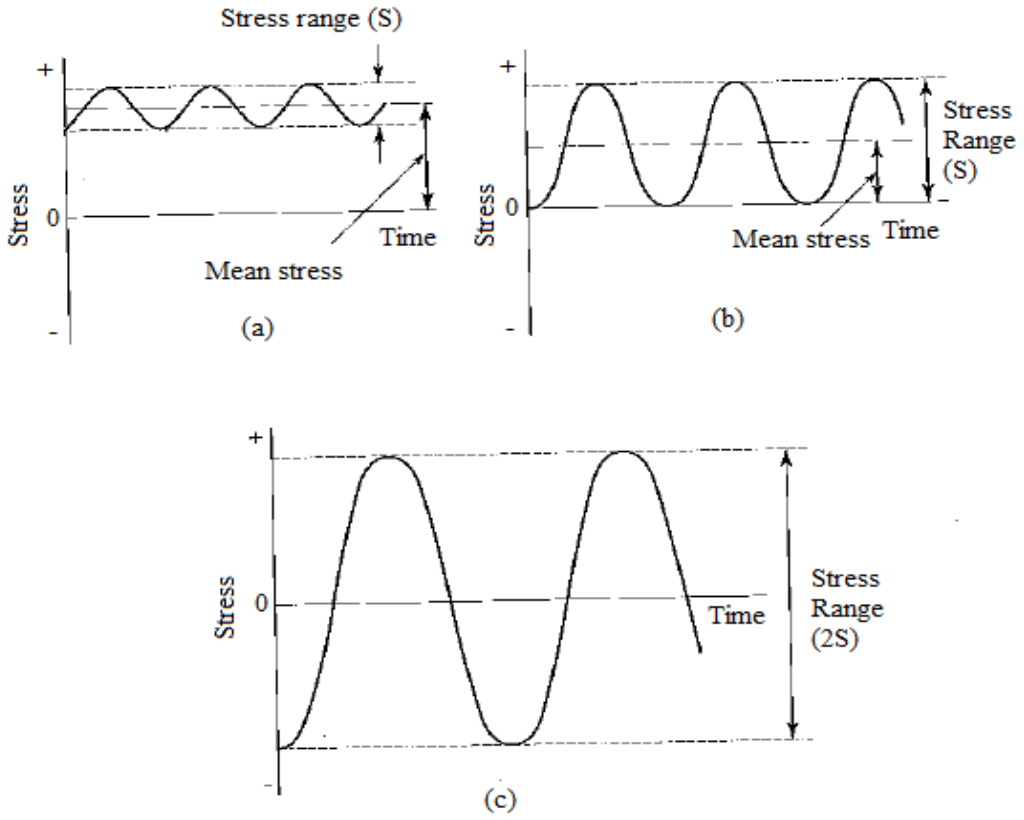

Figure 2.18. Conditions of fatigue loading: (a) fluctuating load; (b) pulsating or repeated load; (c) alternating load [1964Ben].

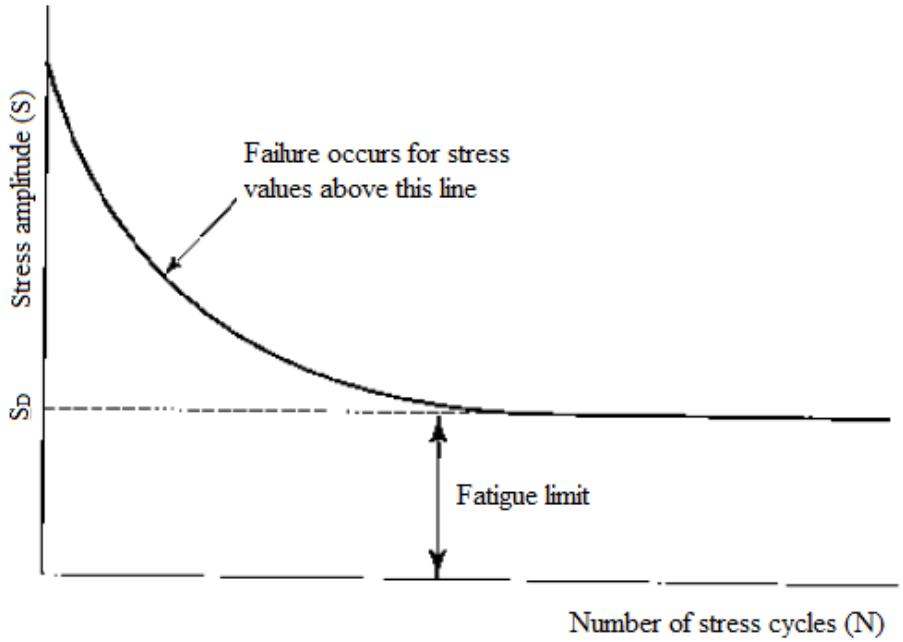

Figure 2.19. Schematic stress reversal curve (S-N) for a typical steel [1964Ben].

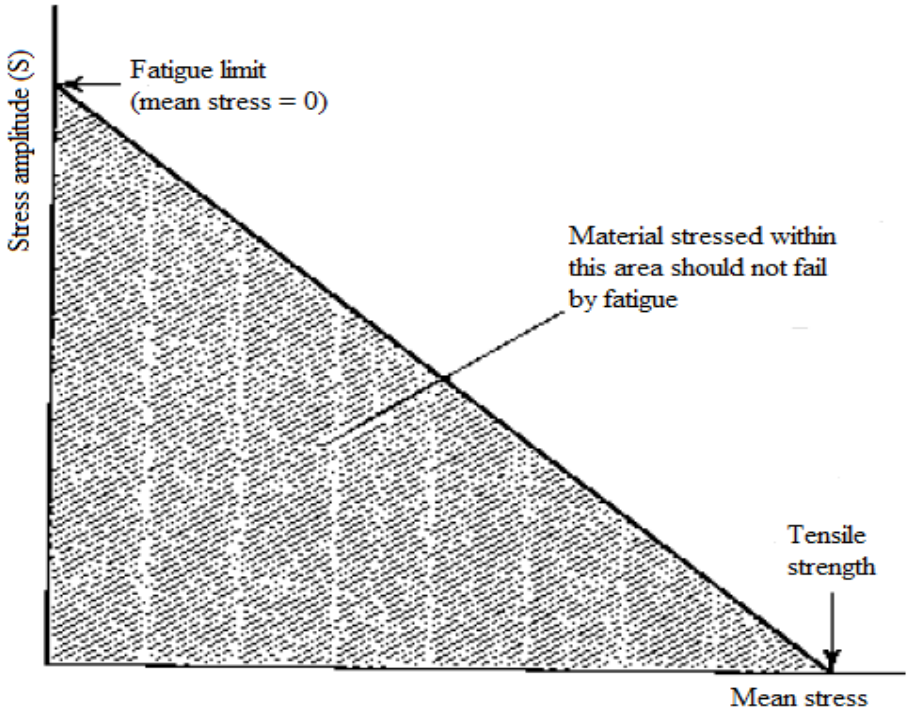

Figure 2.20. The Goodman diagram [1899Goo].

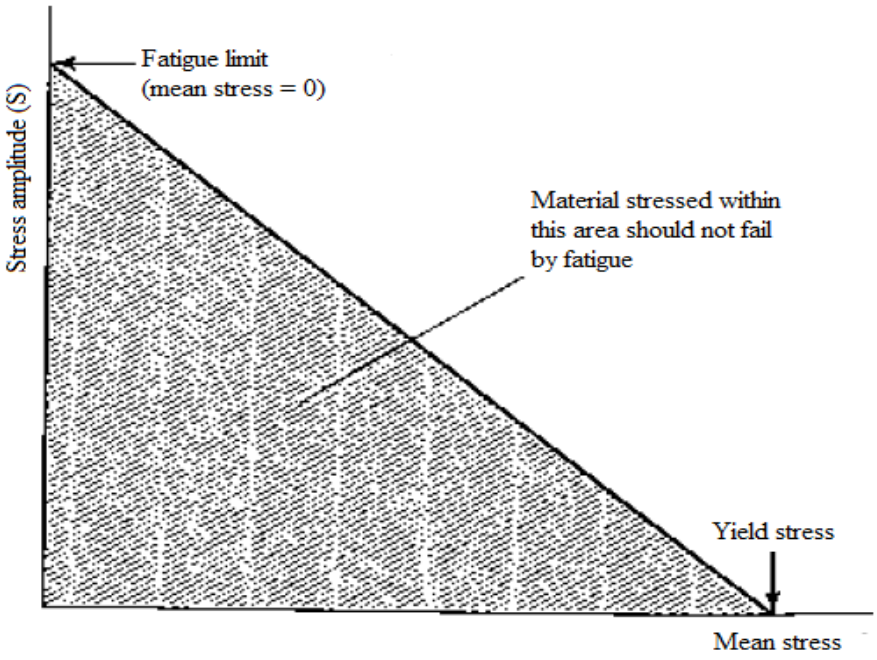

Figure 2.21. The Soderberg diagram [1939Sod].

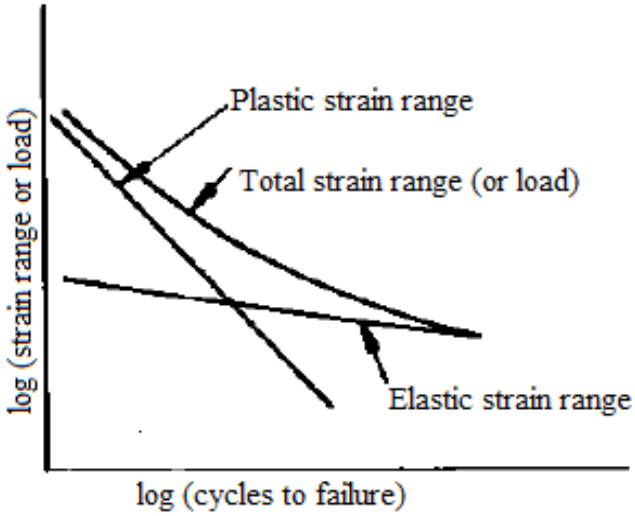

Figure 2.22. Fatigue life data expressed in terms of elastic, plastic and total strain [1983War].

2.7.2. Category of fatigue tests

Fatigue experiments can be categorised as low or high cycle, depending on the number of cycles sustained by the material before fracture. Fatigue failures that occur at cycles less than 10^5 cycles are termed low-cycle fatigue [1954Cof, 1974Kre]. Macroscopic plastic strain takes place in each of the cycles. Above 10^5 cycles, high-cycle fatigue is bound to occur. The macroscopic cyclic plastic straining is what distinguishes low-cycle fatigue from the high-cycle, where the macroscopic deformation is elastic [1974Kre]. A schematic fatigue diagram (S-N) for evaluating low cycle fatigue is shown in Figure 2.22 [1953Man]. Low cycle fatigue (LCF) is based on the Coffin-Manson [1954Cof] relation, where the strain amplitude is the algebraic sum of the elastic and plastic strain, as shown in Equation 2.3. The material under this domain responds to plastic and elastic deformation. In low cycle fatigue, the strain is used.

$$\frac{\Delta\epsilon_p}{2} = \epsilon_f'(2N)^c \qquad \text{Equation 2.3}$$

Low-stress or high cycle fatigue (HCF) is observed at cycles beyond 10^4. In this domain, the material experiences elastic deformation. With HCF, emphasis is on the stress at the endurance or fatigue limit. The data are represented on a Goodman diagram, a plot of alternating stresses against mean stresses, as shown in Figure 2.24 [1953Man].

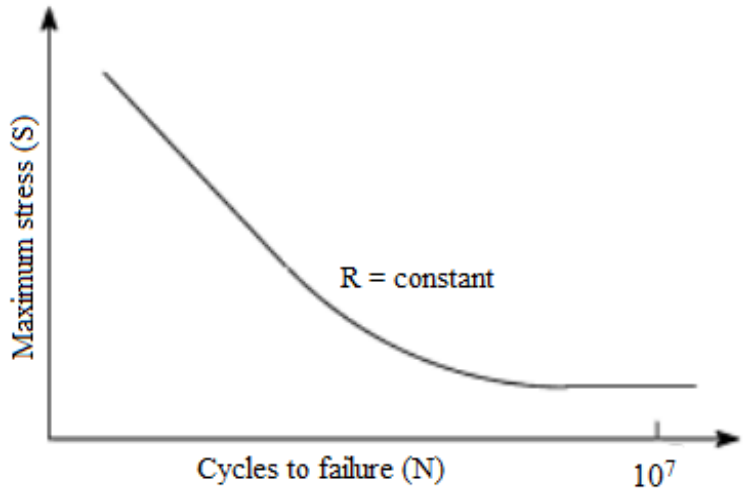

Figure 2.23. Stress-cycle to failure (S-N) curve for a low cycle fatigue (LCF) [1953Man].

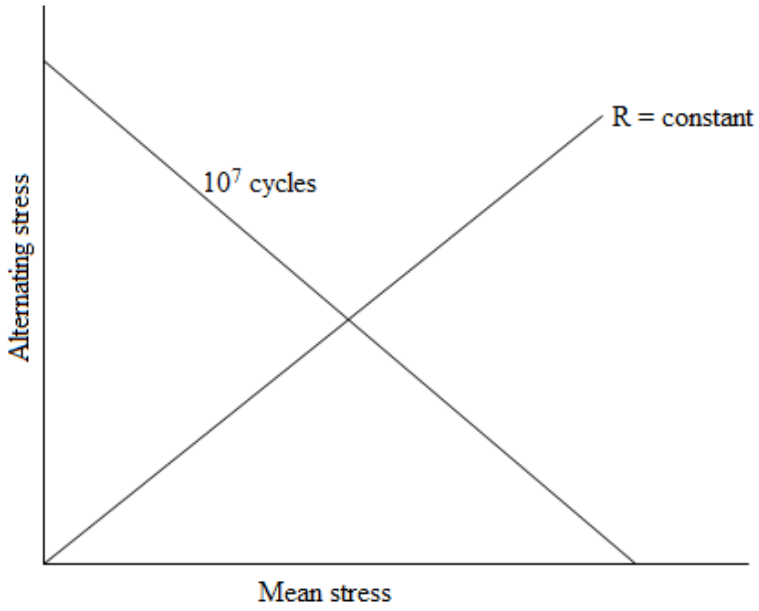

Figure 2.24. Schematic fatigue diagram (Goodman curve) for data in the high-cycle fatigue (HCF) regime [1953Man].

2.7.3. Stages in fatigue

Fatigue failure proceeds in three stages: crack initiation in the area of stress concentrators (near stress raisers), incremental crack propagation and final catastrophic failure.

2.7.3.1. Fatigue Crack Initiation

Crack nucleation during the fatigue process often takes place at a free surface of the material. Extension of the crack is termed the crack growth. During the nucleation process, the crack lengths are in the order of 10μm [1968Tom, 1983Ske, 1983War] and this takes place along the shear plane of the crack tip. During cycling of smooth-surfaced specimens at room temperature, planar arrays of dislocations are formed in the stainless steel. At temperatures above 470ºC, elongated cells are formed [1981Rio]. The change in slip character is consistent with an increase in stacking fault energy (SFE), resulting in an increase in the probability of cross-slip with temperature. The presence of precipitates at the grain boundary mitigates grain boundary migration during high-temperature cyclic deformation [1974Abd, 1981Rio]. The cell size decreases with increasing strain range [1963Seg, 1967Fel, 1973Cha].

Low SFE materials exhibit dislocation bands and these dislocation bands are entangled at low plastic strain ranges. At high strain ranges, elongated cells are observed due to the increase in the tendency of cell formation [1972Lai].

The absence of constraint in surface grains allows the dislocation structure, generated as a result of cycling, to extend out of the free surface grains and produce a microscopically irregular surface [1983War]. These dislocation substructures are known as persistent slip bands (PSBs). Persistent slip band formation begins at a very early stage in the life of the material, and for materials which cyclically harden, is complete on the attainment of saturation hardening after about 10% of life [1981Tom, 1983Ske, 1983War]. Within the PSBs, that extrusions and intrusions are formed, due to some irreversibility in the slip process. Extrusions are thin ribbons of metal of the order of 10μm long and 1μm thick, which protrude from the metal surface, whilst intrusions are crevices of similar dimensions associated with extrusions. Extrusion/intrusion formation occurs rapidly after the appearance of the PSBs intrusions act as transgranular crack nuclei [1983War].

As PSBs represent weak paths in the material, they are clear crack initiation sites, giving crack initiation within a few percent of high strain fatigue life. Typical crack sizes are 1-

10μm [1981Tom, 1983Ske, 1983War]. Since the crack sizes are greater than the dislocation substructures, the initiated cracks behave as a continuum [1983War].

Near-surface crack initiation at particles has been observed in ferritic steel [1973Lan] and probably occurs in austenitic steels, although there is no reported information on this effect. In cast materials, internal cast pores act as stress raisers and promote subsurface crack nucleation [1973Gel]. Internal nucleation has been reported for austenitic welded joints at 550ºC [1980Sch]. Here, internal crack sizes up to 2mm were reported at the weld root, and fatigue life was reduced by a factor of three, when compared to similar test on plate. Reduced fatigue endurances have also been reported for Types 304 and 308 weld metals [1974Bri].

Temperature affects the slip characteristics of a material. For instance, increasing temperature reduces grain boundary strength and accelerates oxidation [1973War]. The combined effect of these processes is to accelerate crack initiation. For temperatures within the creep regime, grain boundaries become progressively weaker with respect to the matrix as the temperature is increased, or the strain rate decreased at a fixed temperature. Austenitic stainless steels exhibited transgranular nucleation at 25°C and 400ºC; intergranular initiation was observed in Types 304 and 347 at 750ºC and 835ºC for strain rates between 10^{-3} and $10^{-5}s^{-1}$ [1973War, 1977Tom]. Type 316 had decreasing strain rate from 10^{-3} to $10^{-6}s^{-1}$ at 625ºC, which caused a change from transgranular to intergranular initiation [1977Tom].

An aspect related to crack initiation is the surface finish of the testpiece. Stress raisers can be generated or induced in the specimen during and after specimen manufacturing. Figure 2.25 shows the variation in finish of Type 316 stainless steel, after grinding, turning and electropolishing [1979War, 1983War].

For the ground condition, the notch peak topography is similar to that of naturally initiated cracks. Thus, cracks grow from machining marks around the entire specimen circumference. For the electropolished surface, initiation occurs by slip processes and cracks are discretely spaced around the surface, as illustrated in Figure 2.26 [1983War]. The stress cycle to a fraction of the expected life at 400°C is followed by ambient

temperature cycling revealing crack initiation and propagation characteristics, because of enhanced oxidation at the higher temperature. The difference in crack density is reflected in enhanced fatigue lives of electropolished specimens. However, at 600°C and 750°C, the lives of machined and electropolished specimens of 20Cr-25Ni-Nb stainless steels tested in air were similar [1979War, 1983War]. This is because at these temperatures, grain boundaries are the prime sites for crack nucleation, and no difference in surface crack distribution was observed for the two surface finishes [1967Sum].

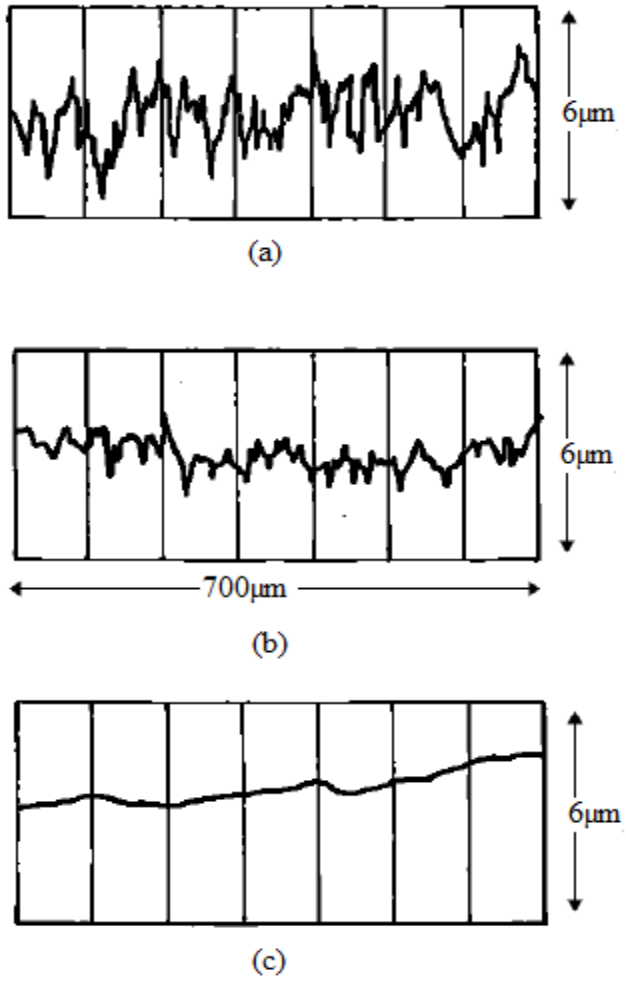

Figure 2.25. Surface roughness profile of surfaces 316 stainless steel specimens: (a) ground finish, (b) turned finish, and (c) electropolished finish [1979War, 1983War].

It is evident that small defects present on the surface of specimens and engineering components in the form of corrosion pits [1979Jou], flaws[1975Mai, 1982Ish] and inclusions [1966Yok, 1981Kun] can significantly reduce high-cycle fatigue strength of

stainless steels. The initiation and subsequent growth of short fatigue cracks (depth 100 μm) may be faster than those of macrocracks [1981Hud].

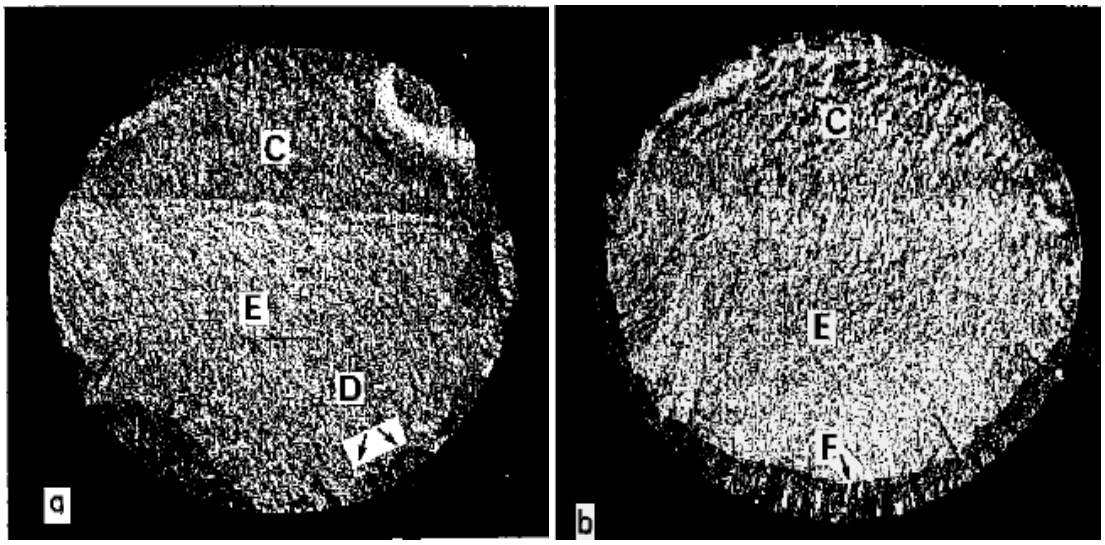

Figure 2.26. Fracture surface of Type 316 stainless steel fatigue specimens tested at 400°C and 25ºC, showing the differences in effect of surface finish on crack initiation and propagation: (a) discrete crack initiation and growth, D, in electropolished specimen, and (b) Circumferential crack initiation and growth, F, from machining marks in the as-ground specimens. Areas of fatigue crack growth and final tensile failure at 25ºC are regions E and C [1983War].

2.7.3.2. Fatigue Crack Propagation

Fatigue crack propagation can be divided into three distinct stages: stage I (short cracks), stage II (long cracks) and stage III (final fracture) [1981Tom, 1983War].

In stage I, the nucleated and initiated cracks propagate along high shear stress planes (45º). The crack propagates until it is decelerated by a microstructural barrier, such as a grain boundary, inclusions, or some pearlitic zones, which cannot accommodate the initial crack growth direction [1981Tom, 1983War]. Therefore, grain refinement is capable of increasing fatigue strength by the insertion of a large quantity of microstructural barriers, i.e. grain boundaries, which have to be overcome in stage I of propagation. Surface mechanical treatments, such as shot-peening and surface rolling, contribute to the increase in the number of microstructural barriers per unit length, due to

the flattening of the grains. Observations of crack tip deformation during crack advance in low-stress and high-strain fatigue revealed that crack extension occurred by sliding off at the inner edge of the crack tip flow bands during the tensile strain increment [1969Tom, 1972Lan, 1983War].

In stage II, when the stress intensity factor K increases as a consequence of crack growth or higher applied loads, slip start to develop in different planes close to the crack tip. While stage I is orientated 45º in relation to the applied load, propagation in stage II is perpendicular to the load direction. An important characteristic of stage II is the presence of surface ripples known as "striations," which are visible with the aid of a scanning electron microscope. Not all engineering materials exhibit striations. They are clearly seen in pure metals and many ductile alloys. In steels, they are frequently observed in cold-worked alloys. The most accepted mechanism for the formation of striations on the fatigue fracture surface of ductile metals is the successive blunting and re-sharpening of the crack tip [1999Rit].

Stage III is related to unstable crack growth as K_{max} approaches K_{IC}. At this stage, crack growth is controlled by static modes of failure and is very sensitive to the microstructure, load ratio, and stress state (plane stress or plane strain loading). Generally crack growth changes from microstructurally sensitive to microstructurally insensitive when the reversed plastic zone size approaches the structural parameter size (usually the grain size) of the material. Macroscopically, the fatigue fracture surface can be divided into two distinct regions, as shown in Figure 2.27 [URLMat]. The first region corresponds to the stable fatigue crack growth and presents a smooth aspect due to the friction between the crack wave faces. Sometimes, concentric marks known as "beach marks" can be seen on the fatigue fracture surface, as a result of successive arrests or decrease in the rate of fatigue crack growth due to a temporary load drop, or due to an overload that introduces a compressive residual stress field ahead of the crack tip. The other region corresponds to the final fracture and presents a fibrous and irregular aspect. In this region, the fracture can be either brittle or ductile, depending on the mechanical properties of the material, dimensions of the part, and loading conditions. The exact fraction of area of each region depends on the applied load level. High applied loads result in a small stable crack

propagation area as depicted in Figure. 2.7a. When lower loads are applied, the crack will have to grow longer before the applied stress intensity factor K, reaches the fracture toughness value of the material, resulting in a smaller area of fast fracture, as shown in Figure 2.27b.

Another macroscopic feature that can be observed in fatigue fractured surfaces are the ratcheting marks. These marks originate when many cracks, nucleated at different points, join together, creating steps on the fracture surface [1996ASM]. Therefore, counting the number of ratchet marks is a good indication of the number of nucleation sites.

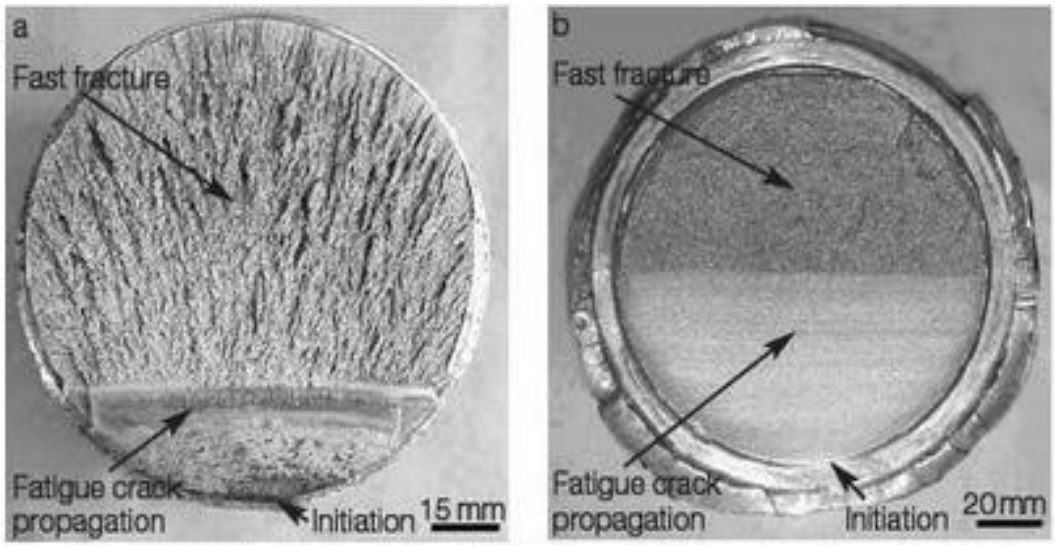

Figure 2.27. Fatigue fracture surface: (a) high applied load, (b) low applied load [URLMat].

2.7.4. Effect of carburising on fatigue strength of AISI 316L stainless steels.

There is a direct relationship between carburising treatment and fatigue strength of materials [1999Gen]. The relative case depth (ratio of the case depth to specimen diameter), which is affected by section size of the material, influences the fatigue performance of case hardened structures. Theoretical and experimental methods have revealed that increasing case depth can improve fatigue strength of carburised steels [1974Lut, 1975The, 1983Mit]. However, improvement in fatigue strength due to case depth is limited [1991Pre]. Deep cases with decreased compressive residual stresses at the surface can cause decreased fatigue strength in the steel. Deep cases do not guarantee

improved fatigue resistance due to the possibility of pitting fatigue and case-crushing (also known as deep-spalling occur due to shear stresses). If the maximum shear stress-to-shear yield strength ratio exceeds 0.55, deep-spalling failure would eventually occur [1961Ped]) [1999Gen]. In order to obtain optimum fatigue strength as a result of case depth, the ratio of the case depth to the specimen diameter should be considered [1966Daw, 1975The]. The relative case area (ratio of case area to the core area) is also a factor that enhances the fatigue performance of carburised steel. The change in fatigue strength due to the effect of relative case depth and case area on carburised AISI 8620 steel is shown in Figure 2.28. At high values of relative case depths and case areas, there is an enhancement in fatigue life. This is due to higher fatigue resistance and the geometrical interdependence of case depth and case area [1999Gen].

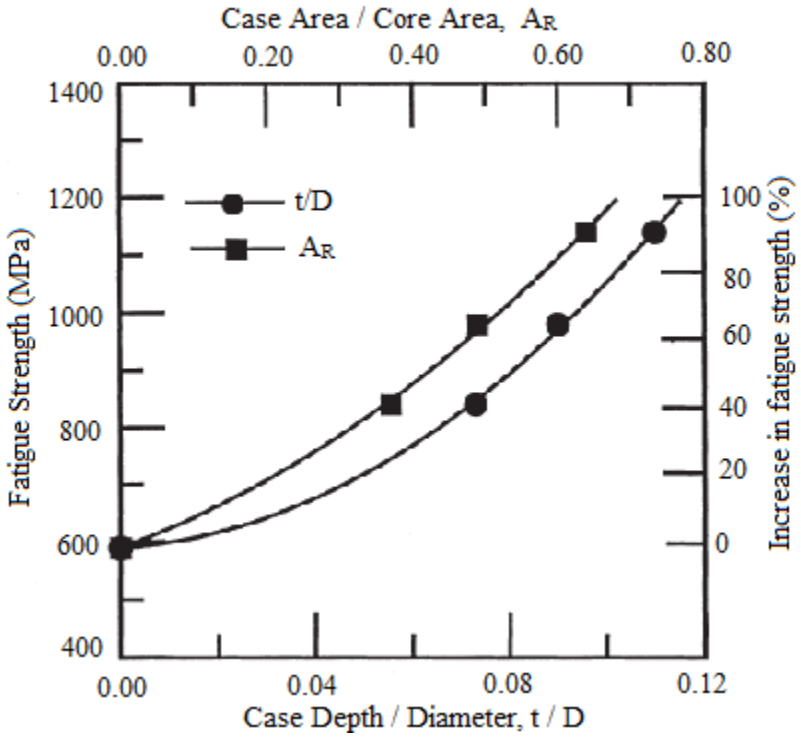

Figure 2.28. Effect of relative case depth and area on the fatigue strength of carburised AISI 8620 steel [1999Gen].

Ceschini *et al.* [2008Ces] showed that AISI 316L stainless steel carburised at low temperatures had both the fatigue strength and the surface hardness improved. There was 40% improvement. The appreciable increase was attributed to high strength in the

carburised case and the high compressive residual stresses induced by the carburising heat treatment [2004Tok, 2006Aki, 2008Ces]. The fatigue strength of the carburised case increased more than the core material, hence crack nucleation and initiation was found at the interface between the carburised case (hardened layer due to carbon diffusion) and the core [2004Tok].

Physical vapour deposition (PVD) hard coatings using TiN [2001Ber, 2004Puc] and ZrN [2004Ber] on the surface of AISI 316L stainless steels also enhanced fatigue strength. Coating thicknesses of approximately 3-3.6µm for TiN [2001Ber], 1.4µm for TiN [2004Puc] and 1.3-2.6µm for ZrN [2004Ber] on the surface of AISI 316L stainless steel were studied. The improved fatigue resistance was perceived as due to the high mechanical strength of the coating to the substrate, the presence of compressive residual stresses within the coating and the excellent adhesion of the coating to the substrate [2001Ber, 2004Puc]. The presence of high compressive residual stresses contributed to the arrest of crack propagation within the coating [2001Ber, 2004Ber, 2004Puc]. Under low alternating stresses, crack nucleation started from the coating [2001Ber, 2004Ber, 2004Puc] and was attributed to the micro-columnar grain structure. Delamination or debonding of coating from the substrate occurred under high applied stresses, which served as site for fatigue cracks.

In summary, the hardening mechanism is attributed to the high compressive residual stresses arising from lattice distortions, which enhance the fatigue strength of the steel. These distortions are as a result of the surface treatment techniques used. Depending on the treatment type, the corrosion resistance of the material may or may not be adversely affected.

CHAPTER THREE

EXPERIMENTAL PROCEDURE

"Theory guides, experiment decides.'

— Izaak Maurits Kolthoff

3. EXPERIMENTAL PROCEDURE

3.1. MATERIALS AND MANUFACTURE OF SPECIMENS

Rods and plates of AISI 316L austenitic stainless steel in the as-rolled condition were purchased from Ultra-Vision, Johannesburg. The tensile specimens were machined with dimensions and tolerances according to ASTM E 8, a standard test method for tension testing of metallic materials, as shown in Figure 3.1.

Fatigue specimens with continuous curvature were machined with dimensions and tolerance of 0.1 shown in Figure 3.2. The specimens were machined with a continuous radius (hour glass).

The standard Charpy impact test specimen according ASTM A370 standard specimen configuration consist of a bar of metal, 55x10x10mm having a notch machined across one of the larger dimensions. The V-notch, 2mm deep, with 45° angle and 0.25 mm radius along the base, is shown in Figure 3.3.

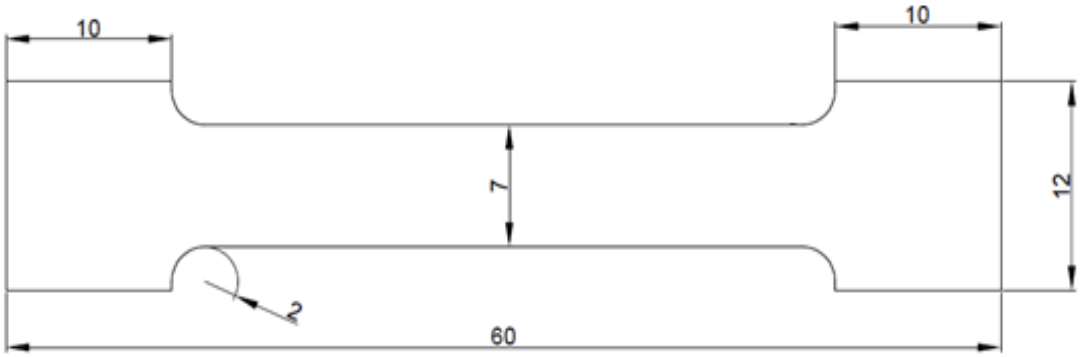

Figure 3.1. Tensile testing specimen.

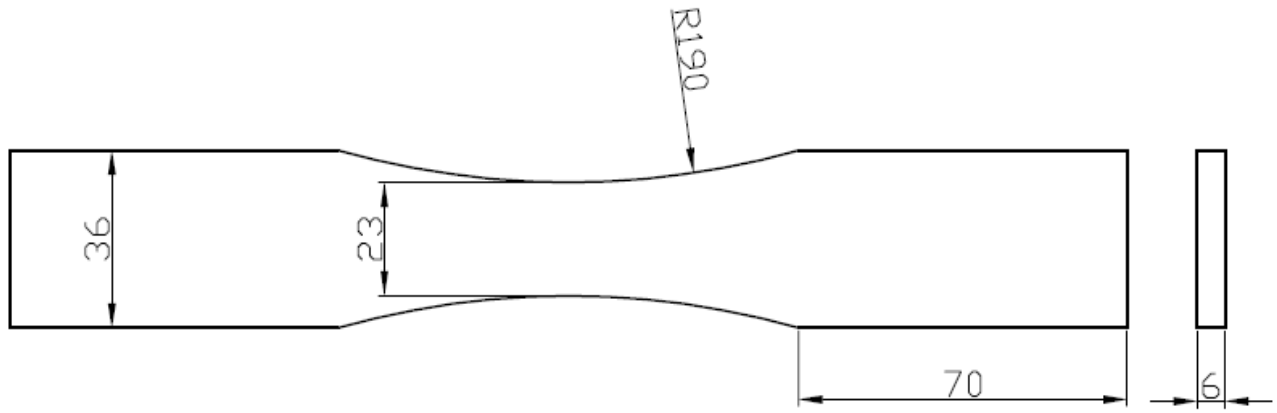

Figure 3.2. Fatigue testing specimen.

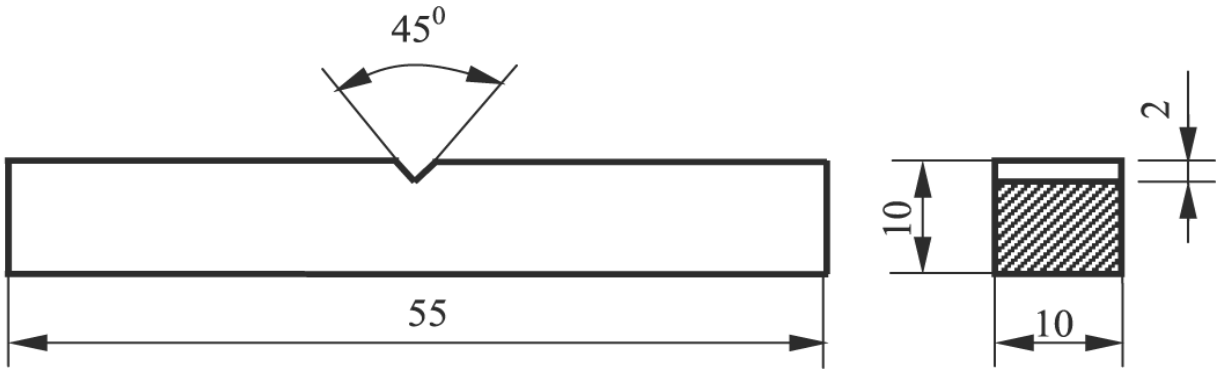

Figure 3.3. Charpy impact test specimen.

3.2. CARBURISING HEAT TREATMENT

A carburising case with lid of dimensions 145x80x80mm was designed and manufactured from mild steel for the carburising heat treatment. Tensile, Charpy impact and fatigue specimens were pack carburised with 60% $BaCO_3$, 30% activated charcoal and 10% NaCl. The carburising heat treatment was carried out in a Lenton muffle furnace at 450ºC, 550ºC, 650ºC, 700ºC and 750ºC for 24 hours, followed by furnace cooling. The Charpy impact specimens were carburised after the notches were cut.

3.3. MECHANICAL TESTS

3.3.1. Tensile testing

Tensile tests of the carburised and as-received specimens were performed using a Tinius Olsen tensile testing machine under a uniaxial load. The stress-strain graphs were plotted with the QMAT installed software. The load at fracture for each specimen was recorded, as well as the diameter at the point of fracture and the final gauge length. Each initial diameter and gauge length was recorded before the application of the load. From the data generated, the ultimate tensile strength, percentage elongation and percentage reduction in area of each sample were calculated. The tests were conducted on three test samples and the mean values were used to estimate the properties.

3.3.2. Fatigue testing

Fatigue tests were performed on the carburised and as-received AISI 316L stainless steel using an "Instron 1342" fatigue testing machine at the Advanced Materials Division, Mintek. The testing was performed in duplicate and at a peak stress of 500MPa with a stress ratio (R) of 0.1 and a frequency of 7Hz.

3.3.3. Charpy impact testing

Charpy impact tests measure the energy absorbed by a standard notched specimen while breaking under an impact load. It is a quality control method used to determine notch sensitivity and impact toughness of engineering materials. It consists of striking specimen machined according to ASTM A370 with a hammer on a pendulum arc, while the specimen is held securely at each end. The hammer strikes opposite the notch. The energy absorbed by the specimen is determined by measuring the decrease in motion of the pendulum arm. The Charpy impact tests were performed on the as-received and carburised samples. The tests were conducted on three test samples and the mean values were used to estimate the properties.

3.3.4. Hardness Test

Hardness measurements on both as-received and carburised specimens were taken from the surface to the core of the specimen. This was done by a Vickers hardness tester using a 500g load and a dwell time of 10s. Graphs of hardness-distance from the surface to the core were plotted to ascertain the effect of carburising heat treatment on surface hardness of the AISI 316L austenitic stainless steel.

3.3.4.1. Correlation between Hardness and Yield Strength

Hardness is the resistance of a material to plastic deformation, and also sometimes an indication of resistance to abrasion. The hardness number is not a true property but rather an empirical value. This empirical value is based on the hardness scale used and its associated experimental methods. A correlation of hardness number and the yield strength of the materials can be estimated from Equation 3.1 [1962McL, URLHar]:

$$\sigma_y = k \times H_v \qquad \text{Equation 3.1}$$

where:

σ_y= yield strength (MPa),
k = constant determined by geometrical factors usually between 2 and 4,
H_v= Vickers hardness number (MPa).

From experiments, Vickers hardness is normally in kg/mm^2 and unit kilogram per millimetre square is equivalent to 9.807MPa. Including the relevant geometrical factors, Equation 3.1 becomes:

$$For\ H_v \leq 175MPa:\ \sigma_y = 3.55 \times H_v \qquad \text{Equation 3.2}$$

$$For\ H_v > 175MPa:\ \sigma_y = 3.38 \times H_v \qquad \text{Equation 3.3}$$

3.4. METALLOGRAPHIC PREPARATION

Cut sections of tested tensile and fatigue samples were prepared for metallographic examination. Water jet cutting was used for the cutting of the specimens so as not to

damage the microstructures of the samples. Pre-grinding of samples was carried out with a 220-grit SiC paper. Initial grinding was carried out with a stable diamond suspension containing lubricants (DiaPro Allegro/Largo) on an MD-Largo magnetic disc on the automated grinding and polishing machine. The surface was ground down to 9 µm. The final grinding process was carried out using a DiaPro Dac suspension on an MD-Dac magnetic disc with a surface finish of about 3µm. The final grinding was followed by a final polishing done with the MD-Chem disc with a surface finish of about 0.14 µm. A colloidal silica suspension (OP-S) was the lubricant used for the final polishing. Chemical etching was carried on all specimens with 15mL HCl, 10mL HNO_3 and 10mL CH_3COOH. The polished surfaces were swabbed with the etchant for about 8 minutes. Alcohol and water were used to clean and rinse the etchant from the surface.

3.5. OPTICAL MICROSCOPY

A Leica DM 6000M optical microscope was used to observe microstructures of the as-received and carburised specimens. Micrographs were obtained at low magnifications of up to 100X.

3.6. SCANNING ELECTRON MICROSCOPY

The microstructures of the as-received and carburised samples were examined with an FEI Nova NanoSEM 200 with an operating voltage of 20kV and a working distance of approximately 7mm for imaging. All micrographs were taken in both secondary electron (SE) mode where high-resolution imaging is influenced by surface morphology and backscattered electron (BSE) mode, by which image contrast is achieved as a function of elemental composition and surface morphology, so that phases with lower average atomic numbers could be identified by their darker contrasts than those with higher average atomic number.

Specific areas of interest and the composition of the as-received and carburised samples were analysed using the energy dispersive X-ray analysis (EDX) detector on the FE1 Nova NanoSEM. The elemental compositions were recorded and discussed.

CHAPTER FOUR

RESULTS

"If you want something new, you have to stop doing something old"

— Peter Ferdinand Drucker

4. RESULTS

4.1. CHEMICAL ANALYSIS

The chemical constituents of the as-received sample were analysed using the spark analysis for the elemental composition as shown Table 4.1.

Table 4.1. Chemical composition of AISI 316L austenitic stainless steel.

Elements	Percentage composition
C	0.0253
Si	0.4240
Mn	1.0000
P	0.0319
S	0.0311
Cr	17.1200
Mo	2.1100
Ni	10.1300
Cu	0.4490
Co	0.1360
Nb	0.0364
N	0.0564
Fe	68.2000
Trace elements	0.2457

4.2. MECHANICAL TESTS

4.2.1. Tensile tests

The effect of the temperature of carburising on the tensile strength and the ductility of carburised and as-received AISI 316L stainless steel is shown in Figures 4.1 and 4.2. The tensile strength was the same for carburising done at 450°C and 550°C, and within the errors (Figure 4.1). At higher carburising temperatures (650°C-750°C), the tensile strength decreased more strongly.

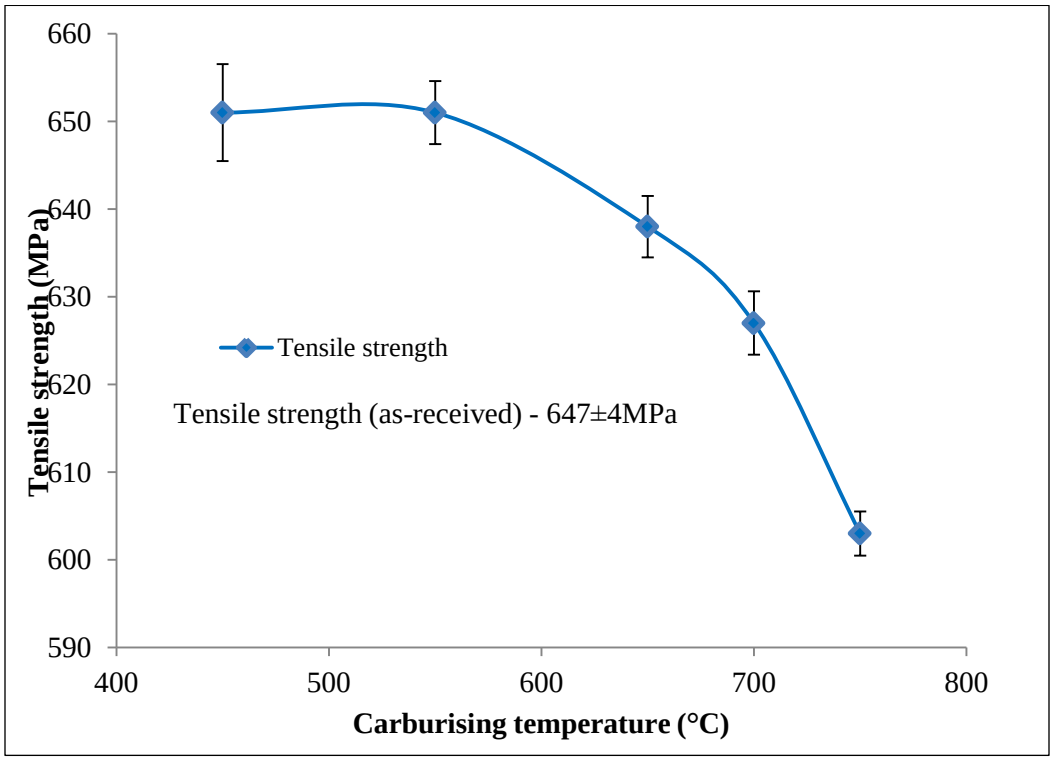

Figure 4.1. Effect of carburising temperature on the tensile strength of AISI 316L stainless steel.

Ductility, quantitatively measured by elongation (%) and reduction in area (%), is shown in Figure 4.2. The elongation decreased moderately with increasing temperature to about 650°C. However above 650°C, the elongation decreased more strongly (Figure 4.2). Although reduction in area decreased with increasing temperature, it decreased more quickly than percentage elongation.

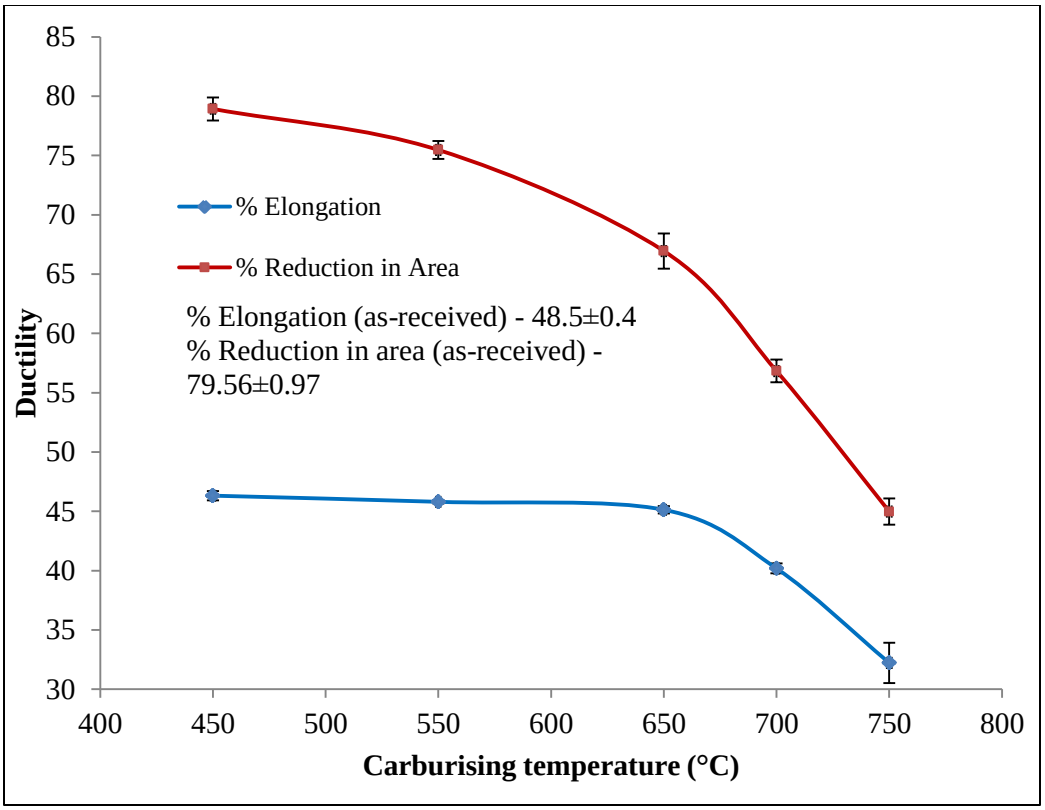

Figure 4.2. Effect of carburising temperature on the ductility of AISI 316L stainless steel.

4.2.2. Hardness tests

The micro-hardness values recorded for the as-received material were between 255±2$HV_{0.5}$ and 248±2 $HV_{0.5}$. The steel carburised at 450°C and 550°C showed only a small difference between the surface and the inside hardness values with much local variation, as shown in Figure 4.3. It was also found that some of the carburising compound was left in the case. Thus, the carburising was not properly effected at these temperatures. However, all samples, including the as-received samples, had slightly higher hardness values at the surface.

Figure 4.4 shows that hardness was higher at the surface, in samples of the carburising temperatures: 650°C, 700°C and 750°C. This is the classic hardness profile, with the hardness being related to the amount of carbon that had diffused inwards.

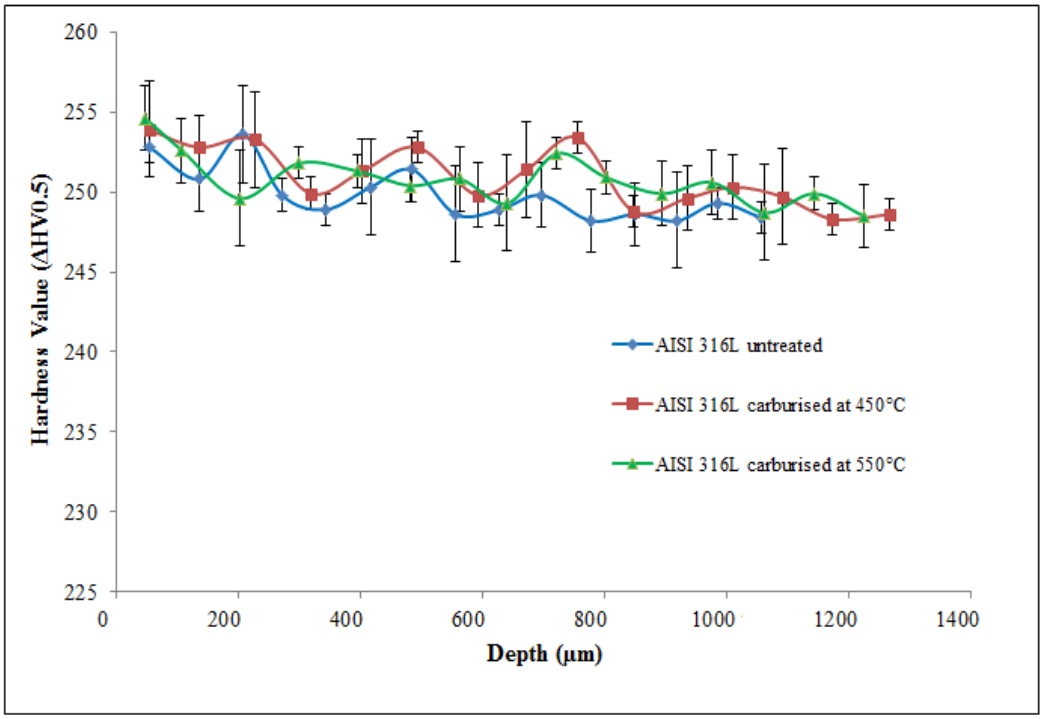

Figure 4.3. Effect of carburising on the hardness of as-received AISI 316L steels and samples treated at 450°C and 550°C.

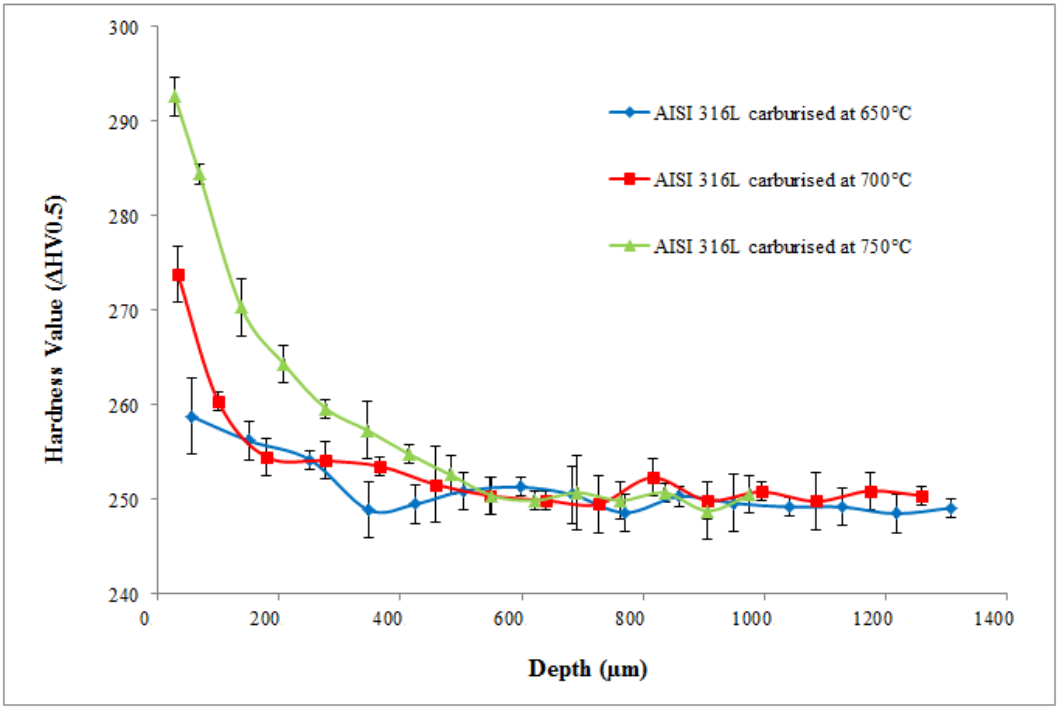

Figure 4.4. Effect of carburising on the hardness of samples of AISI 316L steel carburised at 650°C, 700°C and 750°C.

4.2.3. Impact tests

The impact energy of the as-received AISI 316L stainless steel was 272±2J. After carburising from 450°C-750°C, the impact energies decreased with increasing temperature, as shown in Figure 4.5.

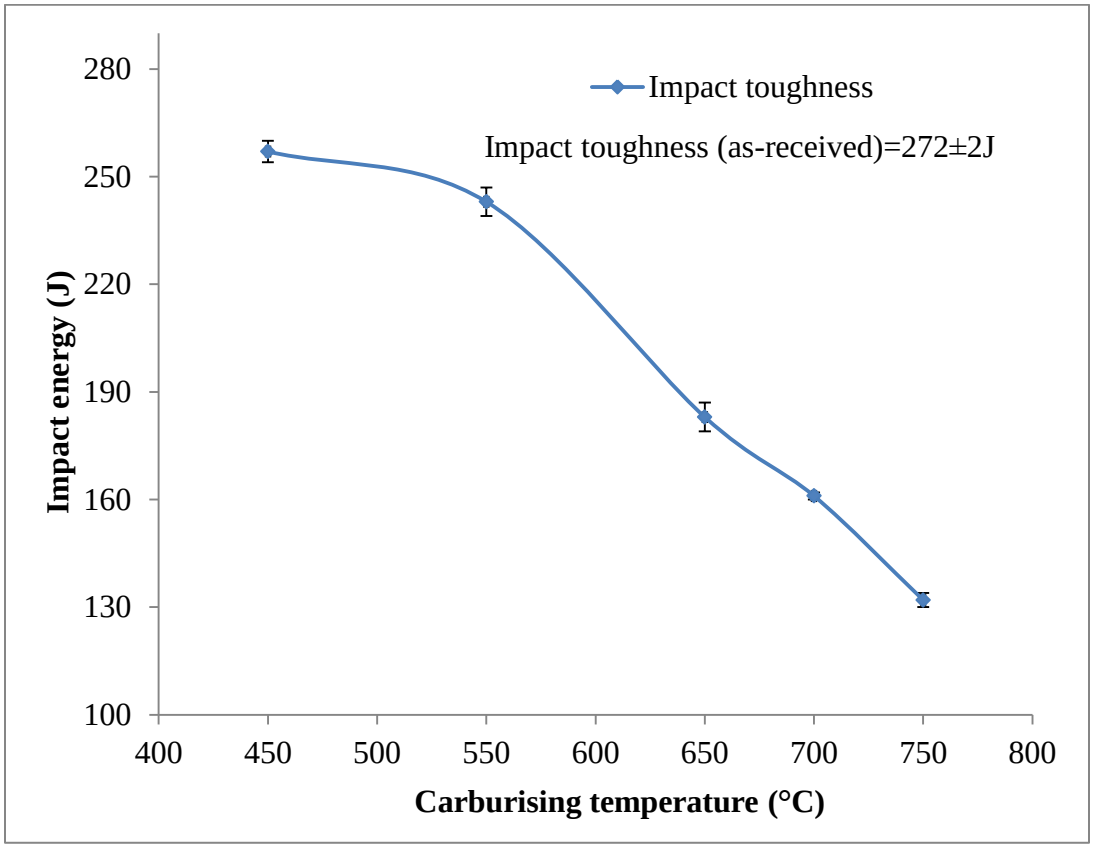

Figure 4.5. Effect of carburising on the impact toughness of AISI 316L stainless steel.

4.2.4. Fatigue tests

The number of cycles to failure (n) of the as-received AISI 316L steel was 59298±2520. Samples carburised at 450ºC to 650ºC showed similar values, which ranged from 51819±5257 to 61455±15076. However, a significant reduction in number of cycles to failure (fatigue strength) was observed for samples carburised at 700ºC (25387±595) and 750ºC (7146±318) as shown in Figure 4.6. For high carburising temperatures (700ºC-

750ºC), the fatigue strength decreased resulting in the low number of cycles to failure. Detailed results with the fatigue parameters are shown in Table 4.2.

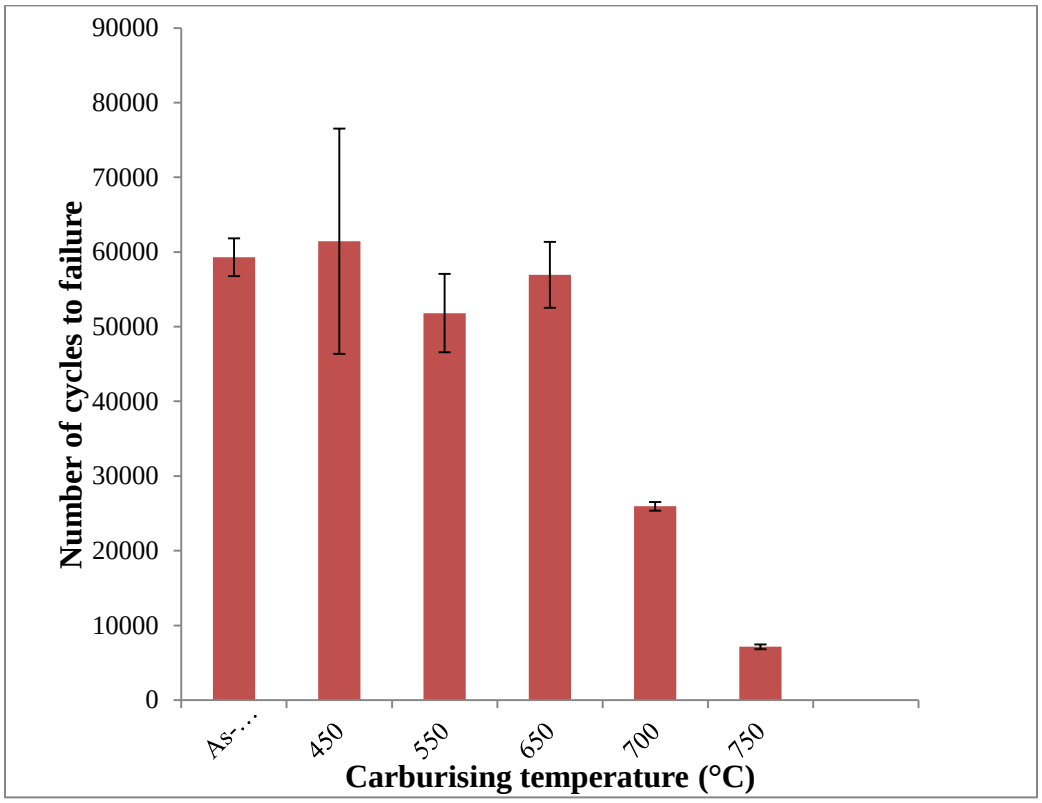

Figure 4.6. Effect of carburising temperature on the fatigue performance of AISI 316L steel.

Table 4.2. Experimental data for fatigue testing of as-received and carburised AISI 316L stainless steel.

Carburising temperature	Designation	Area	Max load	Min load	Cycles to failure
(ºC)		(mm)	(N)	(N)	(n)
As-received	A1	137.8	68900	6890	57110
	A2	141.5	70745	7075	62053
	A3	137.9	68925	6895	58731
	Mean				**59298**
	Deviation				**2520**
450ºC	B1	141.1	70525	7053	50794
	B2	138.9	69465	6947	72115
	Mean				**61455**
	Deviation				**15076**
550ºC	C1	141.2	70585	7059	55536
	C2	141.3	70625	7063	48101
	Mean				**51819**
	Deviation				**5257**
650ºC	D1	139.3	69650	6965	53836
	D2	141.1	70545	7055	60057
	Mean				**56947**
	Deviation				**4399**
700ºC	E1	142.1	71025	7103	24966
	E2	143.5	71745	7175	25807
	Mean				**25387**
	Deviation				**595**
750ºC	F1	140.9	70440	7044	6921
	F2	144.6	72285	7229	7371
	Mean				**7146**
	Deviation				**318**

4.3. MICROSCOPY

4.3.1. Optical microscopy

Figures 4.7 and 4.8 showed the microstructures of the as-received AISI 316L steel. The micrographs showed the austenite grains, slip lines and a few twin boundaries close to the surface (Figure 4.8). There were some dark spots dispersed in the structure. Carburising done at 450°C showed no carburising case (Figures 4.10 and 4.23).

The micrographs of AISI 316L steel carburised at 450°C are shown in Figures 4.9 and 4.10. Figure 4.9 showed the microstructure of the core of the steel with austenite grains with well-defined grain boundaries, few annealing twins and slip lines. Fine carbides were seen within the austenite grains.

The micrographs of AISI 316L steel carburised at 550°C are shown in Figures 4.11 and 4.12. The core of the carburised steel (Figure 4.11) showed distinct austenite grains and boundaries, fairly well distributed annealing twins within the structure, slip lines and fine carbides within the grains and at the grain boundaries. There were no large differences in the grain size distribution within the microstructures of both carburised and as-received samples hence the grain sizes were not measured.

The surface/core microstructure as shown in Figure 4.10 indicated the presence of distinct austenite grains, more annealing twins, slip lines and a few fine carbides compared to the as-received sample (Figure 4.8).

The surface and core of carburised steel at 550°C (Figure 4.12) indicated the austenite grains, well distributed annealing twins, slip lines and some fine carbides. The grains sizes were smaller compared to the as-received and samples carburised at 450°C. There was carburised case observed at this temperature.

The surface and core microstructures of samples carburised above 550°C are shown in Figures 4.13-4.18. Once again, there were austenite grains, annealing twins, slip lines and carbide precipitates which were more distinct. There were more annealing twins and carbides compared to samples treated at and below 550ºC. The carburised case for samples treated at 700ºC and 750ºC were measured as 35μm and 63.5μm respectively.

Figure 4.7. Micrograph of the core of as-received rolled AISI 316L steel.

Figure 4.8. Micrograph showing the surface of as-received rolled AISI 316L steel.

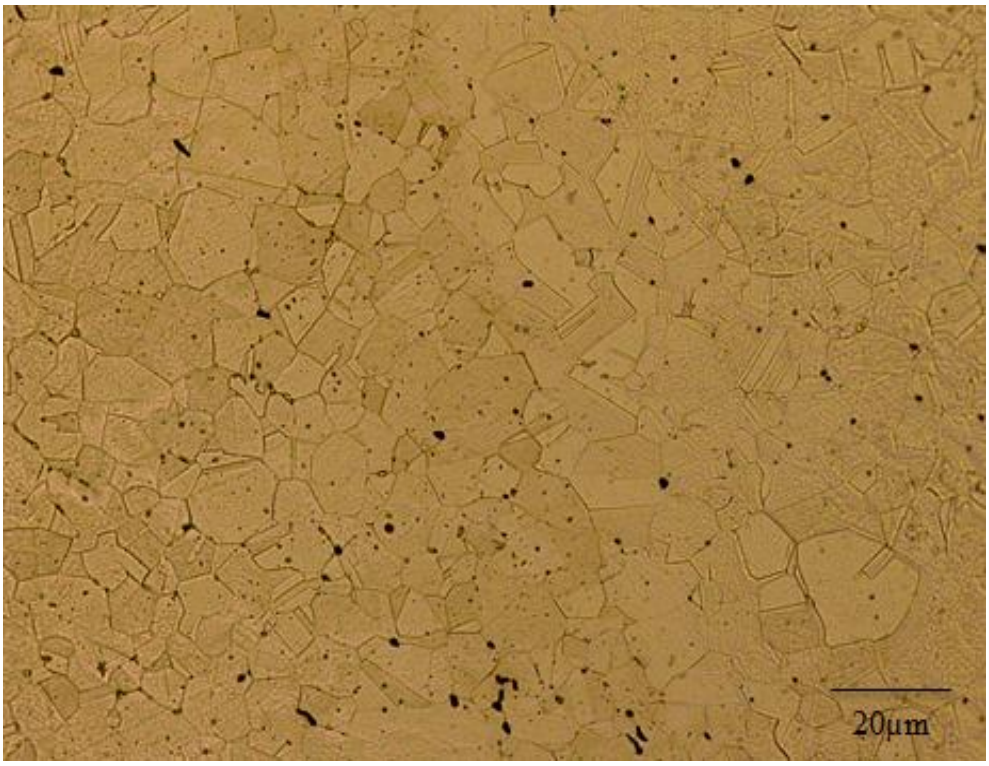

Figure 4.9. Micrograph of the core of AISI 316L steel carburised at 450°C.

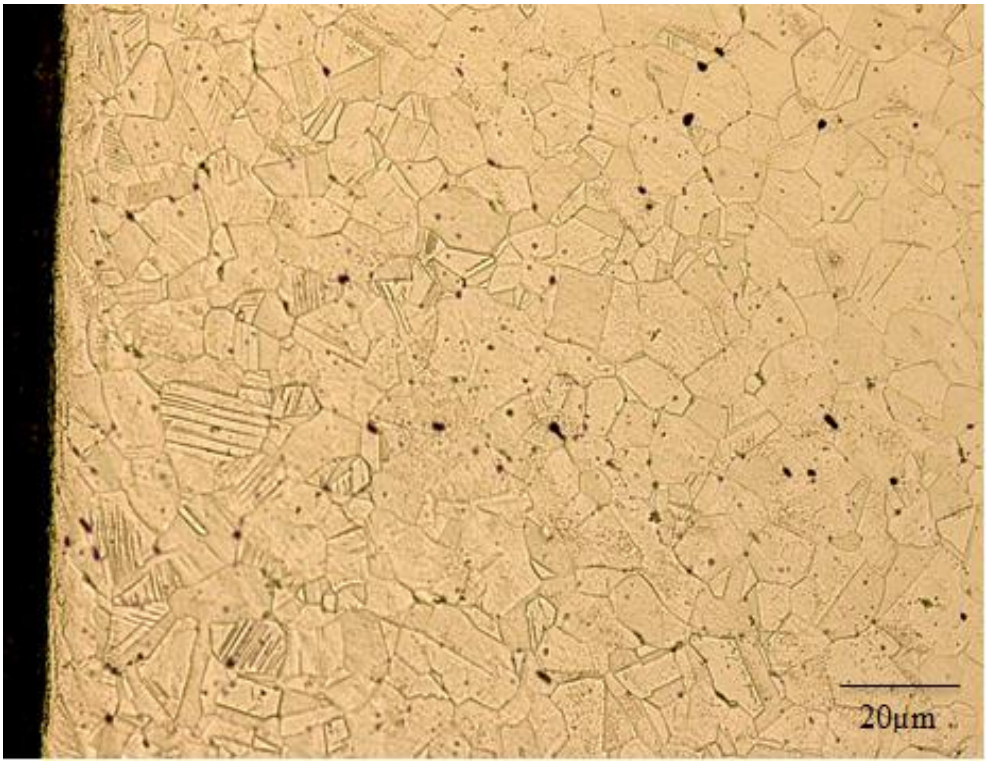

Figure 4.10. Micrograph showing the surface of AISI 316L steel carburised at 450°C.

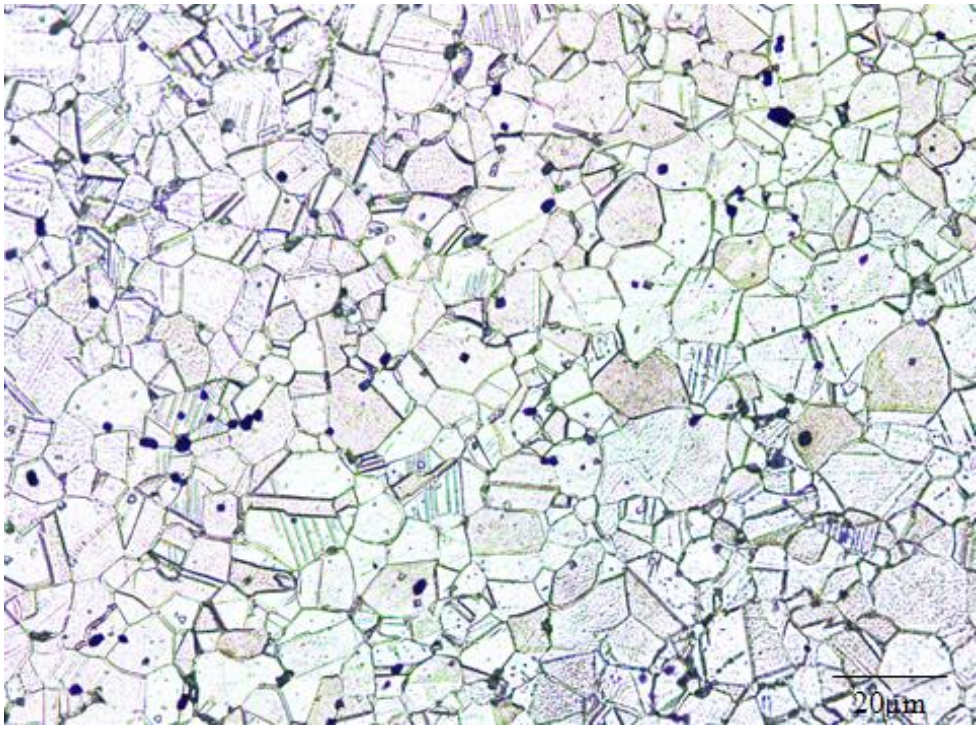

Figure 4.11. Micrograph of the core of AISI 316L steel carburised at 550°C.

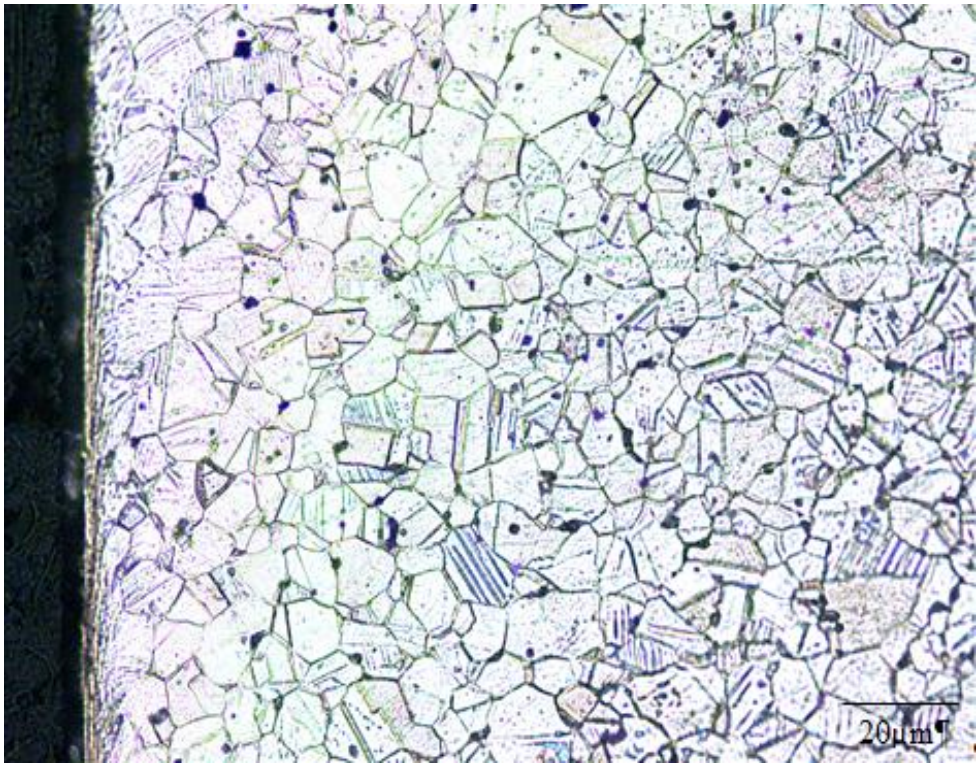

Figure 4.12. Micrograph showing the surface of AISI 316L steel carburised at 550°C.

Figure 4.13. Micrograph of the core of AISI 316L steel carburised at 650°C.

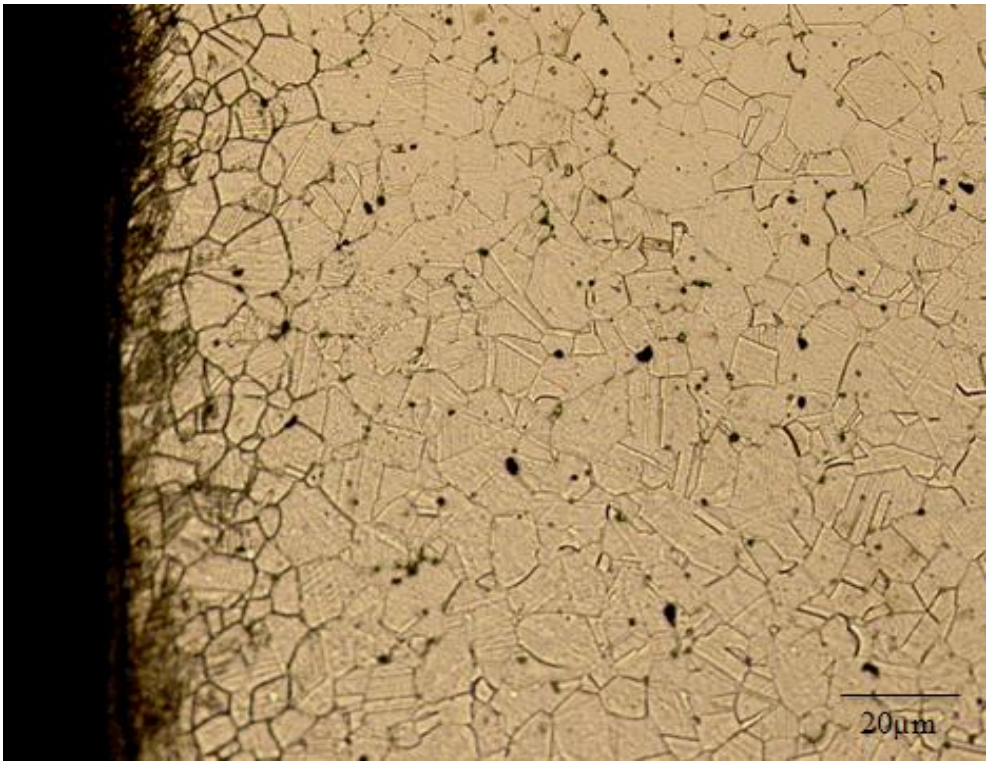

Figure 4.14. Micrograph showing the surface of AISI 316L steel carburised at 650°C.

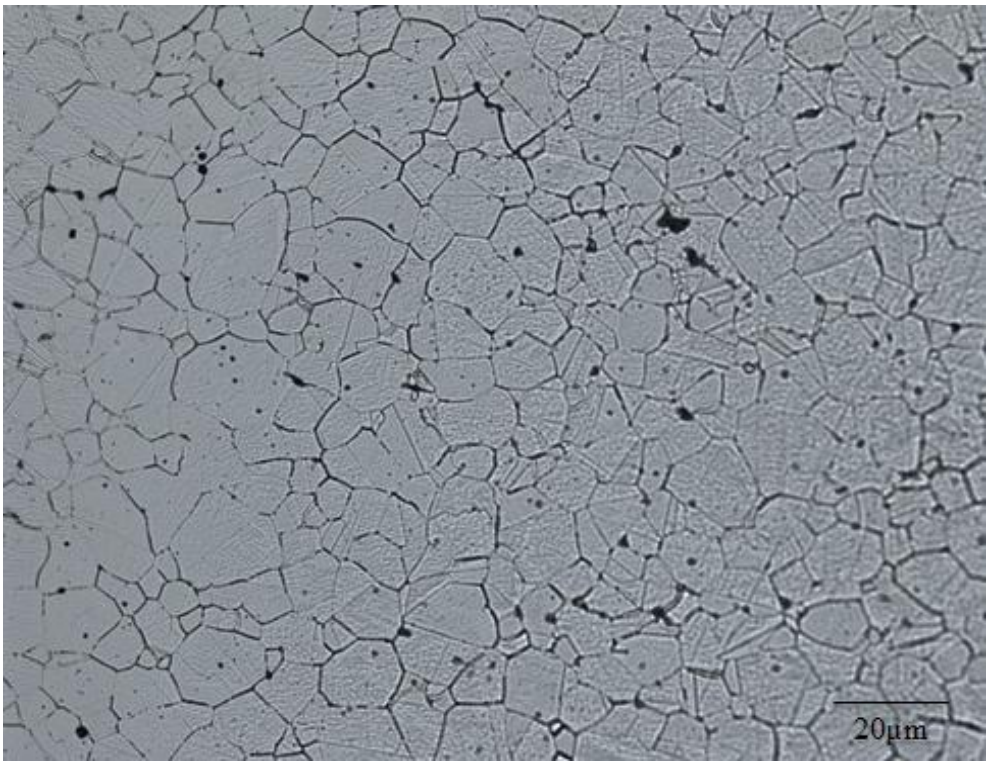

Figure 4.15. Micrograph of the core of AISI 316L steel carburised at 700°C.

Figure 4.16. Micrograph showing the surface of AISI 316L steel carburised at 700°C.

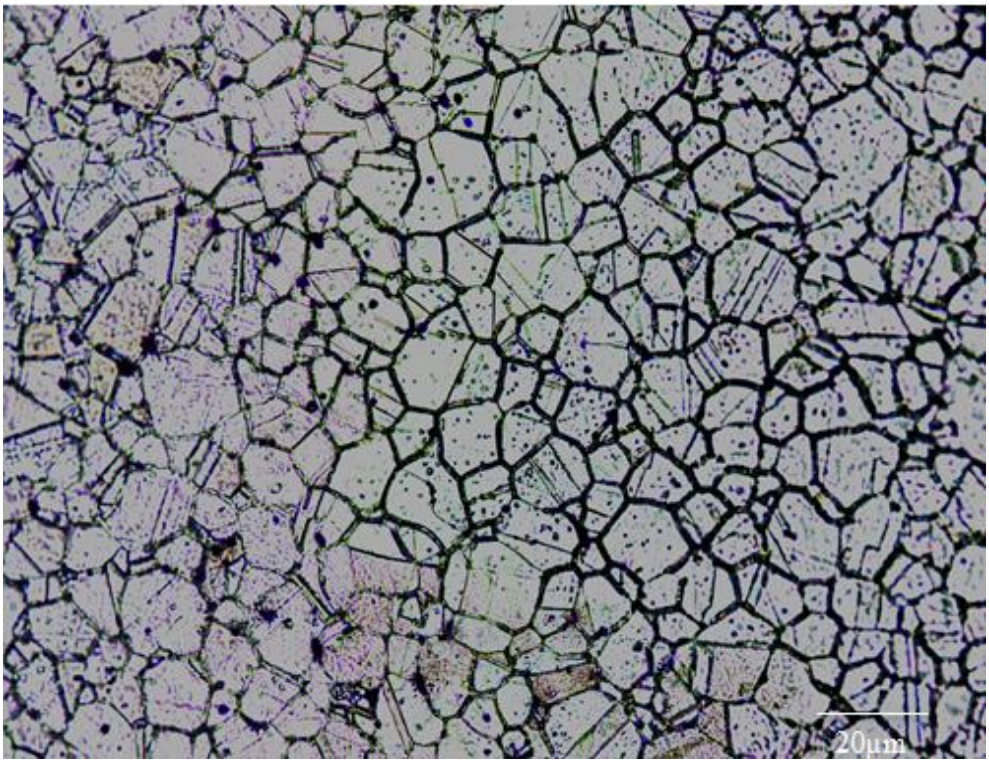

Figure 4.17. Micrograph of the core of AISI 316L steel carburised at 750°C.

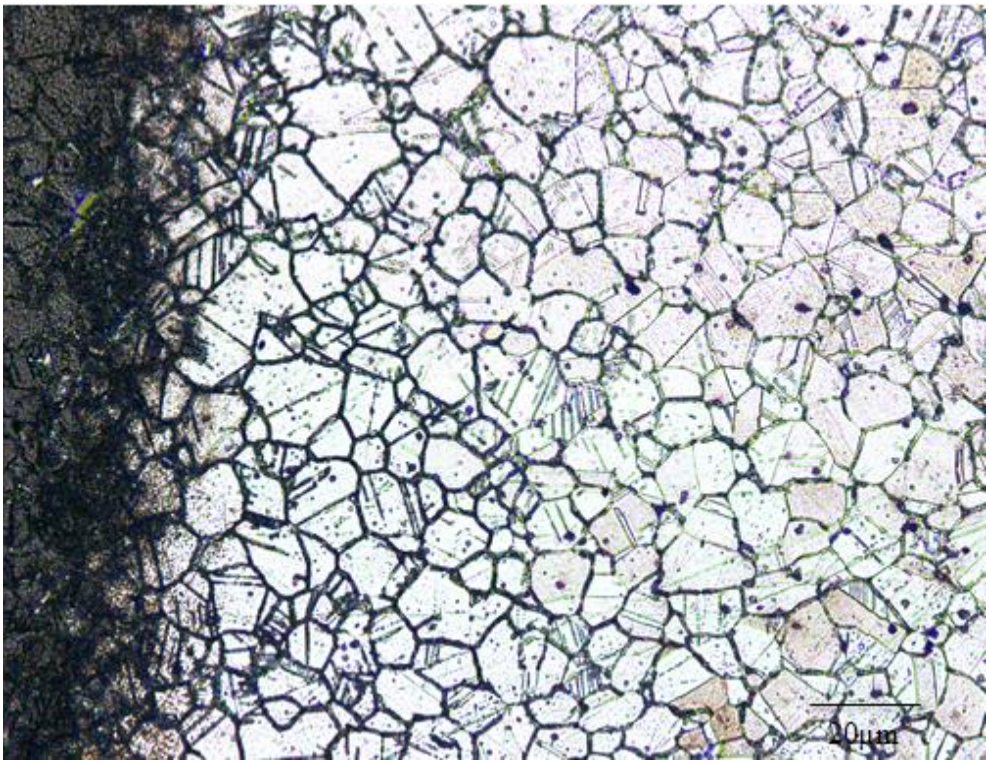

Figure 4.18. Micrograph showing the surface of AISI 316L steel carburised at 750°C.

4.3.2. SEM/EDX analysis of as-received and carburised samples

Microstructures of the core of the as-received samples taken in secondary electron (SE) and backscattered electron (BSE) modes are shown in Figure 4.19 (a) and (b). The micrographs indicated well-defined austenite grains, slip lines, annealing twins and porosity. The white spots were dust particles on the surface of the stainless steel.

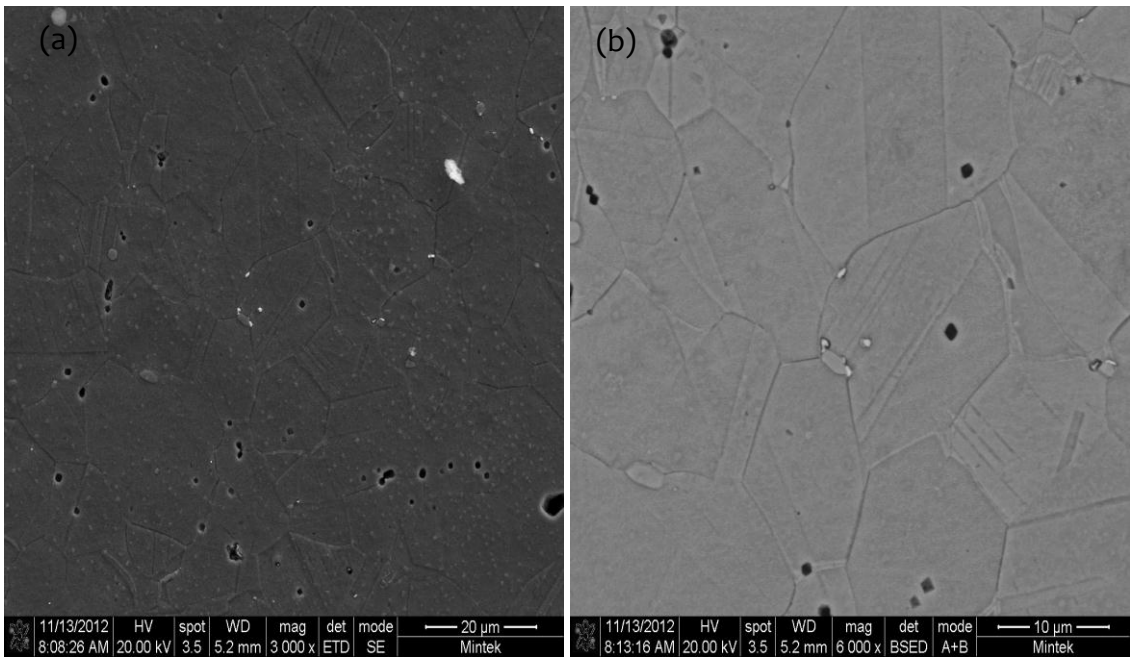

Figure 4.19. SEM images of the core of as-received AISI 316L steel: (a) secondary electron (SE), and (b) backscattered electron (BSE) modes.

Microstructures taken near the surface showed similar characteristics to those at the core, as expected. Figure 4.20 (a) and (b) showed the near surface microstructure of the as-received AISI 316L steel both in SE and BSE modes. Deformations of the surface of the as-received during the mechanical tests are indicated (Figure 4.20) and should not be mistaken for a case since these are as-received materials.

The energy dispersion spectrum analysis carried at both the core and near the surface showed similar characteristics with some amount of oxides present. Figures 4.21 and 4.22 showed the EDX analyses of both the core and near surface. There were more oxides at areas near the surface than to the core, (Tables 4.3 and 4.4). Barium oxide (BaO) and chromium oxide (Cr_2O_3) could be the some of the oxides present in the microstructures.

BaO is a white hygroscopic oxide formed by the decomposition of barium carbonates and salts [URLBar]. Barium carbonate served as the energizer for the carburising process hence decomposing it will give rise to barium oxides within the matrix of the AISI 316L steel. Other oxides could be present due to the presence of trace elements in the chemical analysis as shown in Table 4.1. In both cases, the EDX analysis did not show the presence of carbides.

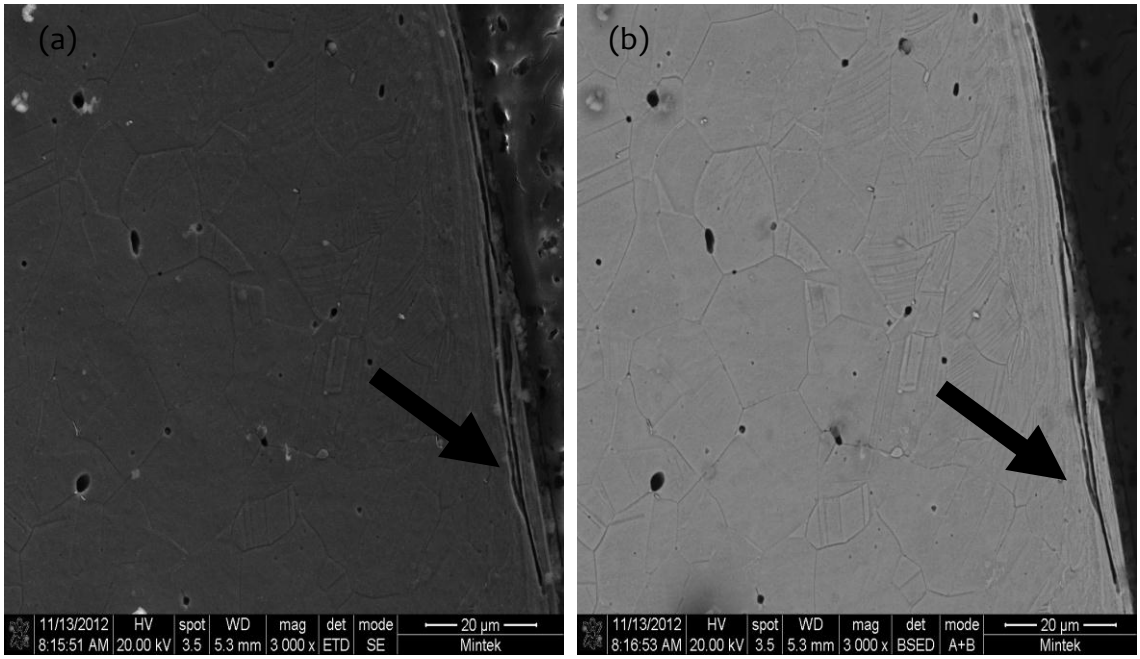

Figure 4.20. SEM images of the surface of as-received AISI 316L steel: (a) secondary electron (SE), and (b) backscattered electron (BSE) modes.

Microstructural characteristics of the core of samples carburised at 450°C and taken in secondary electron (SE) and backscattered electron (BSE) modes are shown in Figure 4.23 (a) and (b). The micrographs showed many pores within the structure.

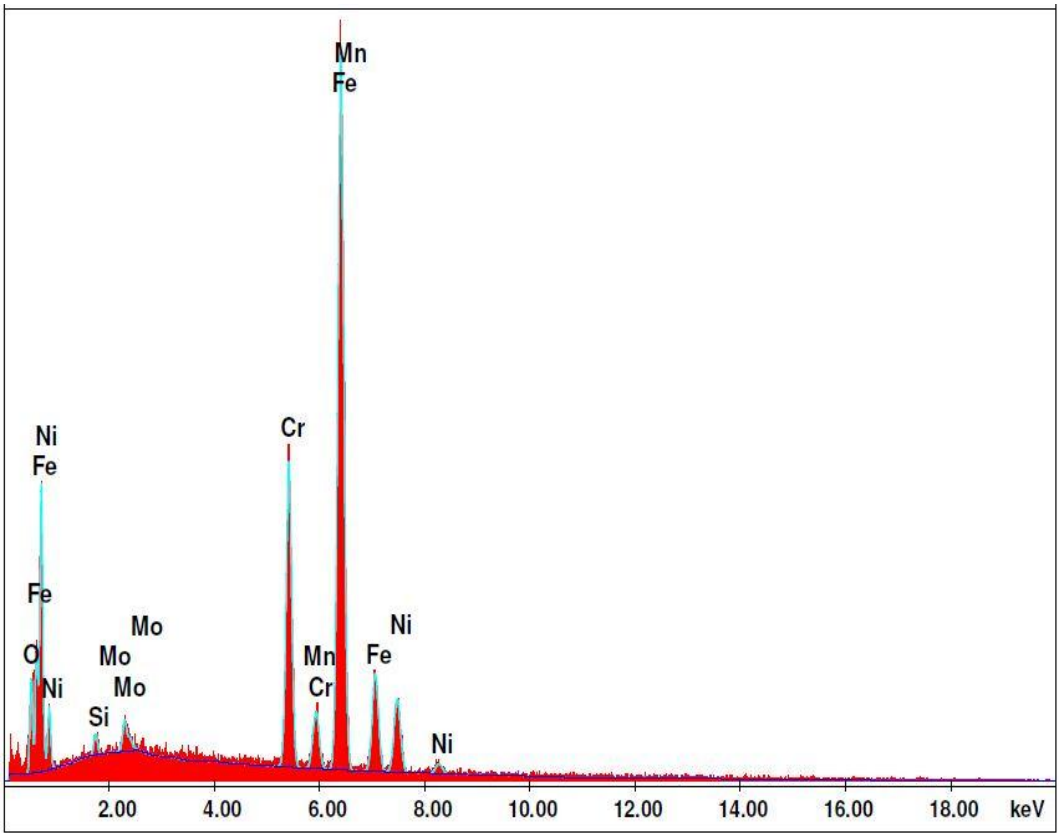

Figure 4.21. Analysis of the core of the as-received AISI 316L steel with EDX.

Table 4.3. EDX elemental compositions of the core of the as-received sample.

Element	Wt%	At%	Z	A	F
O K	3.0	9.6	1.1596	0.3952	1.0034
Si K	0.7	1.2	1.1087	0.4431	1.0016
Mo L	1.9	1.0	0.8945	0.8019	1.0017
Cr K	16.7	16.6	0.9912	0.9874	1.1525
Mn K	1.6	1.5	0.9741	0.9943	1.0107
Fe K	65.3	60.5	0.9933	0.9707	1.0140
Ni K	10.8	9.5	1.0106	0.9037	1.0000
Total	**100.0**	**100.0**			

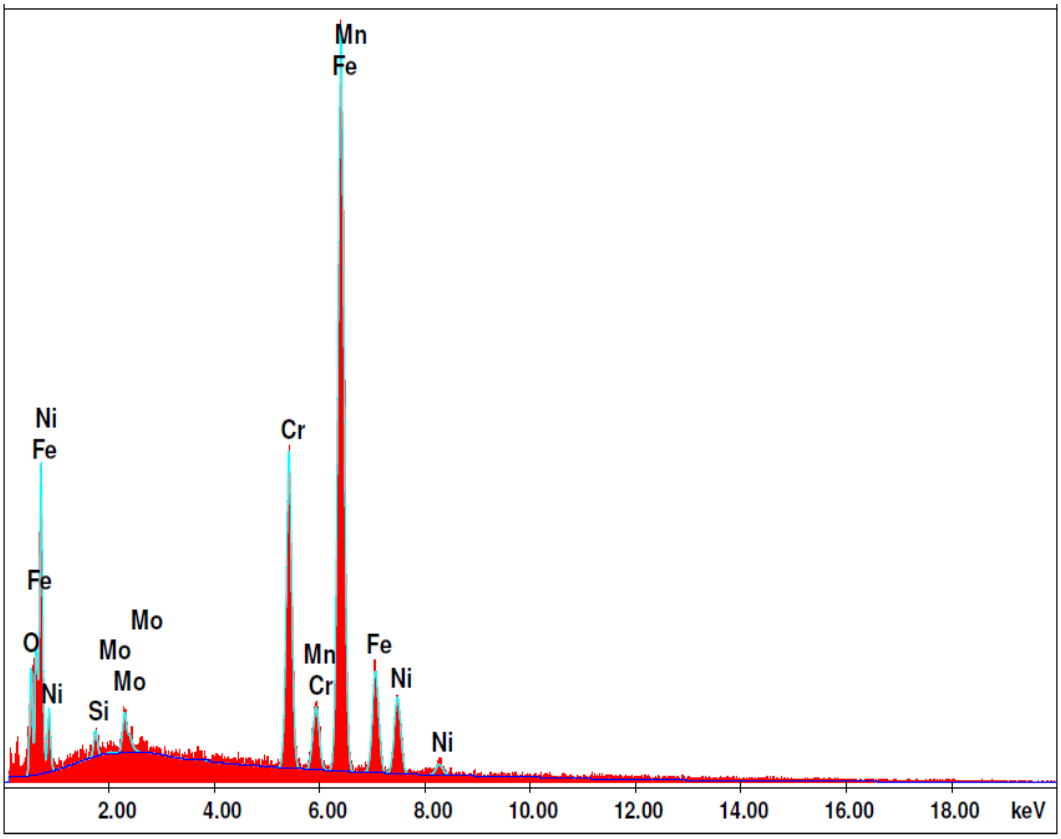

Figure 4.22. EDX analysis of the over near surface of the as-received AISI 316L.

Table 4.4. EDX elemental compositions of the surface of the as-received sample.

Element	Wt%	At%	Z	A	F
O K	3.2	10.3	1.1594	0.3903	1.0033
Si K	0.8	1.4	1.1085	0.4448	1.0017
Mo L	2.3	1.2	0.8943	0.8031	1.0017
Cr K	16.5	16.3	0.9910	0.9868	1.1505
Mn K	1.9	1.8	0.9739	0.9938	1.0105
Fe K	64.7	59.6	0.9931	0.9707	1.0138
Ni K	10.7	9.4	1.0104	0.9043	1.0000
Total	**100.0**	**100.0**			

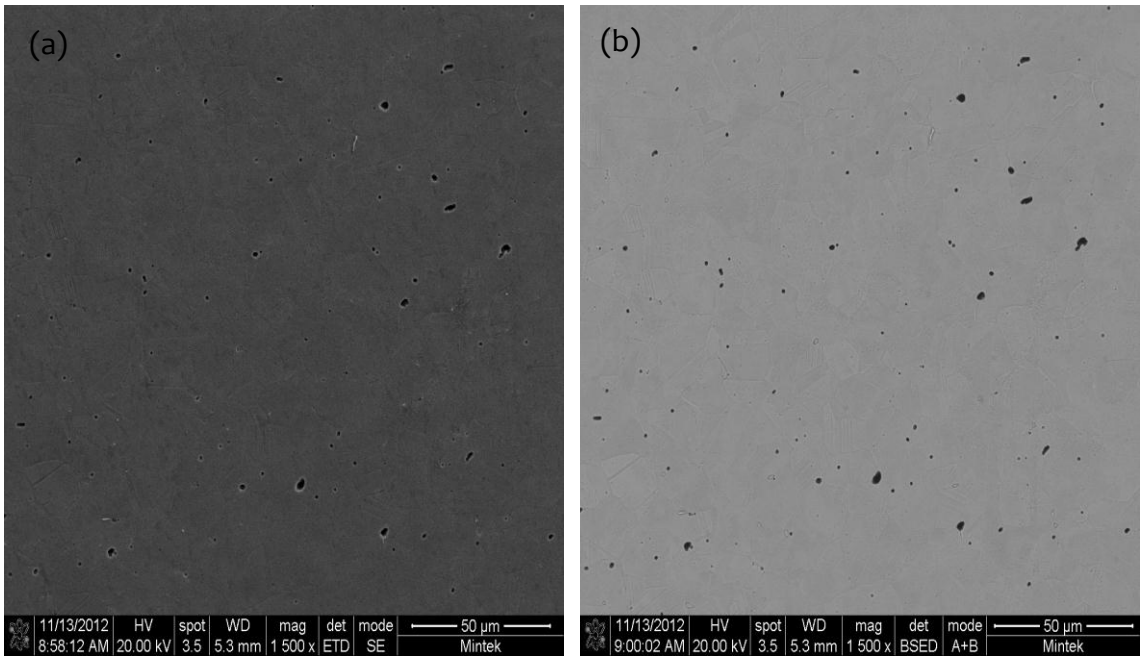

Figure 4.23. SEM images of the core of the sample carburised at 450°C: (a) secondary electron (SE), and (b) backscattered electron (BSE) modes.

Microstructures taken near the surface showed the micro-voids, austenite grains, some annealing twins, precipitates of carbides and oxides. The large and visible dark spots in both micrographs were the pores in the material. The dark and blurry dark spots close to the edge of the materials were carbides and oxides, which were distributed along and within the grains (Figure 4.24). Mechanical deformation was also found on Figure 4.24, which could be as a result of the mechanical testing.

The EDX analysis was carried out on samples carburised at 450°C at the core and near the surface. Analysis of the core revealed a minor presence of carbides and oxides (Figure 4.25). The darker small spots and overall analysis of regions around and close to the surface/edge showed more oxides, carbides and some chlorides (Figure 4.26). The oxides were barium oxide and chromium oxide.

The SEM images of the core of samples carburised at 550°C in SE and BSE modes are shown in Figure 4.27. The micrographs show well-defined austenite grains with some annealing twins and slip lines. The pores were distributed within the structure of the

material, and there were some carbides and oxides resulting from oxidation during the carburization process.

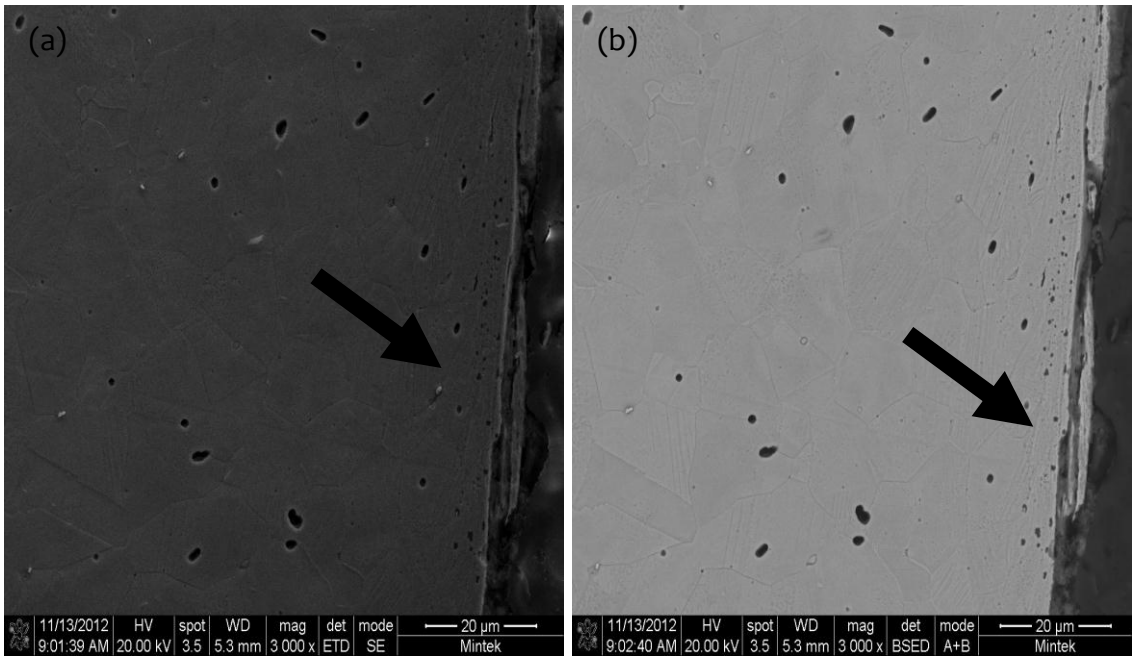

Figure 4.24. SEM images of the surface of the sample carburised at 450°C: (a) secondary electron (SE), and (b) backscattered electron (BSE) modes.

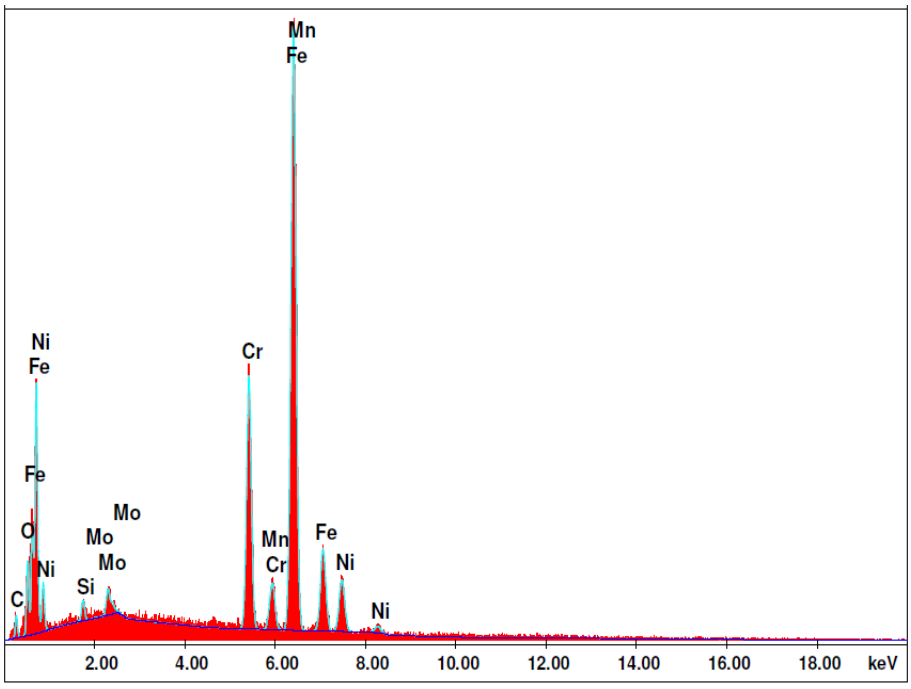

Figure 4.25. EDX analysis of the core of carburised AISI 316L steel at 450°C.

Table 4.5. EDX elemental compositions of the core of sample carburised at 450°C.

Element	Wt%	At%	Z	A	F
C K	4.4	16.4	1.1696	0.1812	1.0004
O K	2.9	8.2	1.1495	0.3680	1.003
Si K	0.7	1.2	1.0992	0.4574	1.0016
Mo L	1.8	0.9	0.8855	0.8179	1.0017
Cr K	16.0	13.9	0.9819	0.9896	1.1531
Mn K	1.5	1.2	0.9649	0.9960	1.0089
Fe K	63.8	51.5	0.9838	0.9731	1.0117
Ni K	8.8	6.8	1.0007	0.9071	1.0000
Total	**100.0**	**100.0**			

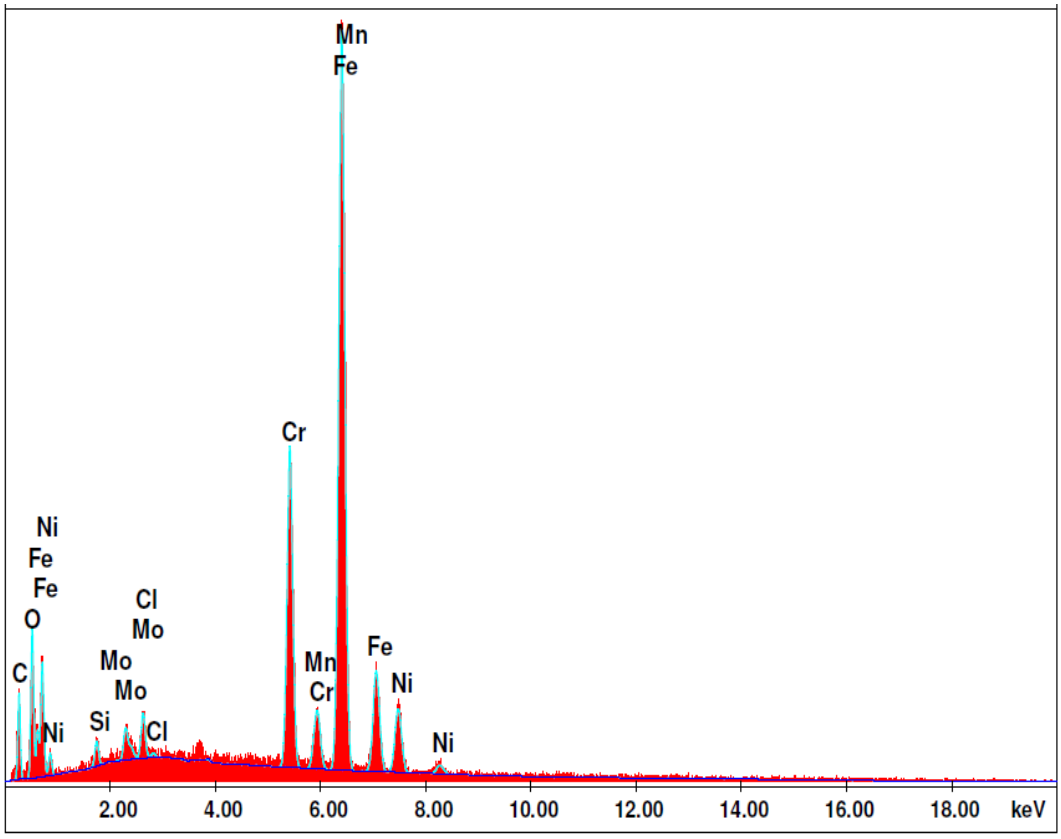

Figure 4.26. EDX analysis of the surface carburised AISI 316L steel at 450°C.

Table 4.6. EDX elemental compositions of the surface of sample carburised at 450°C.

Element	Wt%	At%	Z	A	F
C K	11.6	34.7	1.1482	0.1900	1.0004
O K	4.7	10.6	1.1285	0.3276	1.0027
Si K	0.6	0.8	1.0796	0.4866	1.0017
Mo L	1.6	0.6	0.8670	0.8506	1.0020
Cl K	1.0	1.0	1.0313	0.7880	1.0079
Cr K	14.8	10.3	0.9627	0.9930	1.1448
Mn K	1.3	0.9	0.9458	0.9987	1.0086
Fe K	56.6	36.5	0.9641	0.9773	1.0112
Ni K	7.8	4.8	0.9803	0.9184	1.0000
Total	**100.0**	**100.0**			

Microstructures near the surface of samples carburised at 550°C in SE and BSE modes shown in Figure 4.28 indicated the presence of carbides, nitrides and some chlorides. The chlorides could be due to the etching, while the others were due to the carburising process. Figure 4.28 also shows some mechanical deformation at the edge. Slip lines and annealing twins were fairly distributed through out the material. Defects such as pores were also present within the grains of the material. Mechanically induced deformations were observed on micrographs (Figure 4.28). The average grain size of the as-received specimen, which was determined by the mean lineal intercept method, was 38.4±4.3µm. There was no significant change in average grain size of samples carburised at 450°C and 550°C. It ranged between 39.4±3.2µm – 41.8±4.6µm. The average grain sizes measured for samples carburised at 650°C, 700°C and 750°C were 42.8±4.5 µm, 41.3±3.1µm and 44.6±2.6µm, respectively. The average grain sizes of the samples did not have much influence on the mechanical properties of the AISI 316L steel, as there was not much difference between the values.

The EDX analysis of the core of samples carburised at 550°C as shown in Figure 4.29 revealed oxides and carbides. The analysis done at the surface shown in Figure 4.30 indicated some oxides, carbides, iron and other metals.

Microstructures of the core of the sample carburised at 650°C are shown in Figure 4.31 (a) and (b) in both SE and BSE modes. The microstructure of the core showed the distinct austenite grains, annealing twins and slip lines with some pores. There were also carbides and oxides present within the grains and at the grain boundaries. Micrographs taken near the surface revealed similar characteristics to the core. However, the oxides and carbides were more common at the surface compared to the core. Figure 4.32 (a) and (b) showed the micrographs taken near the surface of the steel. There was a carburised layer of approximately 10μm, with more carbides and oxides than the core as shown by the EDX analysis in Table 4.10. Cracks were nucleate in the hard carburised case as shown in Figure 4.32.

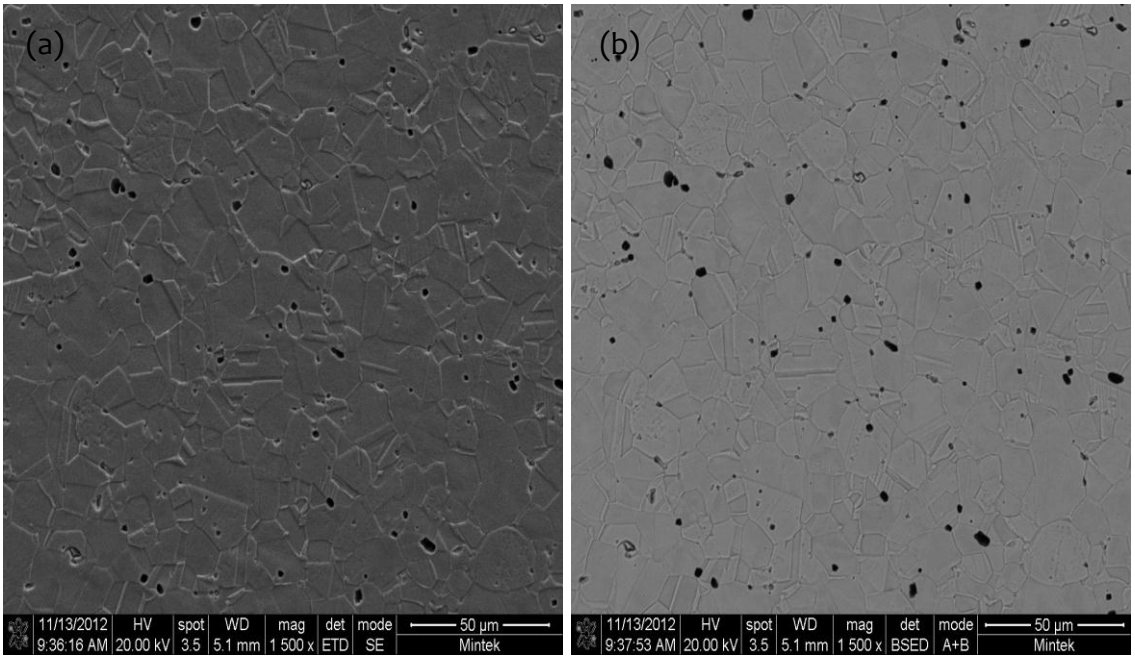

Figure 4.27. SEM images of the core of the sample carburised at 550°C: (a) secondary electron (SE), and (b) backscattered electron (BSE) modes.

At higher carburising temperatures, more chlorides and carbides were found in the sample (Figure 4.33). Analysis done on the near surface also revealed a similar pattern as

that of the core, but with increased oxygen (19.7-26.5 wt%) and carbon (7.6-10.7 wt%), as shown in Figure 4.34.

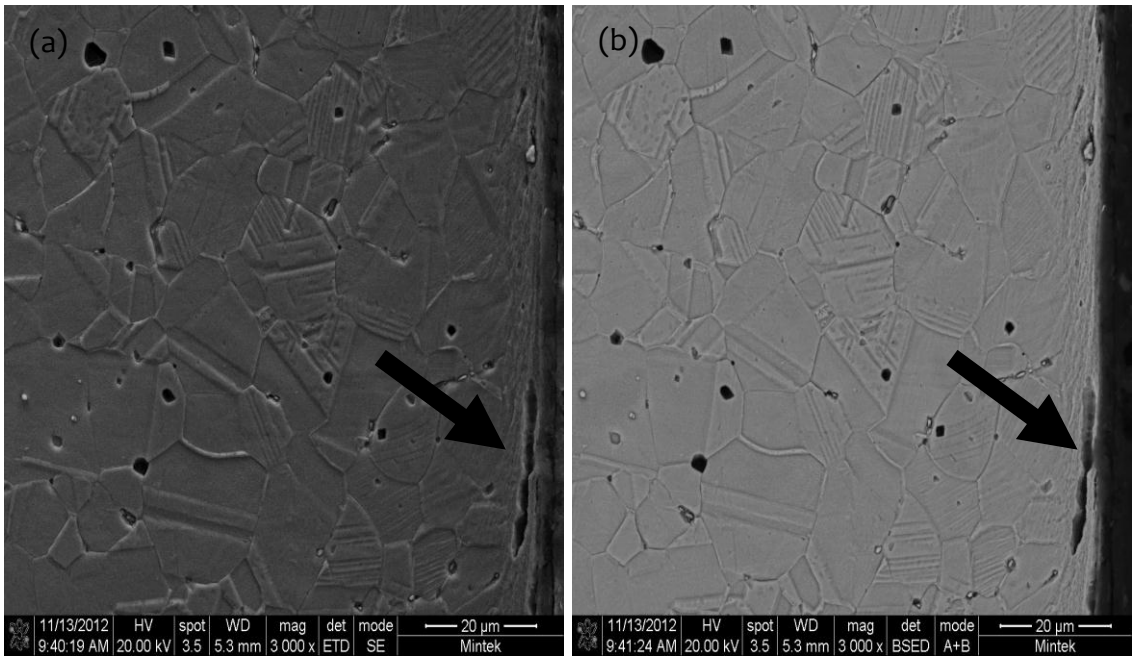

Figure 4.28. SEM images of the surface of the sample carburised at 550°C: (a) secondary electron (SE), and (b) backscattered electron (BSE) modes.

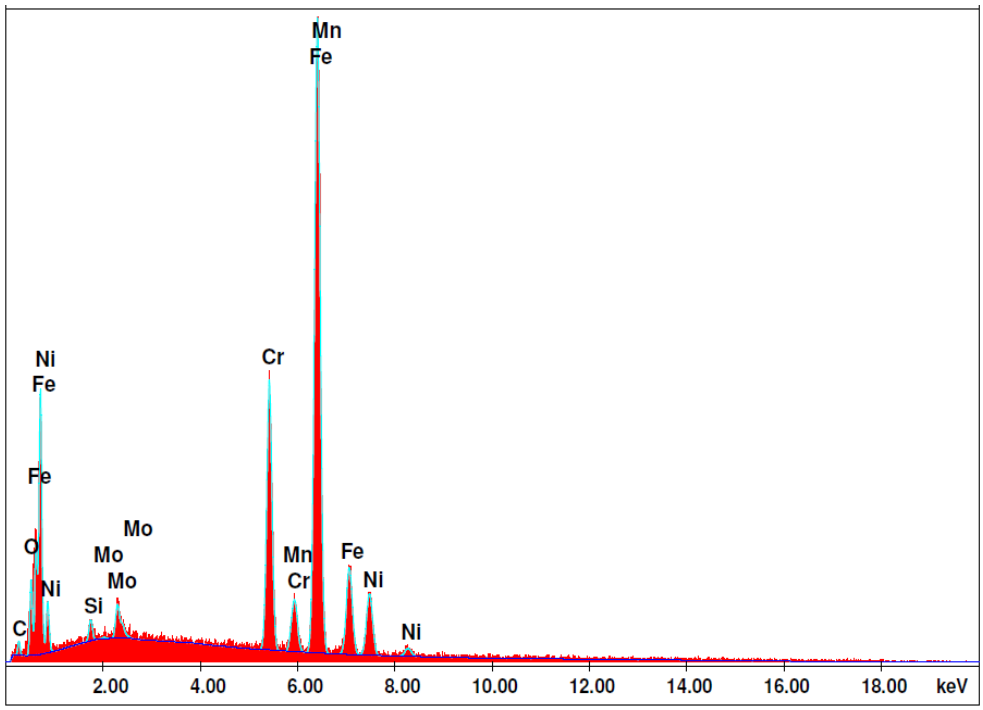

Figure 4.29. EDX analysis of the core of the sample carburised at 550°C.

Table 4.7. EDX elemental compositions of the core of sample carburised at 550°C.

Element	Wt%	At%	Z	A	F
C K	2.7	10.7	1.1743	0.1776	1.0004
O K	2.7	8.1	1.1540	0.3735	1.0032
Si K	0.7	1.2	1.1035	0.4518	1.0017
Mo L	2.2	1.1	0.8895	0.8116	1.0017
Cr K	16.3	14.9	0.9861	0.9881	1.1507
Mn K	1.7	1.5	0.9690	0.9949	1.0099
Fe K	63.8	54.5	0.9881	0.9719	1.0129
Ni K	9.9	8.0	1.0052	0.9061	1.0000
Total	**100**	**100**			

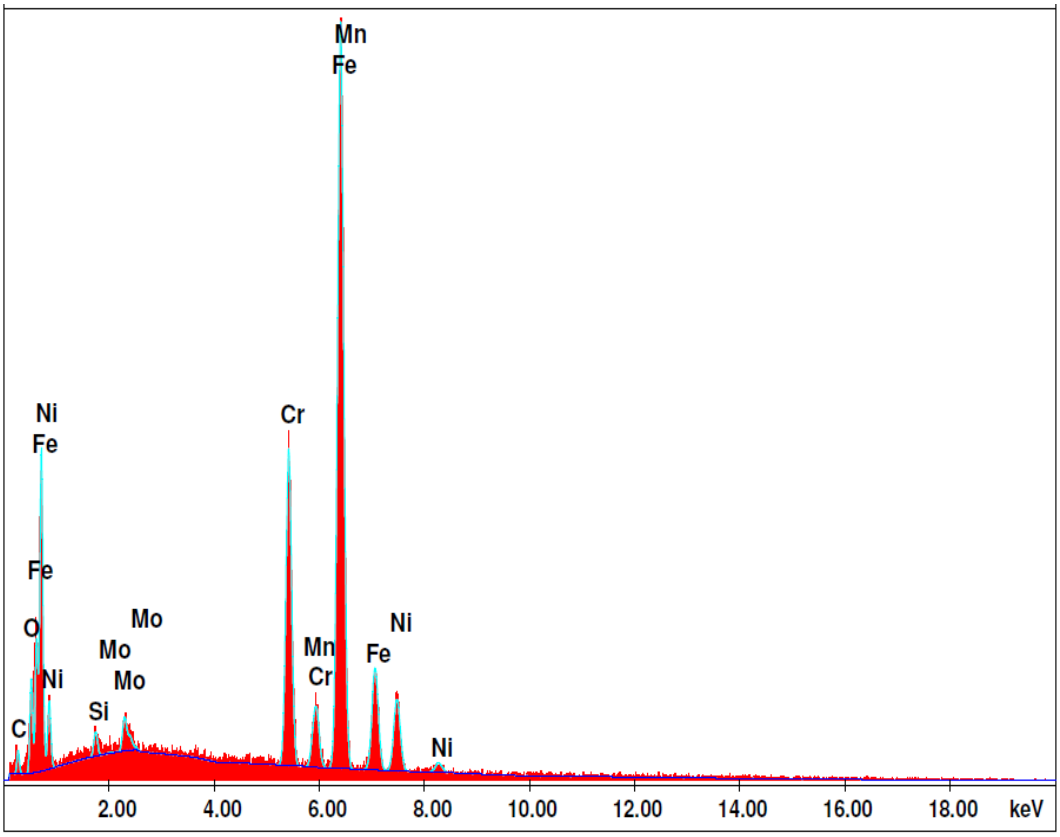

Figure 4.30. EDX analysis of the surface of the sample carburised at 550°C.

Table 4.8. EDX elemental compositions of the surface sample carburised at 550°C.

Element	Wt%	At%	Z	A	F
C K	3.7	14.2	1.1711	0.1799	1.0004
O K	2.9	8.4	1.1509	0.3710	1.0032
Si K	0.7	1.1	1.1006	0.4547	1.0016
Mo L	1.9	0.9	0.8868	0.8150	1.0017
Cr K	16.1	14.2	0.9833	0.9891	1.1515
Mn K	1.7	1.5	0.9662	0.9957	1.0099
Fe K	63.3	52.1	0.9852	0.9728	1.0129
Ni K	9.7	7.6	1.0021	0.9074	1.0000
Total	**100**	**100**			

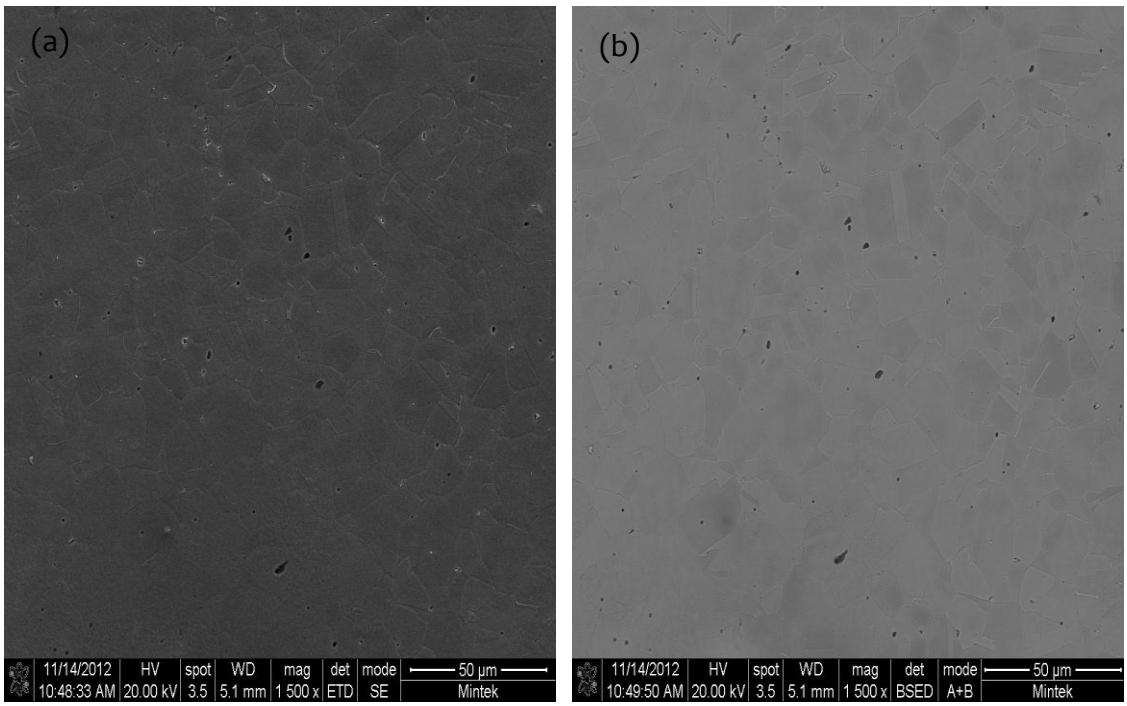

Figure 4.31. SEM images of the core of the sample carburised at 650°C: (a) secondary electron (SE), and (b) backscattered electron (BSE) modes.

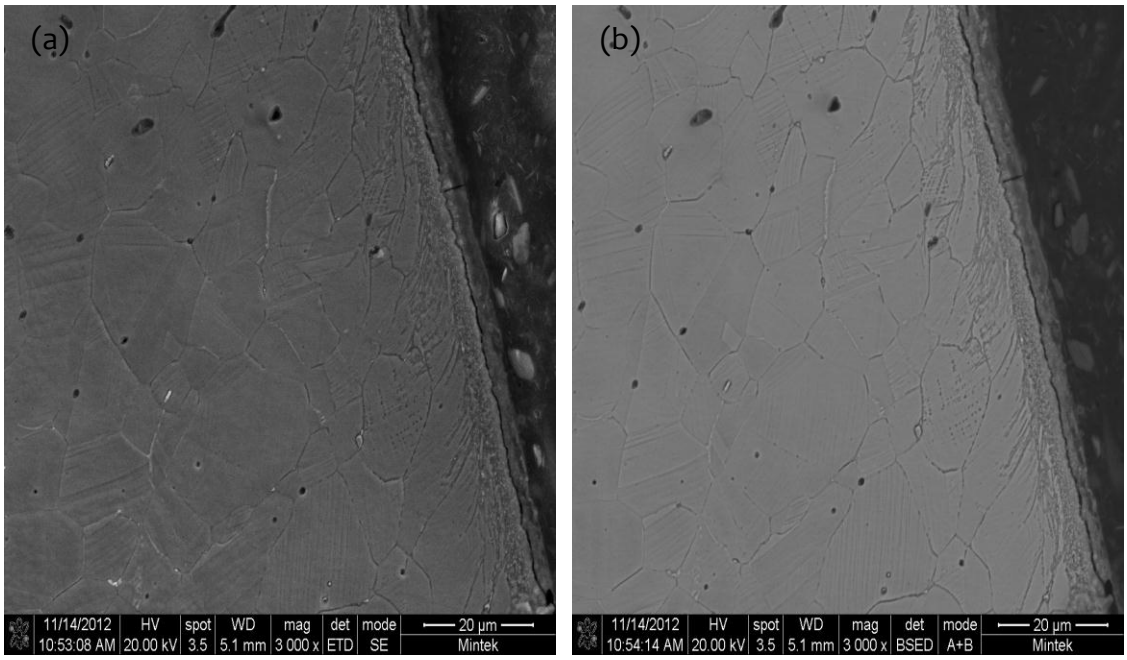

Figure 4.32. SEM images of the surface of the sample carburised at 650°C: (a) secondary electron (SE), and (b) backscattered electron (BSE) modes.

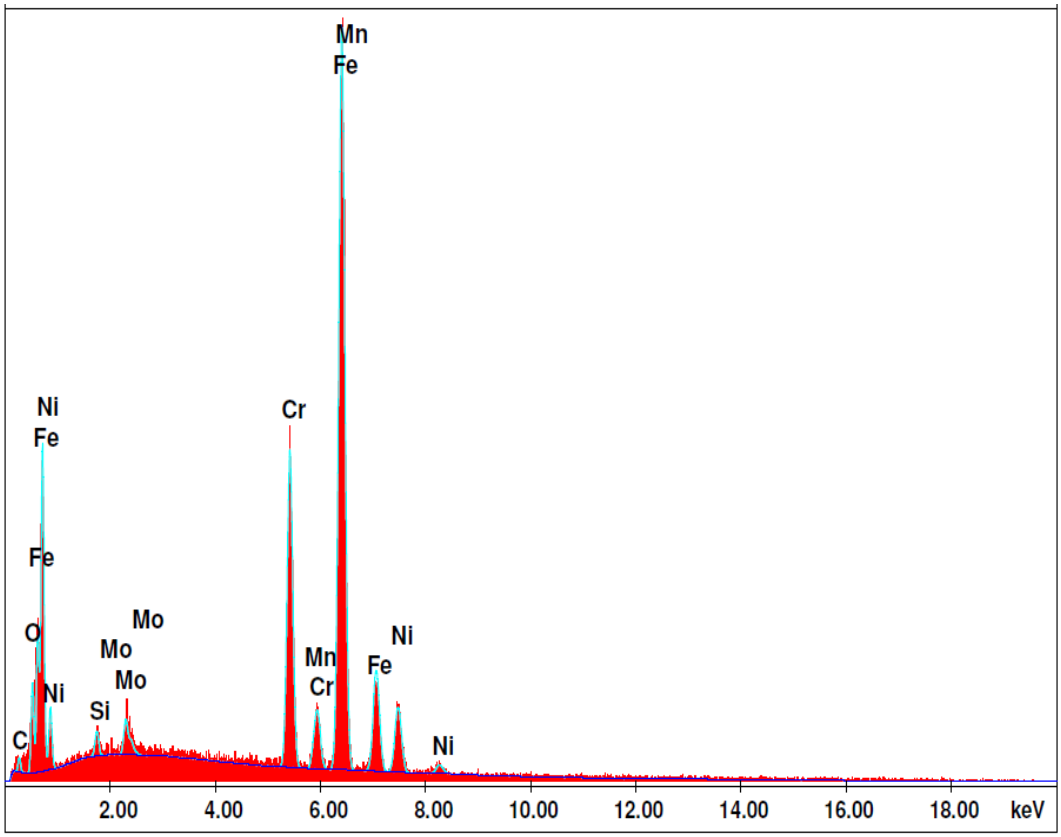

Figure 4.33. EDX analysis of the core of the sample carburised at 650°C.

Table 4.9. EDX elemental compositions of the core of the sample carburised at 650°C.

Element	Wt%	At%	Z	A	F
C K	2.4	9.5	1.1749	0.1783	1.0004
O K	2.8	8.3	1.1547	0.3804	1.0033
Si K	0.7	1.2	1.1041	0.4551	1.0017
Mo L	2.0	1.0	0.8901	0.8131	1.1528
Cr K	16.6	15.3	0.9867	0.9886	1.0091
Mn K	1.6	1.4	0.9696	0.9952	1.0091
Fe K	64.9	55.8	0.9887	0.9719	1.0119
Ni K	9.1	7.5	1.0057	0.9060	1.0000
Total	**100.0**	**100.0**			

At a carburising temperature of 700°C, the microstructures at the core revealed the austenite grains, annealing twins and slip lines. There was grain boundary oxidation and carbides were fairly well distributed throughout the material. Pores were also revealed as shown in Figure 4.35. Similar characteristic features were observed in the micrographs taken near the surface of the steel. However, there were more carbides and oxides present at the surface than the core, as shown in Figure 4.36. The grain boundaries were more visible at areas near the surface due to the carbides and oxides and they were smaller with more slip lines and annealing twins. Figure 4.36 showed carbide and oxide layers that is estimated to be 15μm thick at the surface. Grain boundary oxidation was also found in localised areas throughout the microstructure.

The EDX analysis of the core of samples carburised at 700°C revealed oxides and carbides (Figure 4.37). An analysis of the thin whitish layer and the lined features in Figure 4.36(a) showed the presence of calcium and some chloride, as a result of the chemical etchant, 15mL HCl, 10mL HNO_3 and 10mL CH_3COOH used (Figure 4.38). The presence of more slip lines on the surface of the sample carburised at 700ºC is an indication of excessive plastic deformation within the material. There were some carbides found at the grain boundaries and within the grains (Table 4.11).

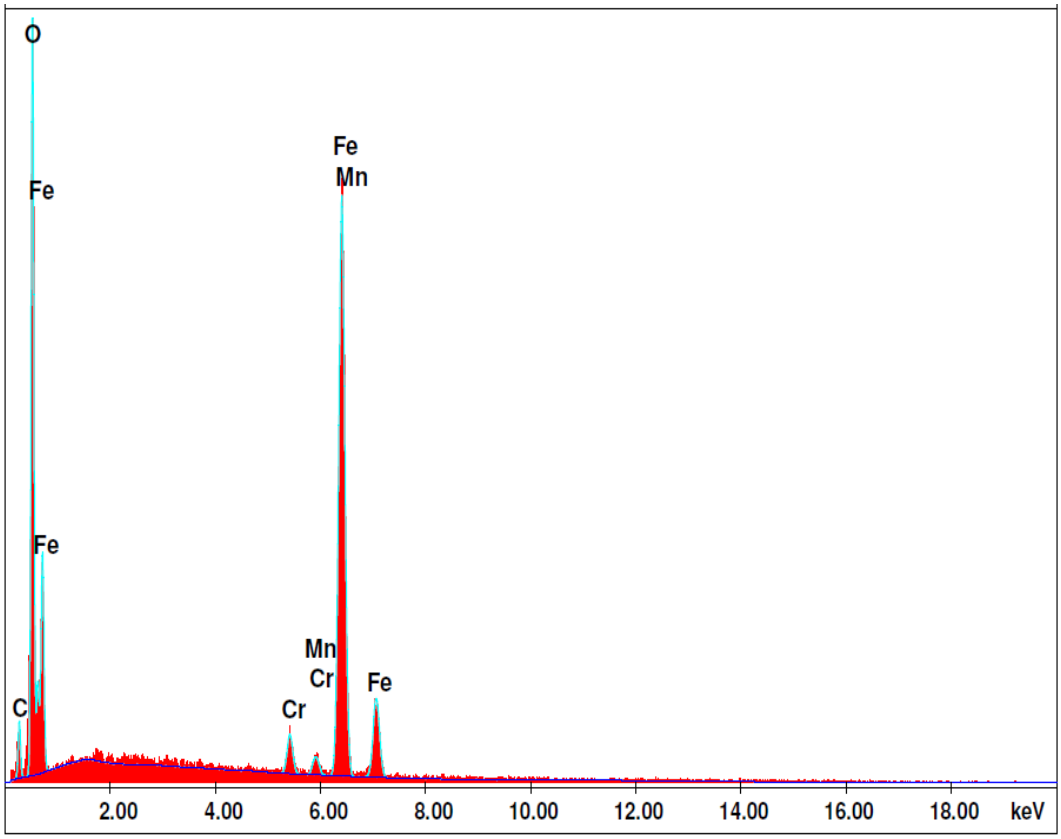

Figure 4.34. EDX analysis of the surface of sample carburised at 650°C.

Table 4.10. EDX elemental compositions of the surface of sample carburised at 650°C.

Element	Wt%	At%	Z	A	F
C K	8.9	20.8	1.1139	0.2252	1.0006
O K	26.4	46.5	1.0950	0.4176	1.0022
Cr K	2.3	1.3	0.9325	1.0024	1.2414
Mn K	1.3	0.7	0.9151	1.0061	1.0000
Fe K	61.1	30.8	0.9325	1.0043	1.0000
Total	**100.0**	**100.0**			

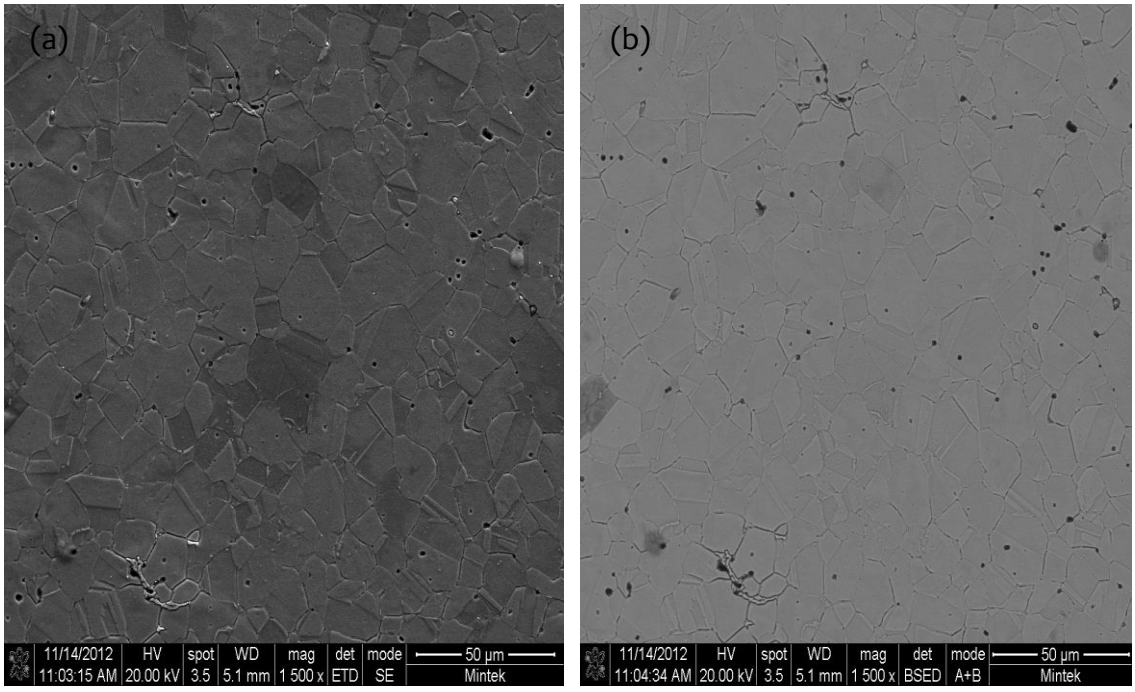

Figure 4.35. SEM images of the core of the sample carburised at 700°C: (a) secondary electron (SE) and (b) backscattered electron (BSE) modes.

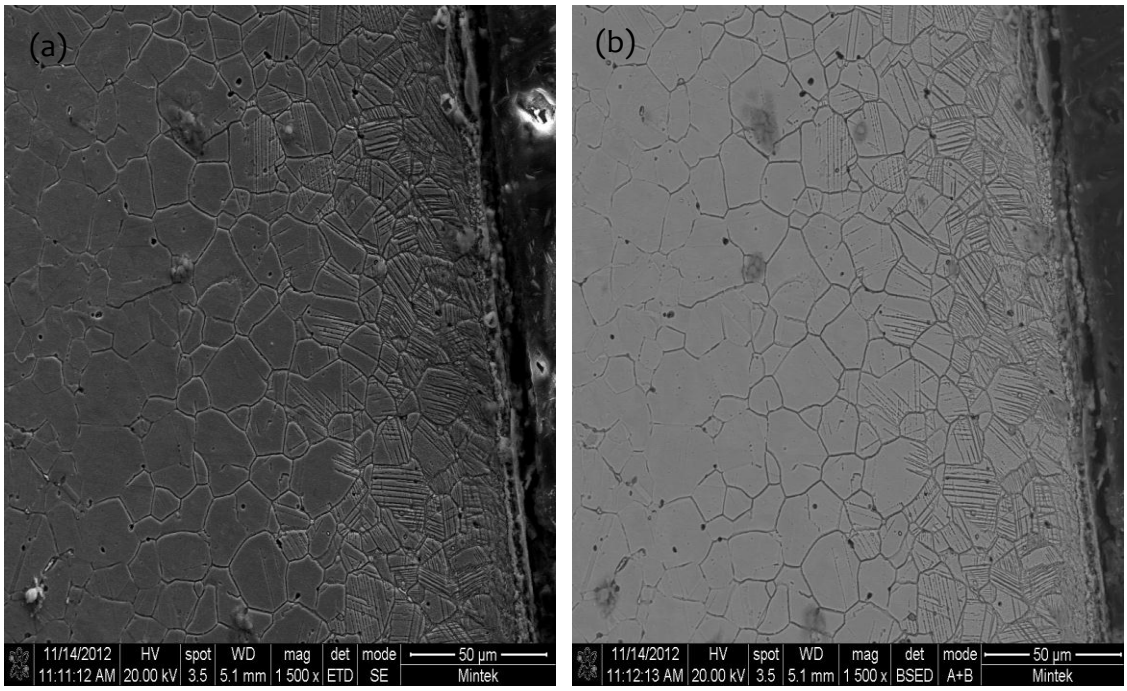

Figure 4.36. SEM images of the surface of the sample carburised at 700°C: (a) secondary electron (SE), and (b) backscattered electron (BSE) modes.

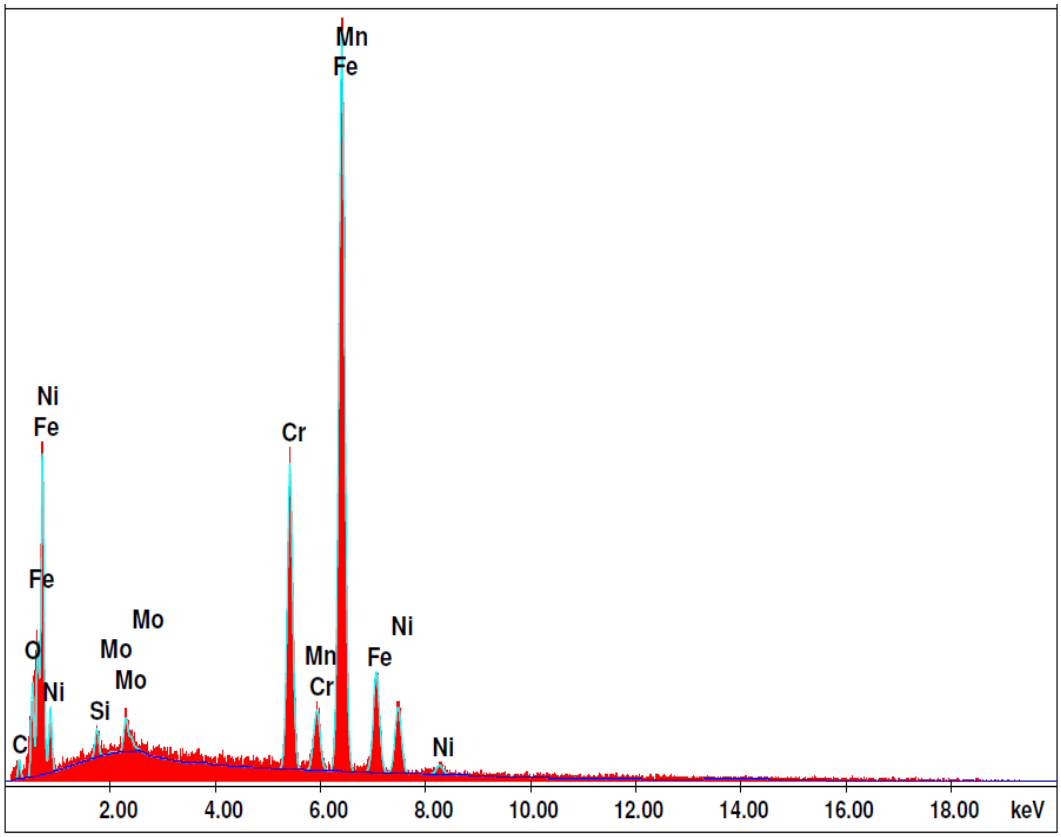

Figure 4.37. EDX analysis of the core of the sample carburised at 700°C.

Table 4.11. EDX elemental compositions of the core of sample carburised at 700°C.

Element	Wt%	At%	Z	A	F
C K	3.1	12.2	1.1725	0.1792	1.0004
O K	2.9	8.5	1.1523	0.3759	1.0032
Si K	0.8	1.3	1.1019	0.4564	1.0017
Mo L	1.9	0.9	0.8880	0.8146	1.0017
Cr K	15.9	14.3	0.9845	0.9890	1.1542
Mn K	1.8	1.6	0.9675	0.9955	1.0092
Fe K	64.4	53.9	0.9865	0.9732	1.0121
Ni K	9.2	7.3	1.0035	0.9069	1.0000
Total	**100.0**	**100.0**			

The outer surface of the microstructure showed some barium, calcium and more chlorides, carbides and oxides. There were higher amounts of oxides and chlorides than

seen before as shown in Figure 4.39. The chemical etchant used was responsible for the higher proportion of chlorides in the structure.

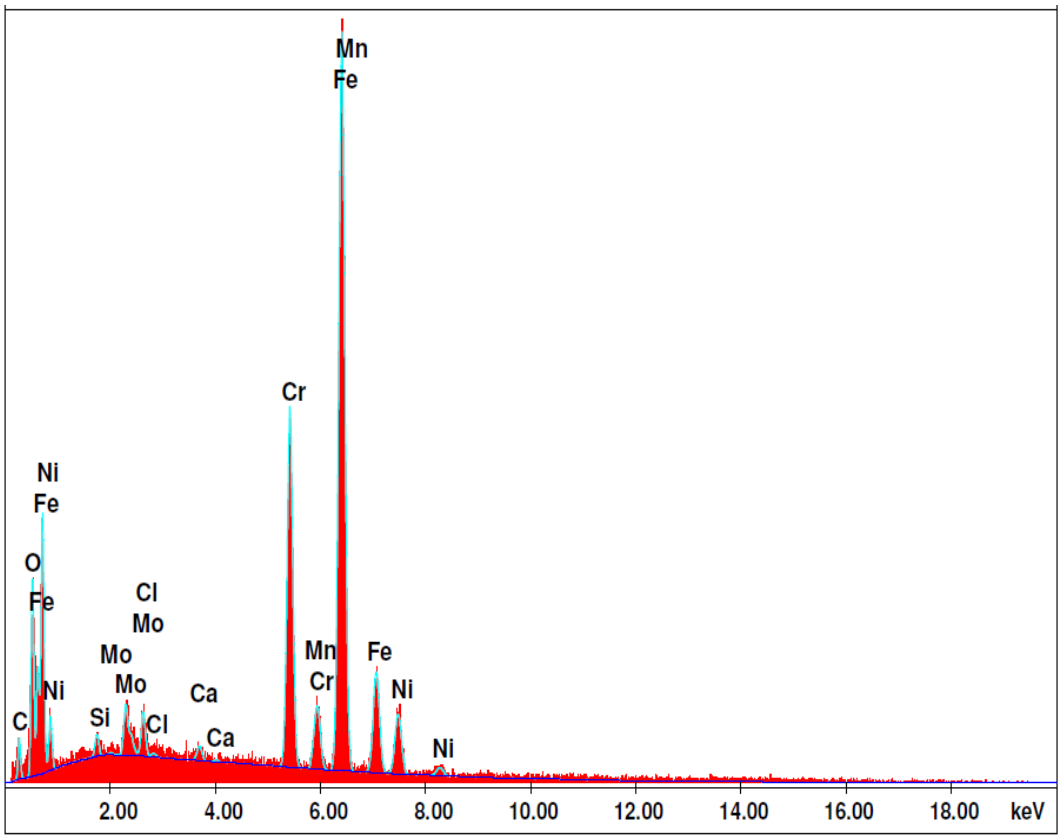

Figure 4.38. EDX analysis of the inner layer and lined feature on the sample carburised at 700°C.

The microstructures of the core of the sample carburised at 750°C both in SE and BSE modes are shown in Figure 4.40, with well-defined austenite grains, annealing twins, slip lines as well as carbides and oxides distributed throughout the grains and on the grain boundaries. The oxide and carbide distributions in these samples were greater than those carburised at lower temperatures. Microstructures taken near the surface showed the carburised case and another layer beneath the surface. The carburised layer had irregular-like features, which were revealed with EDX as mainly chlorides. There were oxides and carbides within the various layers, with the majority found within the case, and some in areas further away from the surface, Figure 4.41. Both the core and surface had voids, and some grain boundary oxidation. The outer layer (III) had more oxides, carbides and chlorides (irregular-shaped structure) than the middle layer (II). The middle layer (I)

showed the austenite grains with some carbides, chlorides and oxides. The oxides, carbides and chlorides decreased as increasing depth from the surface, hence the only difference.

Table 4.12. EDX elemental compositions of the inner layer and the lined feature of the sample carburised at 700°C.

Element	Wt%	At%	Z	A	F
C K	5.8	19.8	1.1597	0.1825	1.0004
O K	5.9	15.0	1.1398	0.3501	1.0028
Si K	0.5	0.8	1.0902	0.4779	1.0020
Mo L	2.5	1.0	0.8769	0.8396	1.0023
Cl K	1.0	1.1	1.0429	0.7772	1.0082
Ca K	0.4	0.4	1.0667	0.9218	1.0386
Cr K	17.1	13.4	0.9730	0.9893	1.1361
Mn K	1.4	1.0	0.9560	0.9957	1.0079
Fe K	58.0	42.3	0.9747	0.9714	1.0102
Ni K	7.5	5.2	0.9913	0.9140	1.0000
Total	**100.0**	**100.0**			

Figure 4.42 shows the EDX analysis of the core of samples carburised at 750°C with the presence of some carbides, but no oxides. Analysis of the carburised inner layer revealed the presence of oxides, carbides and some chlorides as shown in Figure 4.43. The outer carburised layer also showed similar features (Figure 4.44), but in higher proportions, with some barium compounds from the case making chemicals.

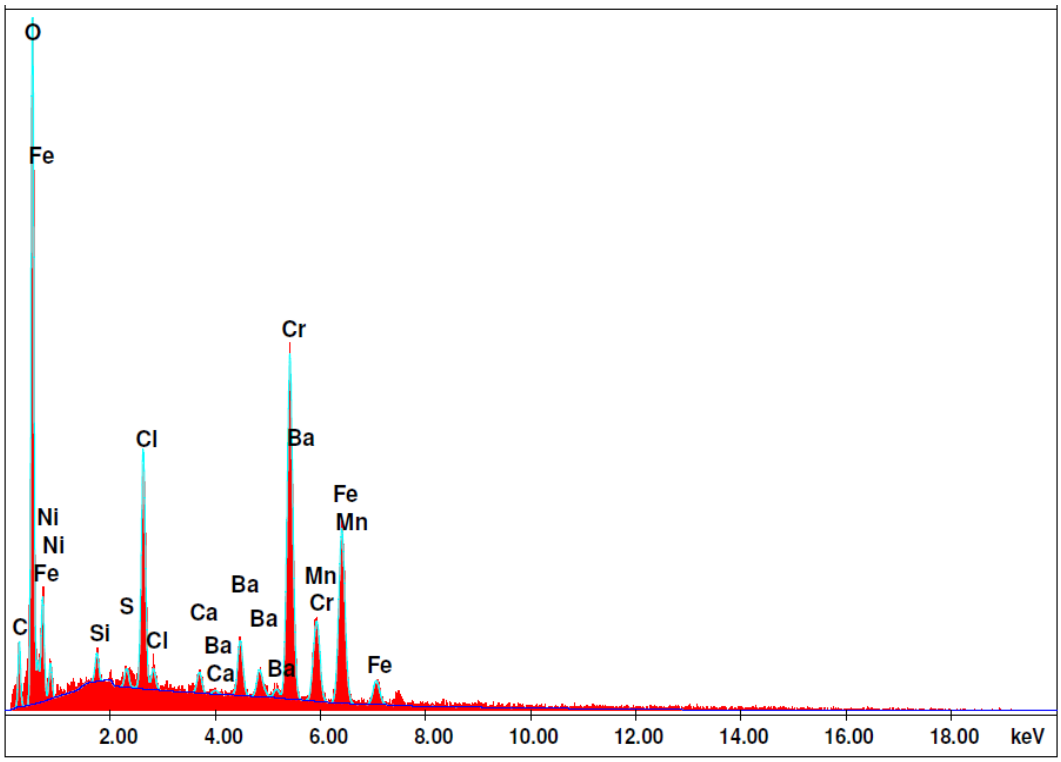

Figure 4.39. EDX analysis of the carburised layer of the sample carburised at 700°C.

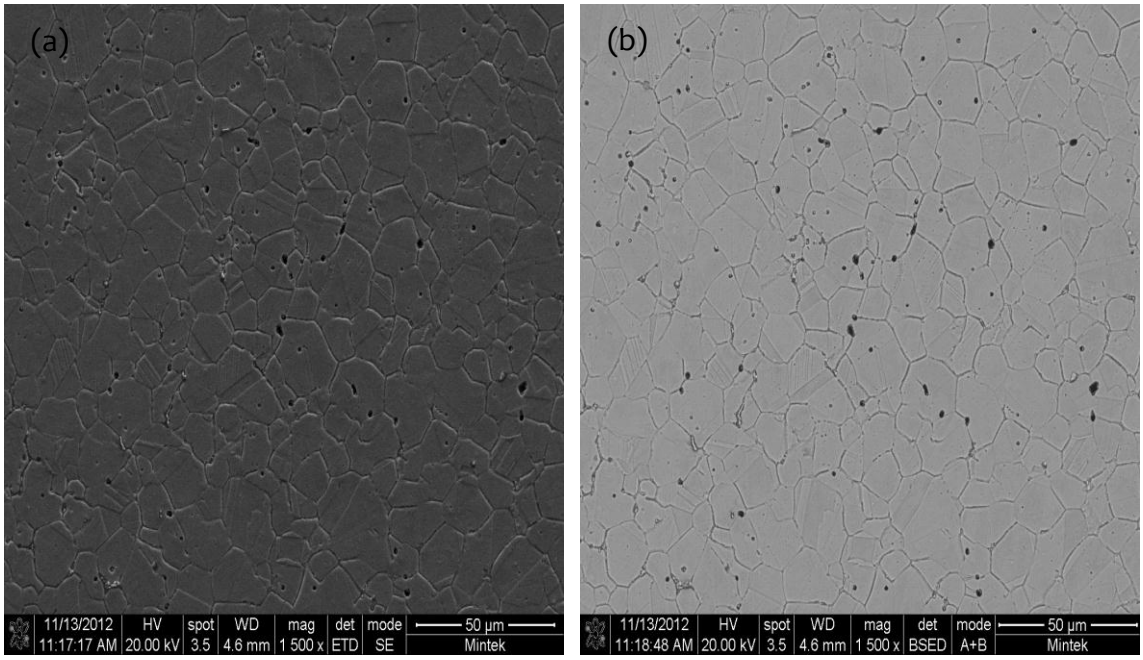

Figure 4.40. SEM images of the core of the sample carburised at 750°C: (a) secondary electron (SE), and (b) backscattered electron (BSE) modes.

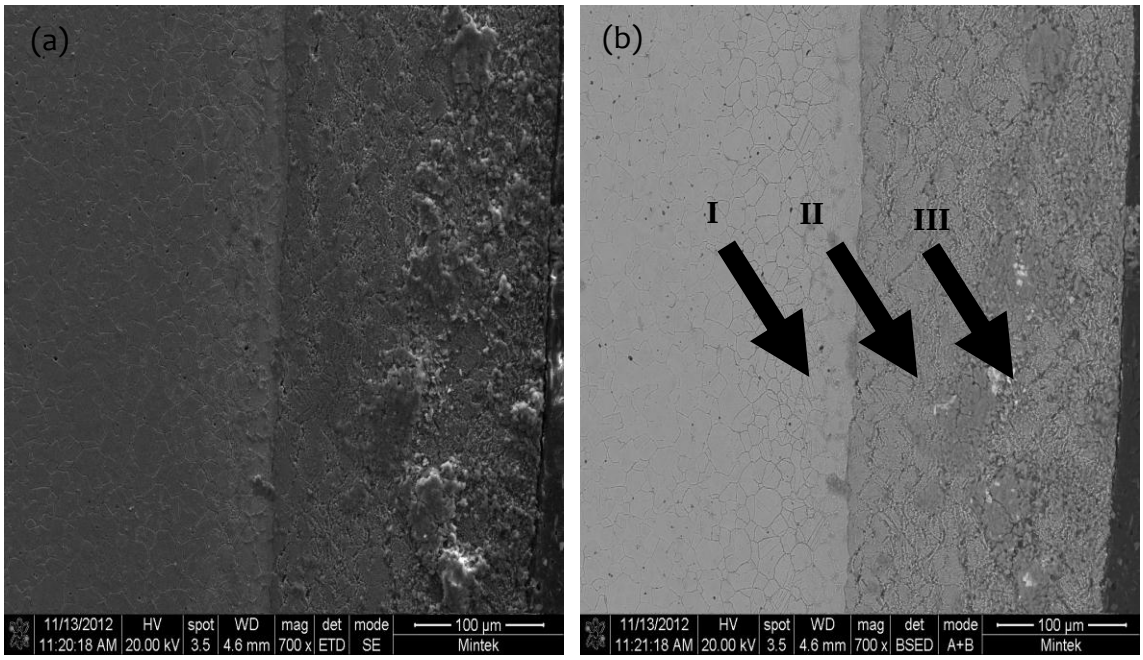

Figure 4.41. SEM images of the surface showing the carburised case of the sample carburised at 750°C: (a) secondary electron (SE), and (b) backscattered electron (BSE) modes showing (i) parent structure (inner layer) (ii) carburised case with oxides and carbides (middle layer) (iii) carburised case with more oxides, carbides and very high chlorides (outer layer).

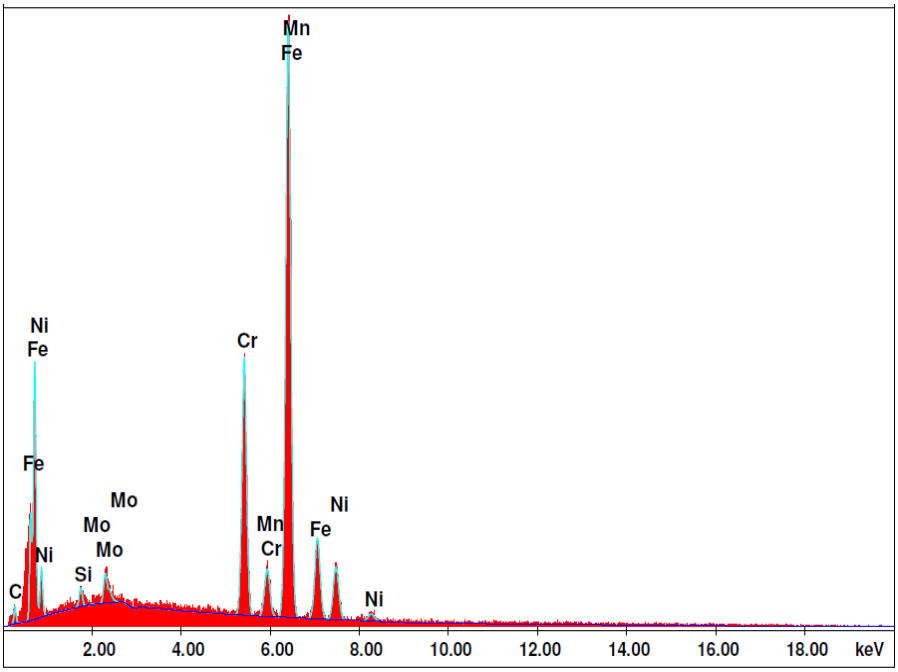

Figure 4.42. EDX analysis of the core of the sample carburised at 750°C.

Table 4.13. EDX elemental compositions of the carburised layer and the lined feature of the sample carburised at 700°C.

Element	Wt%	At%	Z	A	F
C K	10.6	23.9	1.1126	0.1911	1.0004
O K	26.4	44.6	1.0937	0.3434	1.0013
Ni K	6.6	3.1	0.9564	0.2386	1.0001
Si K	0.7	0.7	1.0471	0.5556	1.0028
S K	0.5	0.4	1.0428	0.7663	1.0087
Cl L	5.9	4.5	0.9958	0.8382	1.0083
Ca K	0.7	0.5	1.0215	0.9385	1.0358
Ba L	6.8	1.4	0.7835	1.0716	1.0561
Cr K	21.7	11.3	0.9309	0.9834	1.0374
Mn K	3.3	1.6	0.9143	0.9859	1.0089
Fe K	16.8	8.1	0.9318	0.9540	1.0110
Total	**100.0**	**100.0**			

Table 4.14. EDX elemental compositions of the core of sample carburised at 750°C.

Element	Wt%	At%	Z	A	F
C K	3.5	14.5	1.1782	0.1773	1.0004
Si K	0.7	1.2	1.1071	0.4530	1.0017
Mo L	2.1	1.1	0.8929	0.8108	1.0018
Cr K	17.0	16.1	0.9896	0.9880	1.1530
Mn K	1.6	1.4	0.9725	0.9947	1.0092
Fe K	65.7	57.4	0.9916	0.9709	1.0121
Ni K	9.4	7.9	1.0088	0.9045	1.0000
Total	**100.0**	**100.0**			

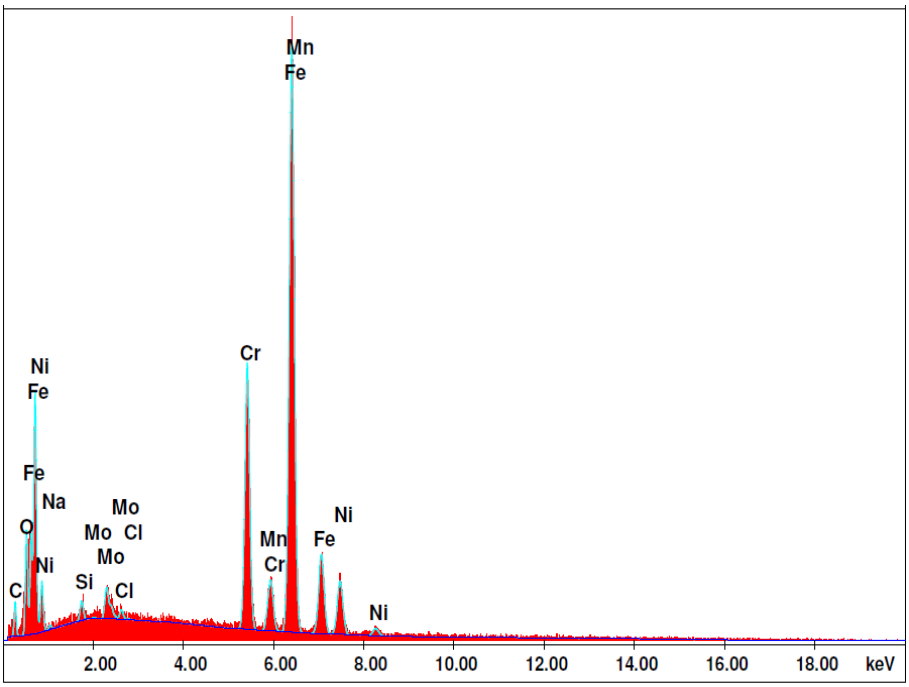

Figure 4.43. EDX analysis of the carburised inner layer on the sample carburised at 750°C.

Table 4.15. EDX elemental compositions of the carburised inner layer of the sample carburised at 750°C.

Element	Wt%	At%	Z	A	F
C K	6.3	21.7	1.1623	0.1843	1.0004
O K	4.0	10.5	1.1424	0.3574	1.0029
Na K	0.3	0.6	1.0682	0.1645	1.0002
Si K	0.6	1.0	1.0926	0.4708	1.0017
Mo L	2.0	0.9	0.8792	0.8310	1.0019
Cl K	0.3	0.3	1.0456	0.7734	1.0081
Cr K	16.4	13.1	0.9754	0.9905	1.1445
Mn K	1.7	1.3	0.9584	0.9967	1.0092
Fe K	59.6	44.4	0.9771	0.9734	1.0119
Ni K	8.7	6.2	0.9938	0.9130	1.0000
Total	**100.0**	**100.0**			

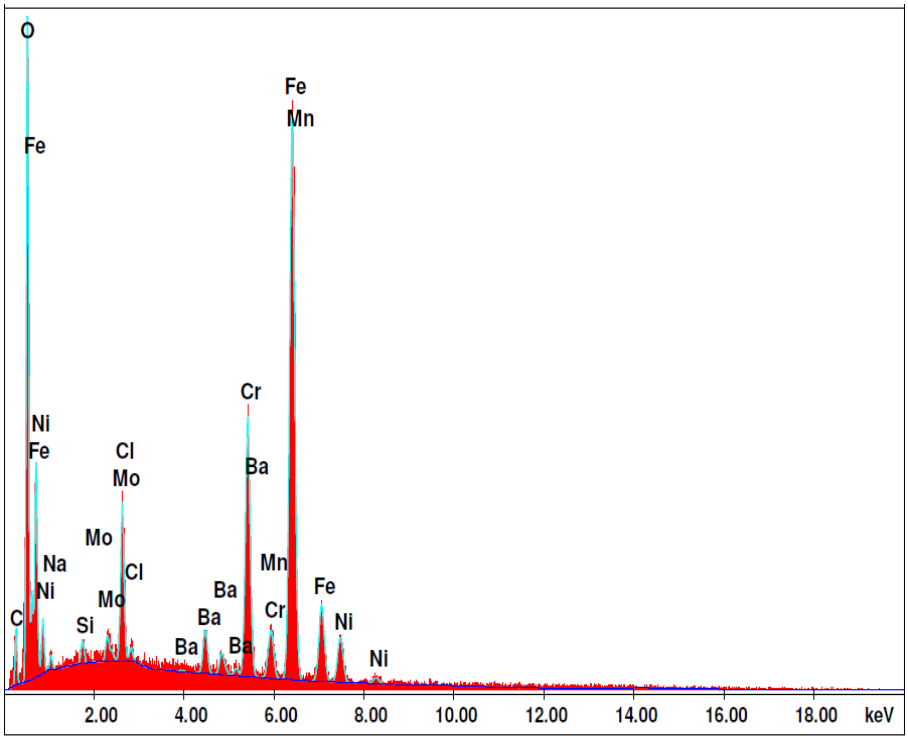

Figure 4.44. EDX analysis of the carburised case of the sample carburised at 750°C.

Table 4.16. EDX elemental compositions of the carburised case of the sample carburised at 750°C.

Element	Wt%	At%	Z	A	F
C K	7.6	19.8	1.1310	0.1896	1.0004
O K	19.7	38.7	1.117	0.3649	1.0018
Na K	0.7	1.0	1.0398	0.1887	1.0002
Si K	0.5	0.6	1.0639	0.5122	1.0021
Mo L	1.2	0.4	0.8526	0.8745	1.0034
Cl K	3.3	2.9	1.0145	0.8071	1.0074
Ba K	4.4	1.0	0.7973	1.0686	1.0712
Cr K	12.5	7.6	0.9475	0.9859	1.1018
Mn K	1.1	0.7	0.9308	0.9897	1.0064
Fe K	43.4	24.4	0.9488	0.9728	1.0085
Ni K	5.5	2.9	0.9646	0.9324	1.0000
Total	**100.0**	**100.0**			

4.4. FRACTOGRAPHY

4.4.1. Macroscopic characteristics of the fatigue fractured surfaces

A visual inspection of the fractured surface of the fatigue specimen indicated the following; ratchet marks and thumbnails. Generally the corners of the fractured surfaces were slightly brighter, which indicated small fatigue cracks and micro-void coalescence [1996ASM, 1999Rit]. There were also less secondary micro-cracks on the surface of the material.

Samples carburised at 450°C, 550°C and 650°C showed secondary cracking along the sides and many fatigue pre-cracks. Secondary cracking and fatigue pre-cracks were minimal on the samples carburised at 700°C and 750°C. Generally, all specimens showed great deal of plastic deformation.

4.4.2. Microscopic characteristics of the fractured surfaces

Fractured surfaces of the as-received AISI 316L steel showed the crack initiation, propagation and rupture zones. Figure 4.45 shows the brittle fracture initiation, which is more of a brittle tearing, rather than a quasi-cleavage mechanism [2005Liu]. When there are shear stresses acting parallel to both the plane of the crack and the crack front, then brittle tearing is facilitated. However, crack propagation sites showed patches of finely spaced parallel marks or striations that are characteristics of fatigue crack growth, are shown in Figure 4.46. The characteristic feature of the final rupture zone was ductile fracture with dimples, with voids nucleated within the fracture as shown in Figure 4.47.

Fractured surfaces of AISI 316L samples carburised at 450°C showed similar initiation, propagation and crack termination patterns. Brittle fracture (tearing) and the presence of secondary cracks within the fractured surface were some of the characteristics features of the initiation stage. Figure 4.48 shows brittle fracture and the presence of the secondary crack shown in black arrow. Crack propagation and the final rupture zones of samples carburised at 450°C are shown in Figures 4.49 and 4.50.

At the carburising temperature of 550°C, the initiation, propagation and rupture stages were similar to the previous treatment temperature. The initiation stage was also predominantly brittle fracture (tearing), with some secondary cracking as shown in Figure 4.51. Fractured surfaces indicating fatigue striations and ductile dimple fracture are shown in Figures 4.52 and 4.53. Although the rupture zone of samples carburised at 550°C showed ductile dimple, it was also associated with a lineal pattern to fracture, like an incremental tearing (Figure 4.53).

The initiation stage of AISI 316L samples carburised at 650°C also showed brittle fracture (tearing) and with dispersed small secondary cracking within the material, shown in Figure 4.54. As the crack propagated, fatigue striations were created on the surface (Figure 4.55), which conforms to previously discussed fractured surfaces. At low magnifications, as shown in Figure 4.56, the rupture zone of the sample carburised at 650°C showed a lineal pattern to the fracture, like an incremental tearing which may be attributed to chemical or microstructural segregation patterns.

Fractographic analysis of samples carburised at 700°C showed similar characteristic features to those treated at 450°C and 550°C. The crack initiation sites showed brittle fracture, which is shown at low magnification in Figure 4.57. As the crack propagated, patches of finely spaced parallel lines or crack arrest marks, striations were found as shown in Figure 4.58. The rupture zone was also found to be ductile fracture characterized by dimples and voids that were nucleated throughout the material, as shown in Figure 4.59.

At the carburising temperature of 750°C, the fractured surfaces of the samples did not show many changes compared to the lower temperature samples. The cracks were nucleated (Figure 4.60) by brittle fracture (tearing), and then crack growth was as a result of fatigue, due to the visible striations within the fracture surface as shown in Figure 4.61.

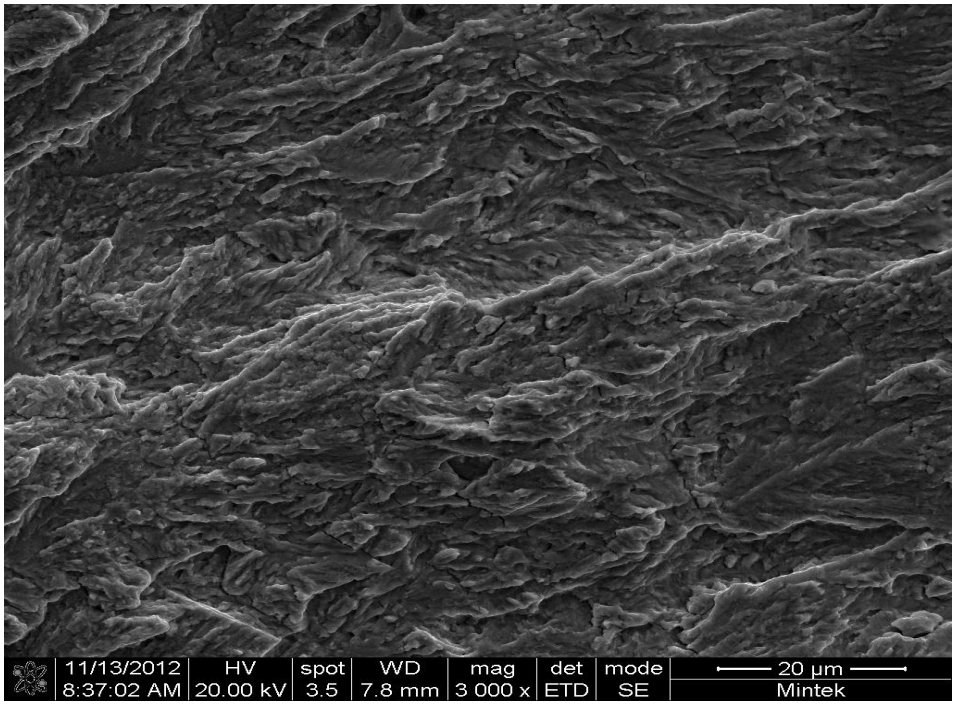

Figure 4.45. Crack initiation zone of the as-received AISI 316L steel showing brittle (tearing) fracture.

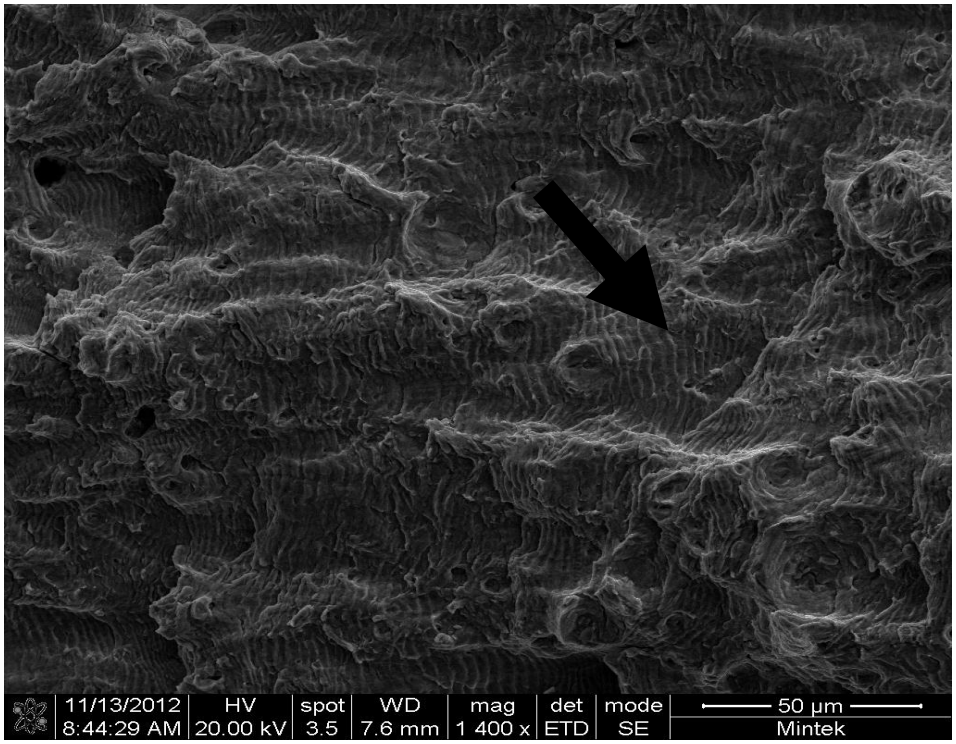

Figure 4.46. Crack propagation zone of the as-received AISI 316L steel showing fatigue striations.

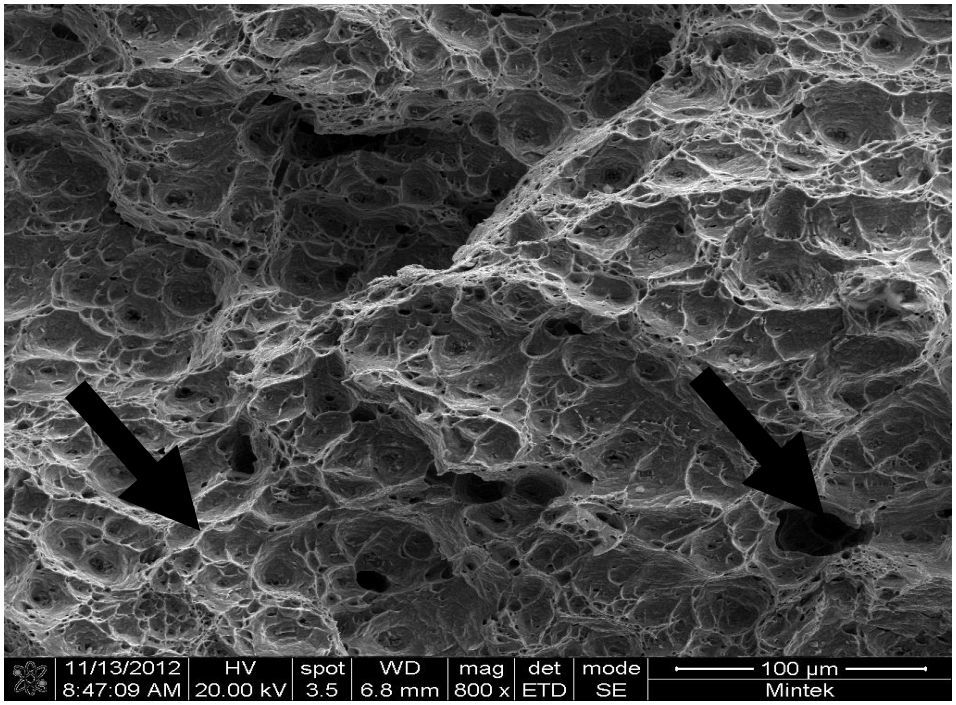

Figure 4.47. Rupture zone of the as-received AISI 316L steel showing ductile dimple fracture.

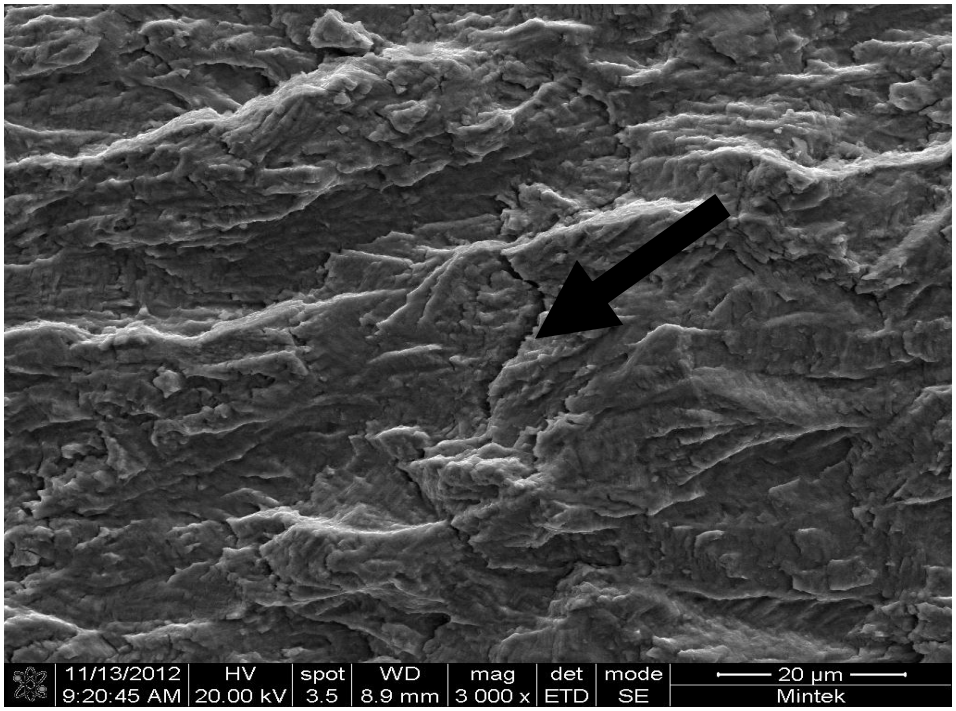

Figure 4.48. Crack initiation zone of AISI 316L sample carburised at 450°C showing brittle (tearing) with dark arrow pointing at secondary cracking within the fractured surface.

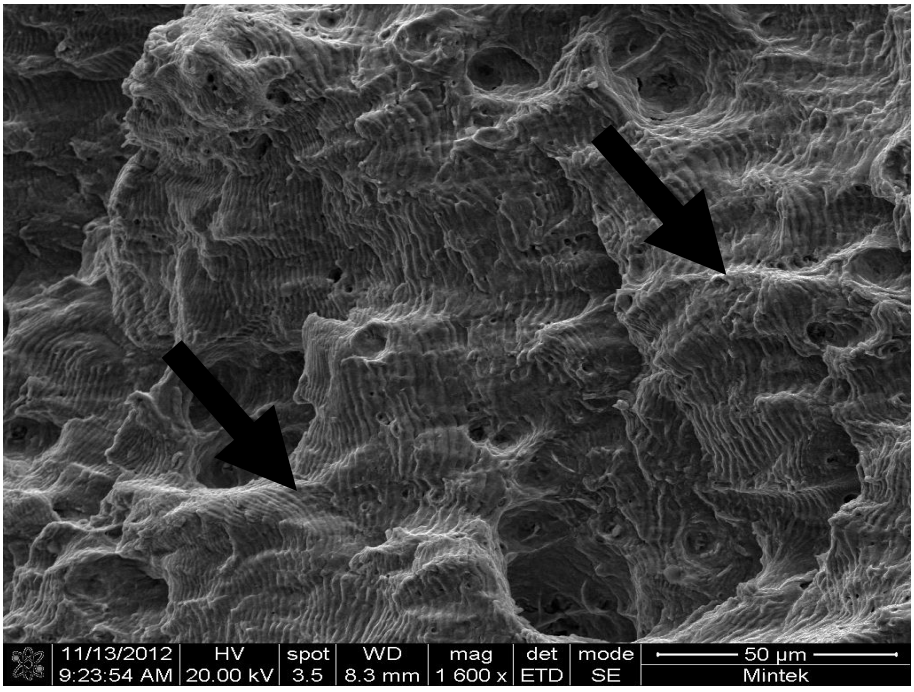

Figure 4.49. Crack propagation zone of AISI 316L sample carburised at 450°C showing fatigue striations.

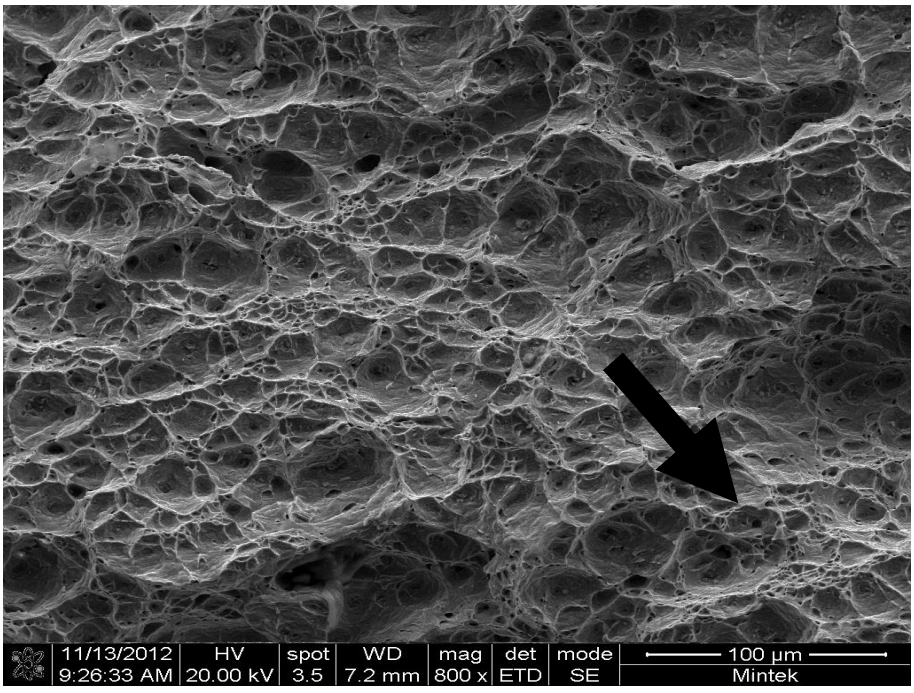

Figure 4.50. Rupture zone of AISI 316L sample carburised at 450°C showing ductile dimple fracture.

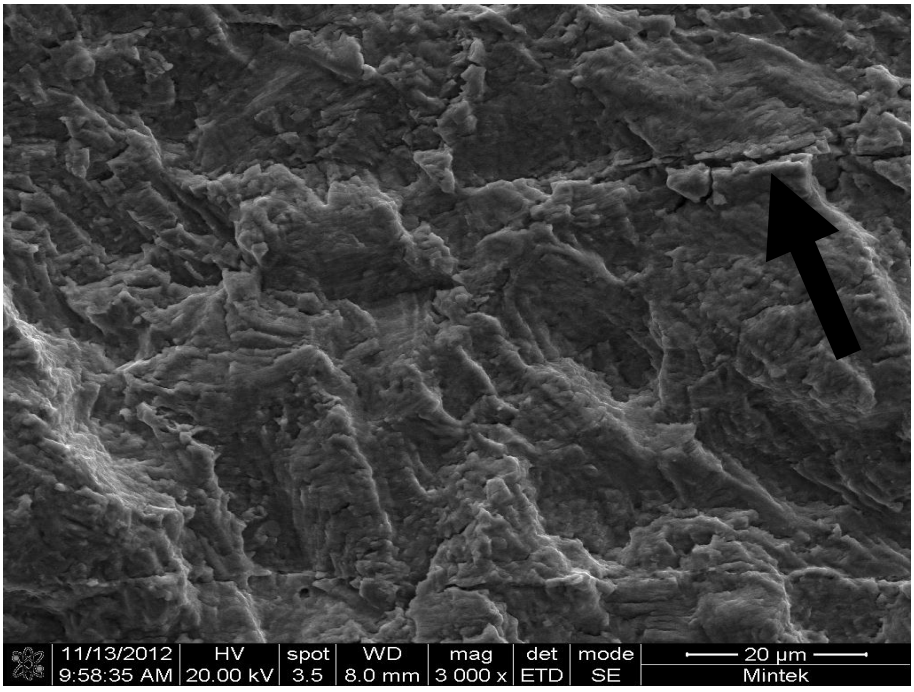

Figure 4.51. Crack initiation zone of AISI 316L sample carburised at 550°C showing brittle (tearing), with the arrow pointing a secondary cracking within the fractured surface.

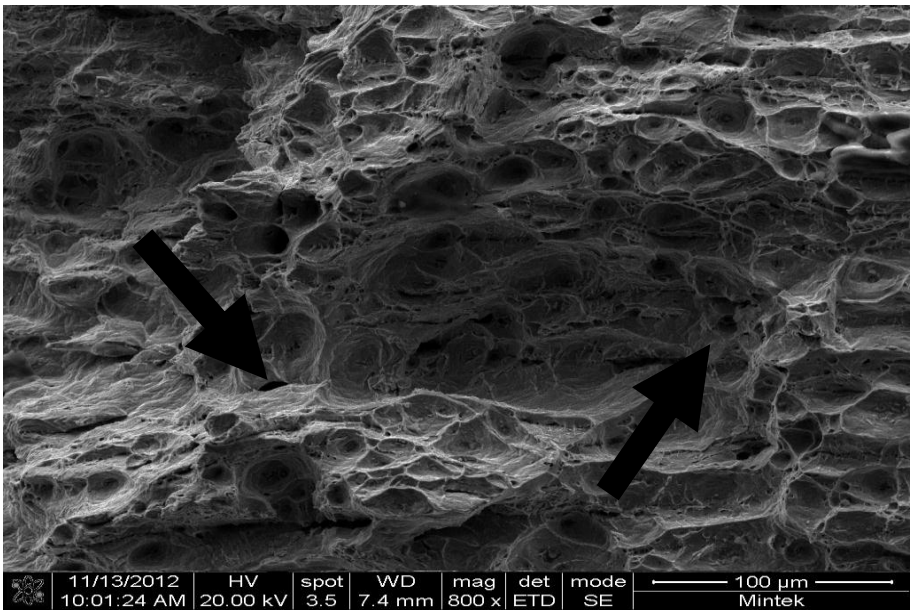

Figure 4.52. Crack propagation zone of AISI 316L sample carburised at 550°C showing less visible ductile striations.

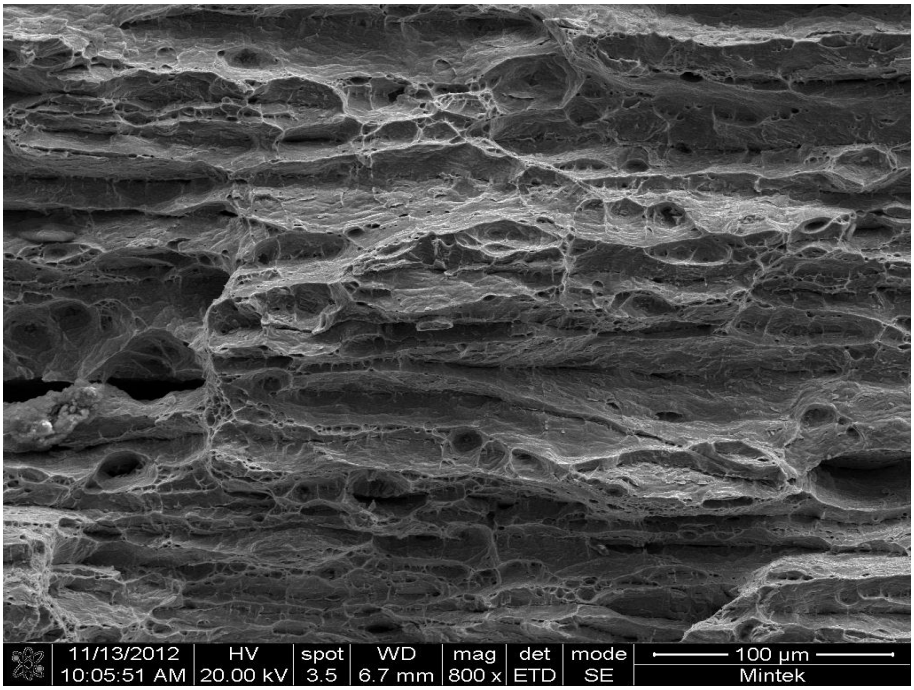

Figure 4.53. Rupture zone of AISI 316L sample carburised at 550°C showing ductile dimples with lineal pattern to fracture.

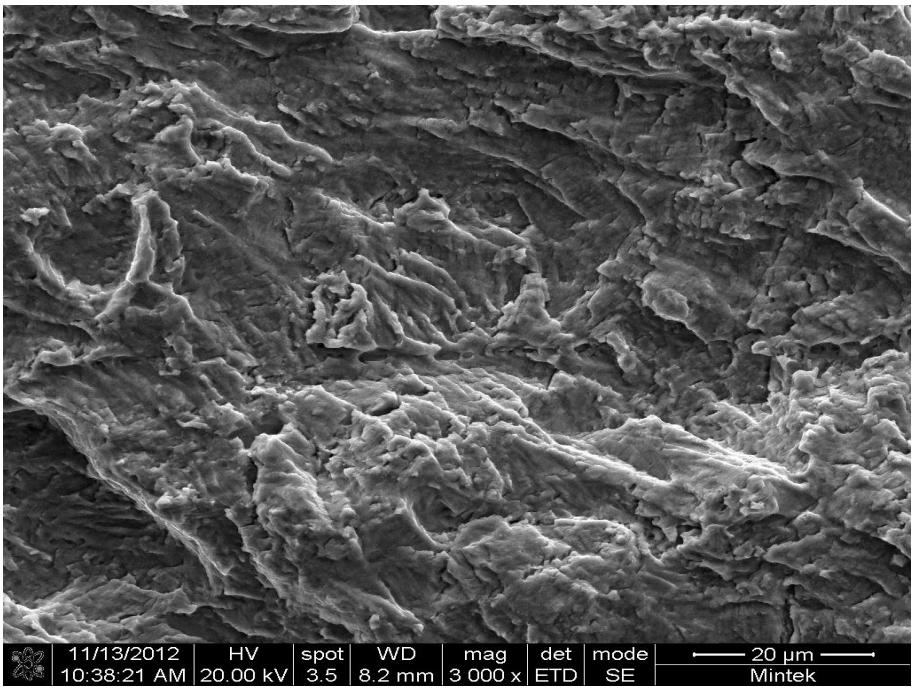

Figure 4.54. Crack initiation zone of AISI 316L sample carburised at 650°C showing brittle (tearing) with dispersed secondary cracking within the fractured surface.

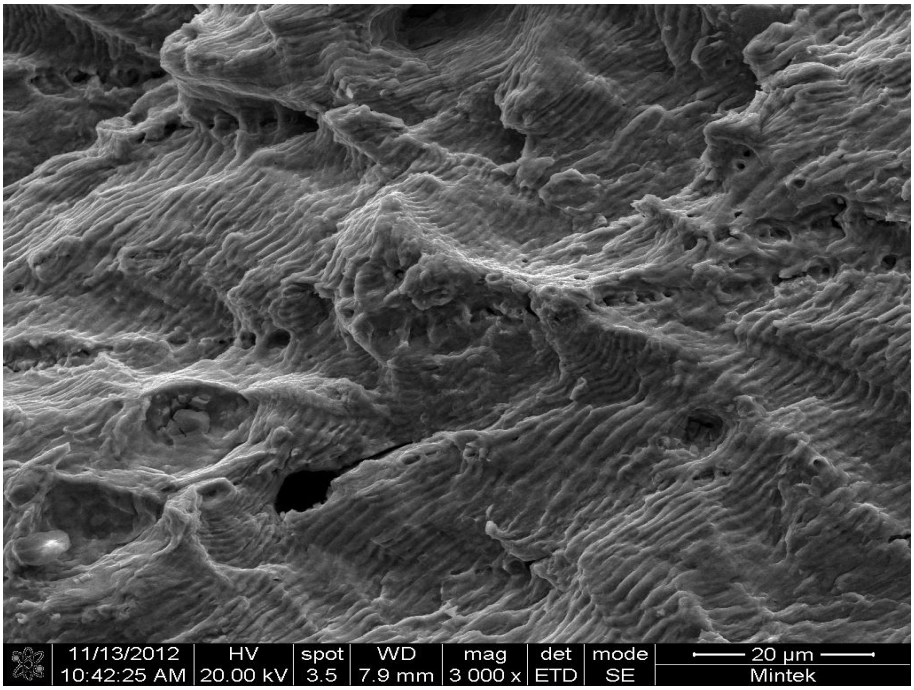

Figure 4.55. Crack propagation zone of AISI 316L sample carburised at 650°C showing fatigue striations.

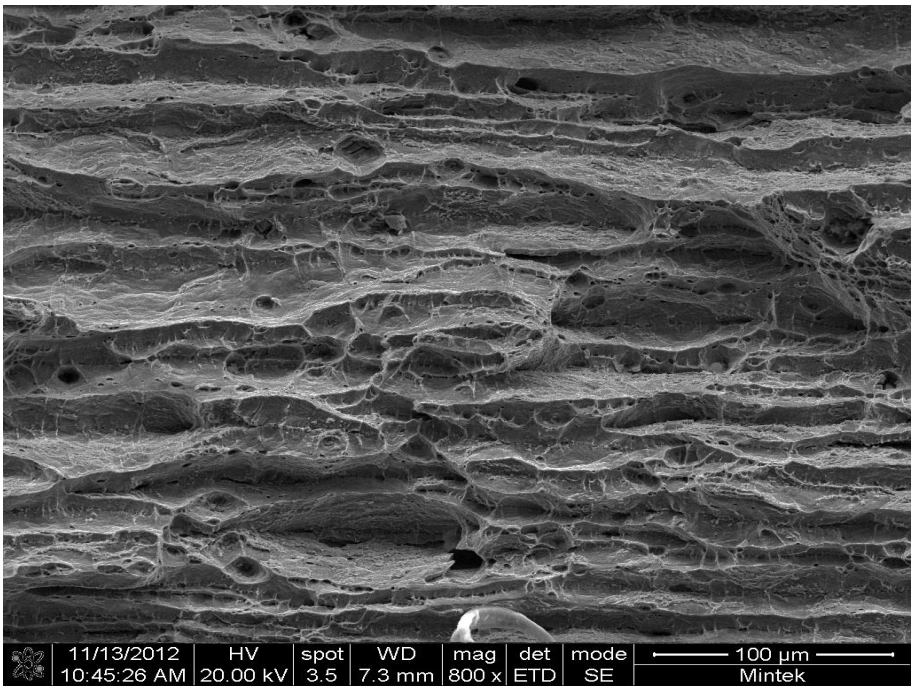

Figure 4.56. Rupture zone of AISI 316L sample carburised at 650°C showing lineal patterns to the fracture.

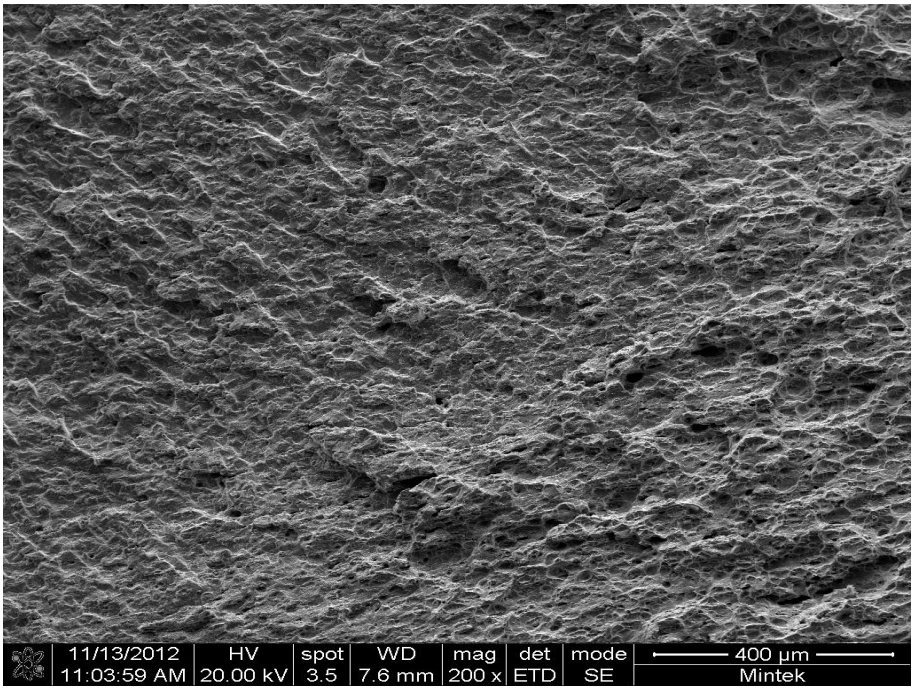

Figure 4.57. Crack initiation zone of AISI 316L sample carburised at 700°C showing brittle (tearing) fracture.

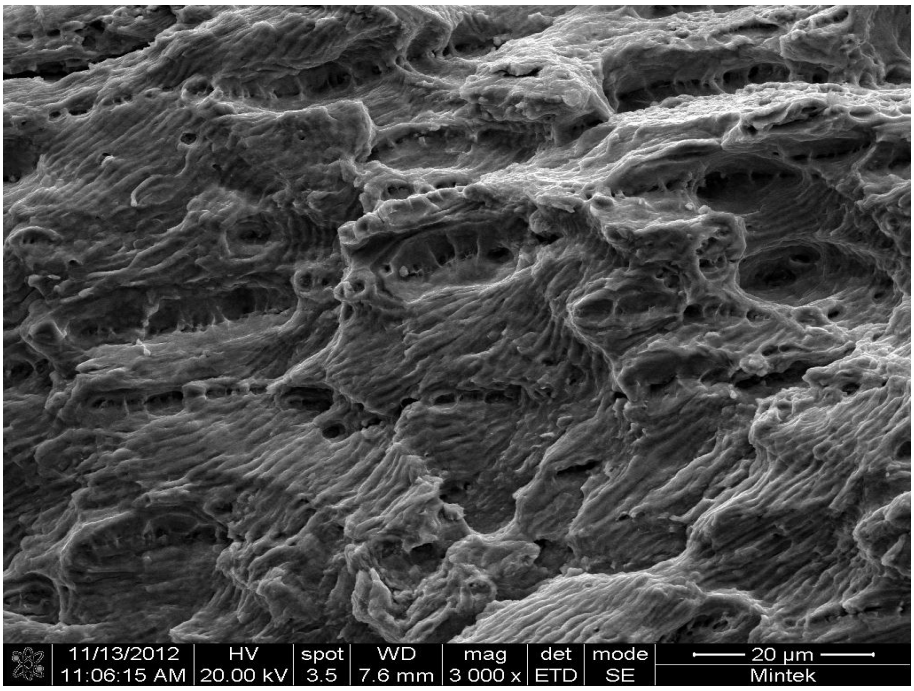

Figure 4.58. Crack propagation zone of AISI 316L sample carburised at 700°C showing fatigue striations.

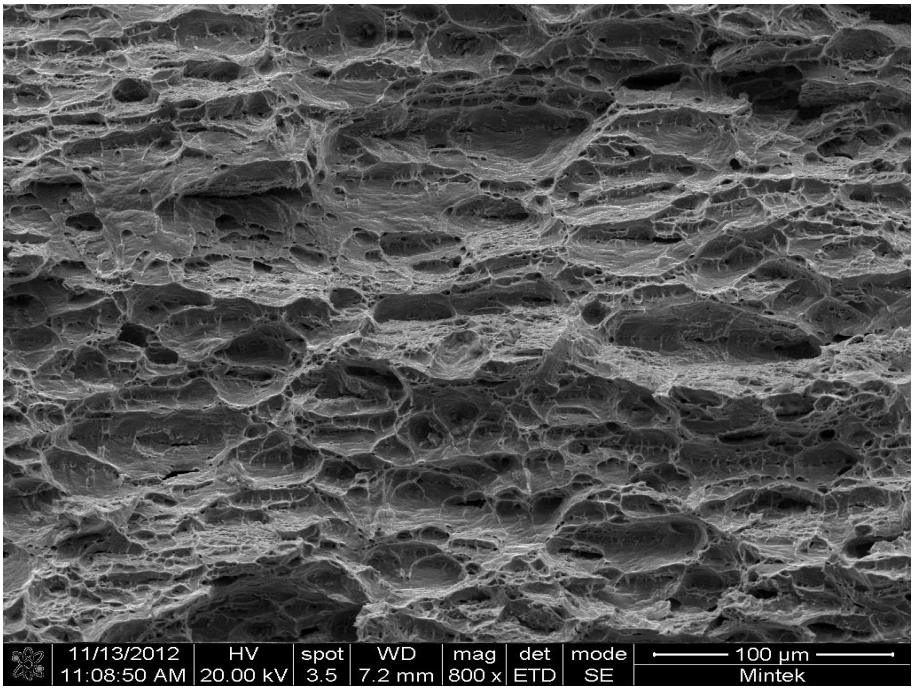

Figure 4.59. Rupture zone of AISI 316L sample carburised at 700°C showing ductile dimple fracture.

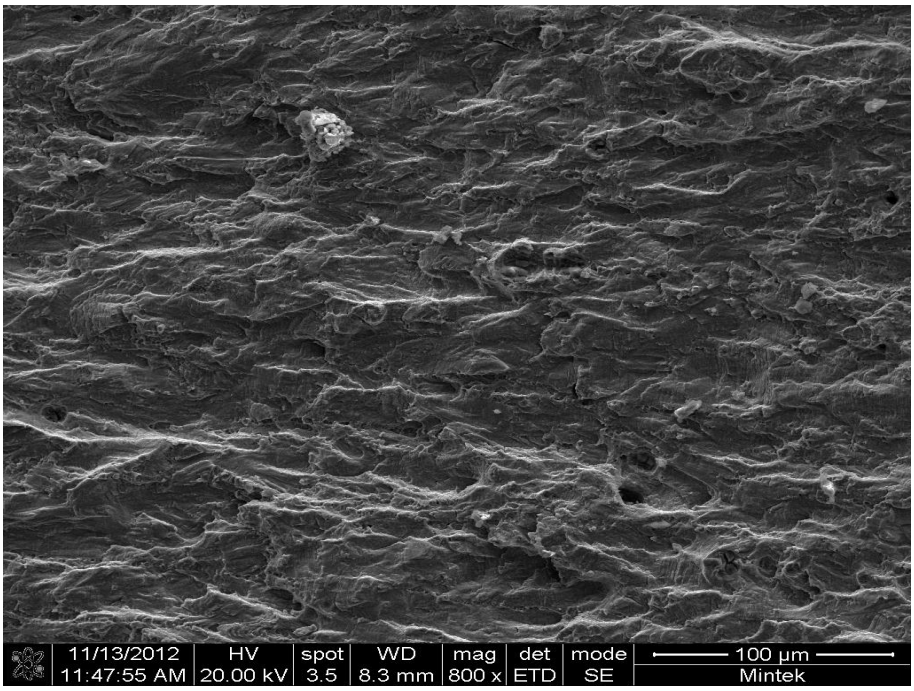

Figure 4.60. Crack initiation zone of AISI 316L sample carburised at 750°C showing brittle (tearing) fracture.

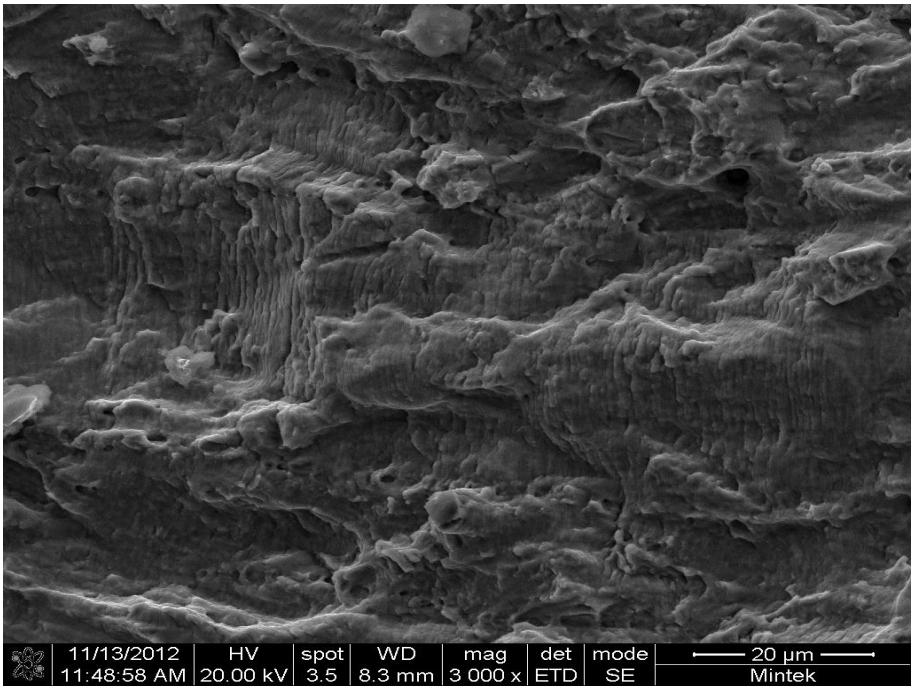

Figure 4.61. Crack propagation zone of AISI 316L sample carburised at 750°C showing fatigue striations.

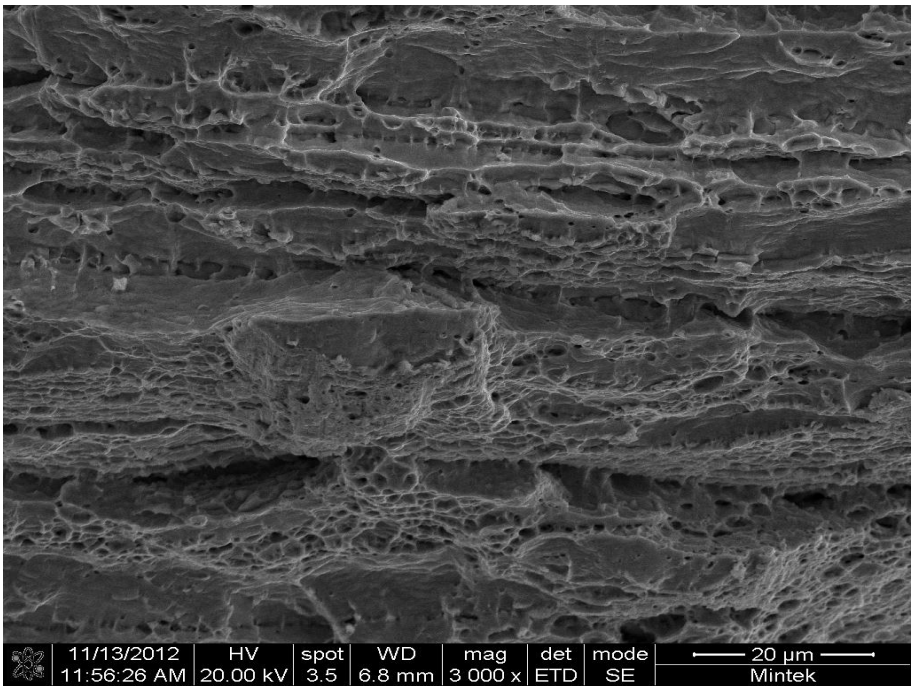

Figure 4.62. Rupture zone of AISI 316L sample carburised at 750°C showing lineal patterns to the fracture.

CHAPTER FIVE

DISCUSSION

"Great minds discuss ideas, average minds discuss events and small minds discuss people."

— Eleanor Roosevelt

5. DISCUSSION

In Figure 4.1, the tensile strength of the as-received sample was 647±4MPa. It then increased slightly at carburising temperatures of 450°C and 550°C, although within the errors, so was not significant. The initial increase could have been due to the formation of fine carbides on the surface and near the surface of the steel. The large decreases above the 550°C carburising temperature showed that the high temperatures were compromising the properties. This compromise could result from carbide precipitation and grain boundary oxidation in the grains and on the grain boundaries. Although there was carbide precipitation, the pack carburising treatment from 450ºC-750ºC did not induce the expanded austenite structure as reported for low plasma carburising temperatures below 450ºC [1999Sun, 2002Bel, 2006Chr]. For low temperature plasma carburising, expanded austenite or S-phase is a face-centred tetragonal (fct) and a thermodynamically metastable structure contributed to improving the mechanical properties of the AISI 316L austenitic stainless steels [1999Sun, 2002Bel, 2006Chr].

For austenitic stainless steels, carburising heat treatment done at temperatures ranges of 450ºC-800ºC result in metal dusting and sensitisation (intergranular corrosion) [1968Sta, 1984Mar, 2005Chu]. However, investigation by pack carburising within the temperature regime of 450ºC to 750ºC suggests no evidence of metal dusting and intergranular corrosion (sensitization) as reported in literature.

Ductility measures the degree of plastic deformation sustained by a material prior to fracture. If little or no plastic deformation occurred, the material is termed “brittle”. The as-received AISI 316L sample had a good ductility and toughness, which is due to the fcc crystal structure possessed by austenitic stainless steel. The fcc crystal structure provides more planes for the flow of dislocations, combined with the low level of interstitial elements (that can help to lock the dislocations) gives the material its good ductility. This also explains why austenitic stainless steels do not have a clearly defined yield point, which is why the proof stress is used. Ductility, quantitatively measured by elongation and reduction in area, decreased with increasing temperature (Figure 4.2), with the

decrease after 550°C being much greater. Above 550°C, the passive Cr_2O_3 barrier of AISI 316L steel was overcome. This allowed for the diffusion of sufficient carbon into the steel. There was less ductility as the carburising temperature increased, which could be due to segregation and brittle grain boundary carbides. The uptake of carbon from the surface of the steel also resulted in surface hardening, reducing the ductility of the stainless steel.

The hardness-depth profile of samples treated at 450°C and 550°C (Figure 4.3) indicated very little change in their surface hardness values, showing that little case hardening had occurred. After carburising, about 10g (of the original 250g) of the carburising compound was left in the case. This showed that the samples were not well carburised at these temperatures. Low rates of carbon diffusion into the surface of the steel resulted in a lower hardness increase. The tenacious Cr_2O_3 surface layer served as an inhibiting barrier for the diffusion of carbon into the steel, since no pre-treatment had been done to remove it, hence the inhibiting barrier was not overcome. This led to the negligible change in the surface hardness of samples carburised at 450°C and 550°C, and specimens treated at these temperatures had about the same values as the as-received samples. The as-received material was not homogenous and had pores within the grains and at the grain boundaries. This could possibly explain the variation observed in the hardnesses of the as-received samples and carburised samples at 450°C and 550°C. At temperatures below 550°C, longer times are required to allowed sufficient diffusion of carbon atoms into the stainless steel for effective carburising [2008Ces]. However, the soaking time for samples carburised 450°C and 550°C was 24 hours, which was not enough to cause adequate carburising of the steel at temperatures below 550°C, thus giving a negligible carbon intake.

Figure 4.4 shows the hardness-depth profile of samples treated at temperatures of 650°C, 700°C and 750°C. The hardness was greater at the surface than the core, as expected and showed a typical carburising profile [1961Bai, 2008Ces]. This indicated an appreciable intake of carbon and carbon enrichment from the carburising, which also explained the greater decrease in the ductility and toughness. The hardening mechanism can be attributed to the expansion experienced by the carburised layer and distortion of the

austenite lattices, resulting in the formation of high density dislocations and stacking faults [2005Tsu1, 2005Tsu2]. These dislocations and stacking faults gave the improvement of surface hardness at temperatures above 650°C. Hardness values associated with surface treated AISI 316L steels by plasma or gas carburising improved at least five times compared to the untreated values [1999Ren, 2000Few, 2006Min]. These high hardness values were achieved by removing formed Cr_2O_3 surface layer by either chemical or mechanical means, which was not done in the current samples, so the hardness increases were less.

The amount of (Charpy) energy absorbed by the AISI 316L steel is shown in Figure 4.5. As the carburising temperature increased, the energy values of the samples decreased, which indicates a decrease in toughness of the material. The decrease in toughness can be attributed to the uptake of carbon, causing surface hardening making and the material more brittle and so less ductile. The stacking faults and high density dislocations due to austenite lattice distortion and expansion as a result of the carburising could also contribute to the decrease in the toughness of the material [URLMat].

Figure 4.6 shows the effect of carburising temperatures on the fatigue strength of AISI 316L stainless steel. The number of cycles to failure for the as-received AISI 316L steel and samples carburised from 450°C-650°C was ranged between 59298±2520 and 61455±15076. The fatigue strength with these treatment parameters were fairly similar and within the margin of errors. As the carburising temperature increased above 650°C, the number of cycles to failure decreased significantly, thus 25387 and 7146 for 700°C and 750°C. Although 316L could not be hardened by heat treatment, carburising heat treatment done at temperatures above 650°C could lead to stress relief which otherwise reduced compressive residual stresses induced in the material since it was rolled [URLStr]. A reduction in compressive residual stresses could led to significant decrease in fatigue strength at temperatures of 700ºC and 750ºC, hence less number of cycles to fatigue failure. The decreased fatigue strength at high carburising temperatures could also due to the microstructural effects of the carburising.

Microstructural observation of all the samples revealed large voids within the materials. (Voids are volume defects in a material in which large number of atoms are missing from

the crystal lattice). These volume defects were probably introduced into the material as a result of the fabrication and processing routes. Figures 4.19 and 4.20 showed large volume defects, slip lines and annealing twins throughout the as-received material. Due to these defects in the AISI 316L steel, any crack induced in the material can easily propagate through the defects which could lead to catastrophic failure. Thus, these volume defects hence served as sites for crack propagation. This led to the lower fatigue strength observed generally in the AISI 316L, although this was not the case for Ceschini *et al.* [2008Ces] and Tokaji *et al*. [2004Tok] who used similar material.

The EDX analysis of the near surface of the as-received showed the presence of oxides in the material (Figure 4.22). Oxides are more ceramic in nature hence very brittle and their presence in the material could reduce the ductility of the AISI 316L steel. As the carburising temperature of the AISI 316L steel increased, more carbides and oxides precipitates were observed which is showed by the EDX analysis by Figures 4.22, 4.25, 4.46, 4.29, 4.30 and very high oxides on the surface of samples treated at 700ºC (Figures 4.39 and 4.44). The entrapment of oxygen was as a result of the carburising procedure. The lid of the carburising was not air tight hence oxygen easily diffused into the material during the carburising process at these relatively high temperatures. These oxides also contributed to the loss in ductility and toughness of AISI 316L steel as shown in Figure 4.2. The exposure of AISI 316L steel to atmospheric oxygen (non air tight lid) resulted in the formation of an oxide film on the surface. A protective thin passive layer was formed on the surface at low temperatures, and as temperature increased the thickness increased considerably and was unacceptably high above the scaling temperature. Generally, in the temperature range of 640ºC-950ºC, elements whose oxides can either melt or form eutectics with chrome oxide (Cr_2O_3) will result in catastrophic oxidation. Grain boundary oxidation was observed at carburising temperatures above 650ºC (Figures 4.35, 4.36, 4.40 and 4.41). Due to the brittleness of oxides and considering the fact that they are located at the grain boundaries can result in catastrophic failures. A brittle grain boundary can serve as a site for crack propagation once the grain is initiated from the surface of the AISI 316L [1979Bri, 2001Zav]. This could explain why there was a very low number of cycles to failure for AISI 316L steel treated at the temperatures; hence the low fatigue strength observed in the material at these temperatures.

There are carbide distributions throughout the steel and the EDX analysis of all the samples showed that as the carburising temperature increases the rate of carbon diffusion also increased resulting in more carbide precipitation in the grains and on the grain boundaries. Embrittlement of the steel is caused by carbon pick-up as a result of the carbide formation or even network of carbides which are formed in the grain boundaries and within the grains. The increase in volume of carbides suggests that the grains are rapidly broken away from the steel surface, which could be given serious grain boundary attack at temperatures above 550ºC.

Other microstructural features observed in all samples were slip lines and some annealing twins. Mechanical or annealing twins are deformation that interacts with dislocation glides. This then provides strain-hardening effect in low stacking fault energy face-centred cubic metals and alloys [2013Ste]. A disruption of a long-range stacking sequence in a material can result either a stacking fault or a twin region. If the change in the sequence is over a few atomic spacing then it is referred to as stacking fault, however, if the change is over many atomic spacing then a twin region is produced. These features also strengthen the material by impeding dislocation movement [2009Ciu]. The presence of annealing twins and/or stacking faults also contributed to the strengthening mechanisms of AISI 316L since they impede the movement of dislocation in the material.

Macrostructural examination of the fractured surface of the specimens indicated small step-like features. Fracture surfaces that have these step-like features indicate that the cracks were initiated from multiple origins. These small step-like features are known as the ratchet marks. As two or more approaching cracks from different levels meet, it creates small step-like features, thus ratchet marks [2002ASM]. Ratchet marks were apparent on the periphery of fractured fatigue surfaces, the step appearance is characteristic whenever fatigue crack emanate from several origins and a principal crack front is subsequently formed [2002ASM]. Multiple crack initiation sites are due to the presence of high stresses or high stress concentrations sites.

The presence of thumbnails in the fractured surfaced showed small fatigue cracks. Most of the thumbnails were at the centre of the fractured surfaces. The position of the

thumbnails also determines the initiation site of the crack that led to the failure [1996ASM]. Thumbnails are derived from machining marks on the surface of the materials. The initiations of cracks are triggered by these marks and other surface defects on the material. Generally, fatigue cracks start at the surface of the material but internal defects, inhomogeneous residual stress distribution and fatigue-resistant structures on the surface of the material (shot peened surface layer, nitrided layer, carburised layer, etc.) can protect against fatigue cracks starting at the surface [1996ASM].

The fractured surface of the as-received and all the carburised samples showed brittle fracture (tearing) at the initiation stage (Figure 4.45). SEM analyses of the fracture surface of the as-received AISI 316L steel showed that crack initiation occurred at the surface, irrespective of the stress level due to the cyclic and fatigue slip bands, as observed by Ceschini *et al.* [2008Ces] The cause of initiation of the cracks could be attributed to surface defects such as machining lines. The brittle tearing is a mode III type of fracture, in which shear stresses act parallel to both the crack front and the plane of the crack. The as-received material was ductile, hence there was some plastic deformation, which resulted in the brittle tearing, instead of brittle fracture characterized by quasi-cleavage with low release energy and without significant plastic deformation. Figure 4.46 shows the crack propagation zone which was characterized by crack arrest marks or striations. This is characteristic of fatigue crack growth, hence crack propagation was mainly fatigue due to the fluctuating stresses. Fatigue crack growth is a slow crack growth, as a result of load variations within the material, hence the corresponding variations in the crack growth rate which appeared as the striations or crack arrest marks (incremental advance patterns of the fatigue crack) shown in Figure 4.46. The final stage of the fractured surface, which is shown in Figure 4.47, was more of ductile dimple rupture, with dimples and presence of more visible microvoids. Ductile dimple fracture formation occurred through the formation and coalescence of microvoids along the fractured path. This was observed in all the crack termination points of the as-received sample. The fractured surface appeared dimpled, as shown in Figure 4.47.

The fracture surfaces for all samples carburised at 450ºC to 750ºC had similar initiation, propagation and crack rupture patterns as to the as-received samples. Most of the

carburised samples also showed the secondary cracking within the materials. This is shown with the arrows on Figures 4.48 and 4.51. The crack initiation stage was mostly brittle tearing fracture, due to the ductile to brittle nature of the AISI 316L steel. The loss in ductility was due to the carbon intake by the AISI 316L steel. Fatigue striations, the most characteristic feature of fatigue failure were also observed (Figures 4.49, 4.55 and 4.58). Due to the presence of these features (striations), it can be said that AISI 316L underwent fatigue crack propagation and then the final fractured surface was by ductile dimple rupture.

Figures 4.53, 4.56 and 4.62 showed more of a mixed mode. There is a lineal pattern to the fracture, like an incremental tearing, which could be due to either chemical or microstructural segregation patterns. The cracks could be running parallel or perpendicular to the hot working directions of the AISI 316L steel.

It is therefore evident that the pack carburising process was not beneficial because it impacted negatively on the mechanical properties of the AISI 316L austenitic stainless steel.

CHAPTER SIX

CONCLUSION

"People don't like to think, if one thinks, one must reach conclusions. Conclusions are not always pleasant."

— Helen Keller

6. CONCLUSION

From the results and discussion, it can be concluded that the mechanical properties of AISI 316L stainless steel were influenced by the process of pack carburisation and the carburising temperature. Mechanical properties such as ductility, toughness, tensile strength and fatigue strength decreased with increasing carburising temperature.

The process of pack carburising had no major influence on samples carburised at temperatures below 550°C due to the tenacious Cr_2O_3 layer that served as a barrier that inhibited the diffusion of enough carbon to improve the surface hardness and other surface-related mechanical properties of the steel. However, at carburising temperatures of 650°C, 700°C and 750°C, the surface hardness improved considerably.

Grain boundary oxidation and precipitates of carbides within the grains and at the grain boundaries were observed at carburising temperatures at and above 650°C which was detrimental to the mechanical properties of AISI 316L stainless steels.

Investigation by pack carburising within the temperature regime of 450ºC to 750ºC suggests no evidence of metal dusting and intergranular corrosion (sensitization) as reported in literature.

The fractured surfaces showed that brittle fracture initiation occurred by brittle tearing, rather than quasi-cleavage. Crack propagation and growth showed patches of finely spaced parallel lines, striations, an indication of fatigue crack propagation. The final rupture zone was characterized by ductile fracture with dimples within the fractured surface.

The pack carburising was unfavourable for AISI 316L steel. The process reduced the mechanical properties compared to the plasma and gas carburising techniques, because it caused carbide precipitation and grain boundary oxidation. Hence, pack carburising is not an appropriate treatment route for improving the mechanical properties of AISI 316L stainless steel, and other processes are preferable.

REFERENCES

"There are no rules here; we're trying to accomplish something."

— Thomas A. Edison

REFERENCES

[1899Goo] J. Goodman, Mechanics Applied to Engineering, Longmans Green, London, UK (1899).

[1903Ewi] J.A. Ewing and J.C.W. Humfrey, The fracture of metals under repeated alternations of stress, Philosophical Transactions of the Royal Society (1903) 241-250.

[1909For] R. Forsythe, The blast furnace and the manufacture of pig iron, Second Edition, David Williams Company, New York, USA (1909).

[1911Mon] P. Monnartz, Iron-chromium alloys with special consideration of resistance to acids, Metallurgie, 8 (7) (1911) 161-176.

[1920Cam] J.M. Camp and C.B. Francis, The making, shaping and treating of steel, Carnegie Steel Company, Pittsburgh, PA, USA (1920).

[1927Bai] E.C. Bain and W.E Griffiths, An introduction to the iron-chromium-nickel alloys, Transactions of the American Institute of Mineral and Metallurgical Engineering, 75 (1927) 166-213.

[1933Bai] E.C. Bain, R.H. Aborn and J.J.B. Rutherford, The nature and prevention of intergranular corrosion in austenitic stainless steels, Transactions of the American Steel Treating Society, 21 (1933) 481-509.

[1936Boy] H.M. Boylston, An introduction to the Metallurgy of Iron and Steel, New York, John Wiley Publishers, USA (1936).

[1937Jen] C.H.M. Jenkins, E.H. Bucknall, C.R. Austin and G.A. Mellor, Some alloys for use at high temperatures. Part IV: The Constitution of the Alloys of Nickel, Chromium and Iron, Journal of Iron and Steel Institute, 136 (1937) 187-222.

[1939Ast] J. Aston and E.B. Story, Wrought Iron - Its manufacture, characteristics and Applications, Second Edition, A.M. Byers Company, Pittsburgh, Pennsylvania, USA (1939).

[1939Sod] C.R. Soderberg, Factor safety and working stress, Transactions ASME, 52 (1939) 13-28.

[1948Uhl] H.H. Uhlig, The Corrosion Handbook, Wiley, New York; Chapman and Hall, London, UK (1948).

[1949Col] F.C. Collins and G.E. Kimball, Diffusion-controlled reaction rates, Journal of Colloid Science, 4 (4) (1949) 425-437.

[1949Sch] A.L. Schaeffler, Constitution diagram for stainless steel weld metal, Metal progress, 56 (1949) 680-680B.

[1949Zap] C.A. Zapffe, Stainless Steels, American Society for Metals (ASM), Materials Park, OH, USA (1949).

[1951Hen] E.K. Henriksen, Residual stresses in machined surfaces, Transactions ASME Journal of Engineering for Industry, 73 (1951) 69-76.

[1951Obe] T.L. Oberle, Properties influencing wear of metals, Journal of Metals, 3 (1951) 438-439.

[1953Arc] J.F. Archard, Contact and rubbing of flat surfaces, Journal of Applied Physics, 24(8) (1953) 981-988.

[1953Hea] A.K. Head, The growth of fatigue cracks, Philosophical Magazine, 44 (7) (1953) 925-938.

[1953Man] S.S. Manson, Behaviour of materials under the conditions of thermal stresses: National Advisory Committee for Aeronautics, NACA-TN-2933, Cleveland, OH, USA (1953).

[1954Bow] F.P. Bowden and D. Tabor, The Friction and Lubrication of Solids, 2nd Edn., Clarendon Press, Oxford, UK (1954).

[1954Cof] L.F. Coffin Jr, The effect of cyclic thermal stresses on a ductile material, Transactions of the ASME 76 (1954) 931-950.

[1954Dar] L.S. Darken and R.A. Oriani, Thermal diffusion in solid alloys, Acta Metallurgica, 2 (6) 841-847.

[1956Arc] J.F. Archard and W. Hirst, The wear of metals under unlubricated conditions, Proceedings of the Royal Society of London A: Mathematical and Physical Sciences 236 (1956) 397-410.

[1959Ehr] G. Ehrlich and D. Turnbull, 'Shock-induced martensitic transformation', Physical Metallurgy of Stress Corrosion Fracture, Interscience, New York, USA (1959).

[1959God] J. Goddard, H.J. Harker and H. Wilman, A theory of the abrasion of solids such as metal, Nature, 184 (1959) 333-335.

[1959Hat] H. Hatwell and A. Berghezan, Nucleation and growth of the chromium precipitates on coherent twin boundaries in austenitic stainless steels; Collection of papers on precipitation processes in steels, Percy Lund Humphries, London, UK (1959).

[1960Pry] L. Pryce and K.W. Andrews, Practical estimation of composition balance and ferrite in stainless steels, Journal of Iron and Steel Institute, 195 (1960) 415-417.

[1961ASM] American Society for Metals, ASM Handbook, The selection of stainless steel for atmospheric and marine corrosion service in "Metals Handbook Vol. 1: Properties and selection of metals' 8th Edn., American Society for Metals, Novelty, Ohio, USA (1961) 552-576.

[1961Bai] E.C. Bain and H.W. Paxton, Alloying Elements in Steels, 2nd Edn., American society of Metals, Metals Park, Ohio, USA (1961).

[1961Ped] R. Pederson and R.L. Rice, Case crushing of carburised and hardened gears, Transactions SAE, 250 (69) (1961) 370-380.

[1961Rab] E. Rabinowicz, L.A. Dunn and P.G. Russell, A study of abrasive wear under three-body conditions, Wear, 4 (5) (1961) 345-355.

[1962Hil] M. Hillert, 'Formation of Pearlite', Decomposition of Austenite by Diffusional Processes, Interscience, London, UK (1962).

[1962McL] D. McLean, Mechanical Properties of Materials, John Wiley, New York, USA (1962).

[1962Ver] D.A. Vermilyea, Proceedings of the First International Congression on Metallic Corrosion, Butterworth, London, UK (1962).

[1963Lan] J.K. Lancaster, The formation of surface films at the transition between mild and severe metallic wear, Proceedings of the Royal Society of London A: Mathematical and Physical Sciences, 273 (1355) (1963) 466-483.

[1963Seg] R.L. Segall, Electron microscopy and strength of crystals, EDX: G. Thomas and J. Washburn, Interscience, New York, USA (1963) 515.

[1964Ben] J.A. Bennett, in Fatigue – An Interdisciplinary Approach, Syracuse University Press, Syracuse, New York, USA (1964) 209-227.

[1964Bra] D.G. Brandon, B. Ralph, S. Ranganathan and M.S. Wald, A field ion microscope study of atomic configuration of grain boundaries, Acta Metallurgica, 12 (1964) 813-821.

[1966Daw] C. Dawes and R.J. Cooksey, Surface treatment of engineering components, Heat Treatment of Metals, Special Reports 95 (47) (1966).

[1966Lew] M.H. Lewis, Precipitation of (Fe, Cr) sigma phase from austenite, Acta. Metallurgica, 14 (1966) 1421-1428.

[1966Oso] K. Osozawa, K. Bohnenkamp and H.J. Engell, Potentiostatic study on the intergranular corrosion of an austenitic chromium-nickel stainless steel, Corrosion Science, 6 (1966) 421-433.

[1966Yok] T. Yokobori and M. Nanbu, Reports of the Research Institute of Strength and Fracture Materials, Tohuku University, Japan (1966) 29.

[1967Fel] C.E. Feltner and C. Laird, Cyclic stress-strain response of F.C.C. metals and alloys: Dislocation structures and mechanisms, Acta Metallurgica, 15 (1967) 1633-1653.

[1967Mar] J.A. Martin and A.D. Eberhardt, Identification on potential failure nuclei in rolling contact fatigue. Trans. ASME, Journal of Basic Engineering, 89 (1967) 932-942.

[1967Slu] C.J. Slunder, A.F. Hoeine and A.M. Hall, Thermal and mechanical treatment for precipitation-hardening stainless steels, National Aeronautics and Space Administration SP-5089 (1967) 1-193.

[1967Sum] G. Sumner, The low endurance fatigue behaviour of 20Cr-25Ni/Nb stainless steel at 25, 650 and 750°C, Conference on Thermal and High strain Fatigue, London, Metal and Metallurgy Trust Monograph, 32 (1967) 295-305.

[1968Col] L. Colombier and J. Hochmann, Stainless and heat resisting steels, St. Martin's Press, New York, USA (1968).

[1968Hor] J. Horvath and H.H. Uhlig, Critical potentials for pitting corrosion of Ni, Cr-Ni, Cr-Fe and related stainless steels, Journal of the Electrochemical Society, 115 (1968) 791-795.

[1968Lan] J.K. Lancaster, Relationship between the wear of polymers and their mechanical properties, Proceedings of the Institute of Mechanical Engineers 183 (16), London, UK 1st September, 1968, 98-106.

[1968Tom] B. Tomkins, Fatigue crack propagation-an analysis, Philosophical Magazine, 18 (155) (1968) 1041-1046.

[1969Sta] C. Stawstrom and M. Hillert, An improved depleted zone theory of intergranular corrosion of 18-8 stainless steel, Journal of Iron and Steel Institute, 207 (18) (1969) 77-85.

[1969Tom] B. Tomkins and W.D. Biggs, Low endurance fatigue in metals and polymers - Part 3: The mechanisms of failure, Journal of Materials Science, 4 (6), (1969) 544-553.

[1970Cih] V. Cihal and I. Kasova, Relation between carbide precipitation and intercrystalline corrosion of stainless steels, Corrosion Science, 10 (12) (1970) 875-881.

[1972Bar] N.C. Barbi and G. Judd, Microstructure and microsegregation effects in the intergranular corrosion of austenitic stainless steel, Metallurgical Transaction A: Physical Metallurgy and Materials Science, 3 (1972) 2959-2964.

[1972Hur] P.L. Hurricks, Some aspects of the metallurgy and wear resistance of surface coatings, Wear, 22 (3) (1972) 291-319.

[1972Lan] J. Lankford and F.N. Kusenberger, On crack tip yielding during fatigue cycling of a high-strength steel, Philosophical Magazine, 26 (6) (1972) 1485-1490.

[1972Wei] B. Weiss and R. Stickler, Phase instabilities during high temperature exposure of 316 austenitic stainless steel, Metallurgical Transactions A, 3A (1972) 851-866.

[1973Cha] K.D. Challenger and J. Moteff, Correlation of substructure with elevated low-temperature low-cycle fatigue of AISI 304 and 316 stainless steels, American Standard for Testing and Materials, STP 520 (1973) 68.

[1973Ede] B. Edenhofer, Carbonitriding in the plasma of glow discharge, Haerterei-Technische Mitteilungen, 28 (3) (1973) 165-172.

[1973Gel] M. Gell and G.R Leverant, Mechanisms of high temperature fatigue at elevated temperature, American Society for Testing and Materials, STP 520 (1973) 37-67.

[1973Lan] J. Lankford and F.N. Kusenberger, Initiation of fatigue cracks in 4340 steel, Metallurgical Transactions A, 4 (1973) 553-559.

[1973War] J. Wareing, B. Tomkins and G. Summer, Fatigue at elevated temperatures American Society for Testing and Materials 520, Philadelphia, USA (1973) 123.

[1974Abd] H. Abdel-Raouf, A. Plumtree and T.H. Topper, Temperature and strain rate dependence of cyclic deformation response and damage accumulation in oxygen-free high thermal conductivity (OFHC) copper and 304 stainless steel, Metallurgical Transactions, 5 (1) (1974) 267-277.

[1974Bri] C.R. Brinkman, G.E Korth and J.M. Beeston, Comparison of strain controlled low cycle fatigue behaviour of stainless steel type 304/308 weld and base material, International Conference on Creep and Fatigue at Elevated Temperature Applications, Philadelphia, Institute of Mechanical Engineers (1974) 218.1-218.11.

[1974Kre] E. Krempl, Influence of state of stress on low-cycle fatigue of structural materials, a literature survey and interpretive report, American Society for Testing and Materials, Philadephia, USA (1974).

[1974Lut] R.G. Luther and T.R.G. Williams, Influence of surface reinforcement on the fatigue strength of low carbon steel, Metallurgia and Metal Forming, 41 (1974) 72-80.

[1975Hal] J. Halling, A contribution to the theory of mechanical wear, Wear, 34 (1975) 239-249.

[1975Mai] P. Maiya (1975), Considerations of crack initiation and crack propagation in low cycle fatigue Scripta Materialia, 9 (1975) 1141-1147.

[1975The] K.E. Thelning, Steel and Its Treatment, 1st Edn., Butterworths, London, UK (1975).

[1977ASM] Carburising and Carbonitriding, Committee on gas carburising, A.S.M.: 1st Edn., American Society of Metals, Metals Park, Ohio, USA (1977).

[1977Dum] J.H. Dumbleton and J.A. Douthett, The unlubricated adhesive wear resistance of metastable austenitic stainless steel containing silicon, Wear, 42 (1977) 305-332.

[1977Tom] B. Tomkins and J. Wareing, Elevated temperature fatigue interactions in engineering materials, Journal of Metal Science, 11 (1977) 414-424.

[1978Bos] A. Bos, A contribution to the theory of wear-the abrasive wear of a soft surface against a rough hard surface, Wear, 50 (1978) 127-144.

[1978Sma] R.F. Smart, Selection of surface treatments, Tribology International, 11 (1978) 97-104.

[1979Bri] C.L. Briant and S.K. Banerji, Intergranular failure in steel: the role of grain boundary composition, International Metals Reviews, 23 (1979) 164-199.

[1979Jou] G.E. Journeaux, J.W. Martin and D.E.G. Talbot, Mechanism of environment sensitive cracking of materials, Proceedings: International conference of Metal Society, Editors: P.P Swann, I.P. Ford, A.R.C. Westwood, Surrey, UK (1979) 322.

[1979Ill] J.M. Illston, J.M. Dinwood and A.A. Smith, Concrete, timber and metals: The nature and behaviour of structural materials, Van Nostrand Reinhold Comp. New York, USA (1979).

[1979Pic] F.B. Pickering, Introduction: The Metallurgical Evolution of Stainless Steel, 1st Edn., The Metal Society, London, UK (1979).

[1979Sed] A.J. Sedriks, Corrosion of Stainless Steels, 1st Edn., John Wiley and Sons, New York, USA (1972).

[1979Str] M.A. Streicher, Stainless steels: past, present and future in 'The Metallurgical Evolution of Stainless Steel' 1st Edn., The Metals Society, London (1979) 442-475.

[1979War] J. Wareing and H.G. Vaughan, Influence of surface finish on low-cycle fatigue characteristics of type stainless steel at 400ºC, Journal of Metal Science, 13 (1) (1979) 1-8.

[1980Hsu] K.L Hsu, T.M. Ahn and D.A Rigney, Friction, wear and microstructure of unlubricated austenitic stainless steels, Wear, 60 (1980) 13-27.

[1980Sar] A.D. Sarkar, Friction and Wear, 1st Edn., Academic Press London, UK (1980).

[1980Sch] B. van der Schaaf, M.I. de Vries and J.D. Elen, The effect of irradiation on creep, fatigue and their interaction in DIN/4948 stainless steel at 823K, In Proceedings: Conference on Engineering Aspects of Creep, Institute of Mechanical Engineers, Sheffield, UK (1980) 153.

[1981Kun] T. Kunio, M. Shinizu, K. Yamada, K. Sakarn and T. Yamamoto, The early stage of fatigue crack growth in martensitic steel, International Journal of Fracture, 17 (2) (1981), 111-119.

[1981Hud] S.J. Hudak, Small crack behaviour and the prediction of fatigue life, Transactions of the ASME, Journal of Engineering Materials and Technology, 103(1) (1981) 26-35.

[1981Rio] E.R. De Los Rios and M.W. Brown, Cyclic strain hardening of 316 stainless steel at elevated temperatures, Fatigue and Fracture of Engineering Materials and Structures, 4(4) (1981) 377-388.

[1981Sly] J. Slycke and T. Ericsson, A study of reactions occurring during the Carbonitriding process, Journal of Heat Treatment, 2 (1981) 3-19.

[1982Bar] F.T. Barwell, The contribution of particle analysis to the study of wear of metals, Wear, 90 (1982) 167-181.

[1982Har] D.R. Harries, Physical metallurgy of Fe-Ni-Cr austenitic stainless steels, Mechanical behaviour and nuclear applications of stainless steel at elevated temperatures, International Conference of Mechanical Behaviour and Nuclear Applications of stainless steel at elevated temperatures, Metal Society, Varese, Italy, 20th-22nd May 1982.

[1982Ish] H. Ishi, Y. Sakakibara and R. Ebara, Effect of heat treatments on the corrosion fatigue properties of 13 PCT chromium stainless steel in 3 PCT NaCl aqueous solution, Metallurgical Transactions, 13 A (1982) 1521-1529.

[1982Woo] D.S. Wood, Mechanical properties data needs in type 316 steel for fast reactors, International Conference of Mechanical Behaviour and nuclear Applications of Stainless steel at Elevated Temperature, Metal Society, Varese, Italy, 20th-22nd May 1982.

[1983Cam] T.B. Cameron, D.E. Diesburgy and C. Kim, Fatigue and overload fracture of carburised steels, Journal of Metals, 62 (1983) 35-37.

[1983Mit] E.J. Mittemeijer, Fatigue of case-hardened steels: role of residual macro and micro stresses, Journal of Heat Treating, 3 (2) (1983) 114-119.

[1983Qui] T.F.J. Quinn, Review of Oxidational wear, Part I: The origin of oxidational wear, Tribology International, 16 (5) (1983) 257-271.

[1983Ske] R.P. Skelton (Ed.), Fatigue at High temperature, Applied Science Publishers Limited, London, UK (1983).

[1983War] J. Wareing, in Fatigue at High Temperatures, Chapter 4, Eds., R.P. Skelton, Applied Science Publishers Limited, London, UK (1983) 135-187.

[1984 Cih] V. Cihal, Intergranular Corrosion of Steels, Materials Science Monographs; 18, Elsevier Science Publishers, London, UK (1984).

[1984Hal] E.L. Hall and C.L. Briant, Chromium depletion in the vicinity of carbides in sensitized austenitic stainless steels, Metallurgical Transactions A, 15A (1984) 793-811.

[1984Keo] S.R. Keown, The history of alloy steels with special reference to Sheffield contributions, Perspectives in Metallurgical Development, The Metals Society, Sheffield, UK (1984) 36-46.

[1984Pic] F.B. Pickering, Physical Metallurgical Development of Stainless Steel, Stainless Steel, Institute of Metals, London, UK (1984) 2-28.

[1984Mar] P. Marshall, Austenitic stainless steels; Microstructure and mechanical properties, Elsevier Applied Science Publishers Ltd, New York, USA (1984).

[1984Smi] A.F. Smith, The friction and sliding wear of unlubricated 316 stainless steel at room temperature in air, Wear, 96 (1984) 301-318.

[1984Str] K.N. Strafford, P.K Datta and C. Googan (Eds.), Coatings and Surface treatments for corrosion and wear resistance, Eliis Horwood, Chichester, U.K (1984).

[1984Van] G.F. Vander Voort, Metallography, Principles and Practice, Materials Science and Engineering Series, McGraw-Hill Inc., New York, USA (1984).

[1984Whi] R.D. Whittle and V.D. Scott, Sliding-wear evaluation of nitrided austenitic alloys, Metallurgical Technology, 11 (1984) 231.

[1985Bog] H.E. Boger and T.L. Gall, Metals Handbook, American Society for Metals, Metals Park, OH, USA (1985).

[1985Par] G. Parrish, and G.S. Harper, Production gas carburising, 1st Edn., Pergamon, Oxford, UK (1985).

[1985Zha] Z.L. Zhang and T. Bell, Structure and corrosion resistance of plasma nitrided stainless steel, Surface Engineering, 1 (1985) 131-136.

[1986But] E.P. Butler and M.G. Burke, Chromium depletion and martensite formation at grain boundaries in sensitised austenitic stainless steel, Acta Metallurgica, 34 (1986) 557-570.

[1986Chi] T.C. Chivers, Nuclear Tribology, a personal perspective, Tribology International, 19 (1986) 225-233.

[1986Mas] T.B. Massalski (Editor in Chief), Binary Alloys Phase Diagram, Volume 1 (EDX: J.L Murray, L.H. Bennett and H. Baker), American Society for Metals, Metals Park, OH, USA (1986).

[1986Rob] W.H. Roberts, Some current trends in tribology in the UK and Europe, Tribology International, 19 (6) (1986) 295-311.

[1986Sed] A.J. Sedriks, Effects of alloy composition and microstructure on the passivity of stainless steels, Corrosion, 42 (1986) 376-389.

[1986Smi] A.F. Smith, The friction and sliding wear of unlubricated 316 stainless steel in air at room temperature in the load range 0.5-90N, Wear, 110 (1986) 151-168.

[1987Bel] T. Bell, Surface engineering: a rapidly developing discipline, European Journal of Engineering Education, 12 (1987) 27-32.

[1987Lim] S.C. Lim, M.F. Ashy and J.H. Brunton, Wear rate transitions and their relationship to wear mechanisms, Acta Metallurgica, 35 (6) (1987) 1343-1348.

[1988Bud] K.G. Budinski, Surface Engineering for Wear Resistance, Prentice Hall Inc., New Jersey, USA (1988).

[1988Dea] P.A. Dearnley, A. Namvar, G.G.A. Hibberd and T. Bell, Some observations on plasma nitriding austenitic stainless steels, Proceedings of the 1st International Conference on Plasma Surface Engineering 1, EDX: E. Broszeit, W.D. Munz, H. Oechsner, K.T. Rie and G.K. Wolf, DGM Informationsgesellchaft, Garmisch-Partenkirchen (1988) 219-226.

[1989Bon] K. Bongartz, W.J. Quadakkers, R. Schulten and H. Nichel, A mathematical model describing carburization in multi-element alloy systems, Metallurgical Transactions A, 20A (1989) 1021-1028.

[1989Gra] S. Grainger, Engineering Coatings - Design and application, Abington Publishing, Cambridge, UK (1989).

[1990Bel] T. Bell, Surface engineering: past, present and future, Surface Engineering, 6 (1990) 31-40.

[1991Bhu] B. Bhushan and B.K. Gupta, Handbook of Tribology: Materials, Coatings and Surface Treatments, McGraw Hill Books Co., New York, USA (1991).

[1991Fig] L.S. Figiel, On Damascus Steel, Atlantis Arts Press, Atlantis, Fla, USA (1991).

[1991Pre] S. Preston, Bending fatigue strength of carburising steel SS2506, Materials Science Technology, 7(2) (1991) 105-110.

[1991Rob] W.H. Roberts, Surface engineering and tribology in general engineering in 'Surface engineering and heat treatment: past, present and future' 1st Edn., The Institute of Metals, London, UK (1991).

[1991Sun] Y. Sun and T. Bell, Plasma surface engineering of low alloy steel, Materials Science and Engineering A: Structural Materials, properties, Microstructure and Processing, A140 (1991) 419-434.

[1992Bel] T. Bell, Surface engineering: its current and future impact on tribology, Journal of Applied Physics, 25 (1992) A297-A306.

[1992Bro] C.R. Brooks, Principles of the surface treatment of steels, Technomic Publishing Company, Inc. Pennsylvania, USA (1992).

[1992Lub] A.A. Lubrecht, R.S. Dwyer-Joyce and E. Ioannides, Analysis of the influence of indentations on contact life. Proceedings of 18th Leeds-Lyon Symposium on Tribology (Eds., D. Dowson, C.M. Taylor and M. Godet) Elsevier, Amsterdam, Netherlands (1992) 173-181.

[1992Mad] R. Maddin, A History of Martensite: Some thoughts on the early hardening of iron, 'Martensite', EDX.: G.B. Oslon and W.S. Owen, ASM International, USA (1992) 11-19.

[1992Rab] E. Rabinowicz, Frictional fluctuations in 'Fundamentals of friction: macroscopic and microscopic processes' 1st Edn., Kluwer Academic Publishers, London, UK (1992) 25-34.

[1993Kwo] H.S. Kwon and S.P. Jang, Effects of Ni on stress corrosion susceptibility of high-Cr ferritic stainless steels in hot Cl^- solution, Corrosion Science, 49 (1993) 802-808.

[1994BSI] British Standard EN 10052:1994, 'Vocabulary of heat treatment terms for ferrous product', BSI, London, www.bsi-global.com.

[1994Wil] D.L. Williamson, O. Ozturk, R. Wei and P.J. Wilbur, Metastable phase formation and enhanced diffusion in fcc alloys under high dose, high flux nitrogen Surface and Coatings Technology, 65 (1994) 15-23.

[1995Tav] A.A. Tavassoli, Assessment of Austenitic Stainless Steels, Fusion Engineering and Design, 29 (1995) 371-390.

[1996Asm] Fatigue and Fracture, ASM Handbook 19, ASM International, The Materials Information Society, Materials Park, Ohio, USA (1996) 713-731.

[1997Vor] B.I. Voronenko, Austenitic-ferritic stainless steel: a state-of-the-art review, Metal Science and Heat Treatment, 39 (9-10) (1997) 428-437.

[1999Ash] M.F. Ashby, Materials selection in mechanical design, 2nd Edn. Butterworth Heinemann, Oxford, UK (1999).

[1999Bed] J. Beddoes and J.G. Parr, Introduction to Stainless Steels, 3rd Edn, ASM International, Materials Park, OH, USA, (1999) 1-6.

[1999Gen] K. Genel and M. Demirkol, Effect of case depth on fatigue performance of AISI 8620 carburized steel, International Journal of Fatigue, 21 (1999) 207-212.

[1999Li] X.Y. Li, Characterisation of low temperature plasma nitrided austenitic stainless steel, PhD thesis, Metallurgy and Materials, The University of Birmingham, UK (1999).

[1999Mar] K. Marchev, R. Hidalgo, M. Landis, R. Vallerio, C.V. Cooper and B.C. Giessen, The metastable m phase layer on ion-nitrided austenitic steels Part 2: crystal structure and observation of its two-dimensional orientation anisotropy, Surface and Coatings Technology, 112 (1999) 67-70.

[1999Rit] R.O. Ritchie, Mechanisms of fatigue-crack propagation in ductile and brittle solids, International Journal of Fracture, 100 (1999) 55-83.

[1999Ren] N. Renevier, P. Collignon, H. Michel and T. Czerwiec, Low temperature plasma nitriding of AISI 316L austenitic stainless steel, Surface and Coatings Technology, 111 (1999) 128-133.

[1999Sto] T.A. Stolarki, Basic principles of tribology: friction in 'Tribology in machine design' 1st Edn., Butterworth Heinemann, Oxford, UK (1999) 13-19.

[1999Sun1] Y. Sun, X.Y. Li and T. Bell, Low temperature plasma carburising of austenitic stainless steels for improved wear and corrosion resistance, Surface Engineering, 15 (1999) 49-54.

[1999Sun2] Y. Sun, X.Y. Li and T. Bell, Structural characteristics of low temperature plasma carburised austenitic stainless steel, Materials Science and Technology, 15 (1999) 1171-1178.

[1999Sun3] Y. Sun, X.Y. Li and T. Bell, X-ray diffraction characterisation of low temperature plasma nitrided austenitic stainless steels, Journal of Materials Science, 34 (1999) 4793-4802.

[1999Vor] B.I. Voronenko, Austenitic-ferritic stainless steel: a state-of-the-art review, Metal Science and Heat Treatment, 39 (9-10) (1999) 428-437.

[2000Car] Francois Cardarelli, Materials Handbook-A concise desktop reference, 2nd Edn, Springer, London, UK (2000).

[2000Few] M.P. Fewell, D.R.G. Mitchell, J.M. Priest, K.T. Short and G.A. Collins, The nature of expanded austenite, Surface and Coatings Technology, 131 (2000) 300-306.

[2000Ley] A. Leyland and A. Matthews, On the significance of the H/E ratio in wear control: a nanocomposite coating approach to optimised tribological behaviour, Wear, 246 (2000) 1-12.

[2000Lia] W. Liang, X. Bin, Y. Zhiwei and S. Yaqin, The wear and corrosion properties of stainless steel nitride by low-pressure plasma-arc source ion nitriding at low temperatures, Surface and Coatings Technology, 130 (2000) 304-308.

[2000Par] S. Parascandola, W. Moller and D.L. Williamson, Successful nitriding of austenitic stainless steel: the diffusion mechanism of nitrogen and the role of the surface oxide layer, Stainless steel 2000, Osaka, Japan (2000) 201-214.

[2000Sch] M. Schwind, J. Kallqvist, J.O. Nilsson, J. Argen and H.O. Andren, Sigma-phase precipitation in stabilized austenitic stainless steels, Acta Materialia, 48 (2000) 2473-2481.

[2000Tim] R.L. Timings, Engineering Materials II, 2nd Edn., Pearson Education Limited, Essex, UK (2000).

[2001Ber] J.A. Berrios, D.G. Teer and E.S. Puchi-Cabrera, Fatigue properties of a 316L stainless steel coated with different TiNx deposites, Surface and Coatings Technology, 48 (2001) 179-190.

[2001Dav] J.R. Davis, Surface Engineering for Corrosion and Wear Resistance, ASM International, Materials Park, Ohio, USA (2001).

[2001Li] X.Y. Li, Low temperature plasma nitriding of 316 stainless steel – Nature of S-phase and its thermal stability, Surface Engineering, 17 (2001) 147-152.

[2001Mat] M. Matula, L. Hyspecka, M. Svoboda, V. Vodarek, C. Dagbert, J. Galland, Z. Stonawska and L. Tuma, Intergranular corrosion of AISI 316L steel, Material Characterization, 46 (2001) 203-210.

[2001Sun] Y. Sun, X.Y. Li and T. Bell, In Stainless steel 2000 – Thermochemical surface engineering of stainless steel, (Eds., T. Bell and K. Akamatsu). London, Maney Publishing, The Institute of Materials (2001) 263-273.

[2001Zav] P.D. Zavattieri and H.D. Espinosa, Grain level analysis of crack initiation and propagation in brittle materials, Acta Materialia, 49 (2001) 4291-4311.

[2002Aok] K. Aoki and K. Kitano, Surface hardening for austenitic stainless steels based on carbon solid solution, Surface Engineering, 18 (2002) 462-464.

[2002ASM] Failure Analysis and Prevention, ASM Handbook 11, ASM International, The Materials Information Society, Materials Park, Ohio, USA (2002).

[2002Bel] T. Bell, Surface engineering of austenitic stainless steel, Surface Engineering, 18 (6) (2002) 415-422.

[2002NAC] National Association of Corrosion Engineers (NACE) Internal, History Congressional Study: Corrosion costs and preventative strategies in the United States, a supplement to materials performance, Houston, Texas, USA (2002).

[2002Sun] Y. Sun and T. Bell, Dry sliding wear resistance of low temperature plasma carburised austenitic stainless steel, Wear, 253 (2002) 689-693.

[2002Tha] S. Thaiwatthana, X.Y. Li, H. Dong and T. Bell, Comparison on properties of nitrogen and carbon S phase on low temperature plasma alloyed 316 stainless steel, Surface Engineering, 18 (2002) 433-437.

[2003Gra] H.J. Grabke, Metal dusting, Materials and Corrosion, 54 (10) (2003) 736-746.

[2003Li] X.Y. Li and H. Dong, Effect of annealing on corrosion behaviour of nitrogen S phase in austenitic stainless steel, Materials Science and Technology, 19 (2003) 1427-1434.

[2003Sob] W.O. Soboyejo, Mechanical Properties of Engineered Materials, Marcel Dekker Inc., New York, USA (2003).

[2003Sun] Y. Sun and T. Bell, Low temperature plasma nitriding characteristics of precipitation hardening stainless steel, Surface Engineering, 19 (2003) 331-336.

[2003Tha] S. Thaiwatthana, X.Y. Li, H. Dong and T. Bell, Corrosion wear behaviour of low temperature plasma alloyed 316 austenitic stainless steel, Surface Engineering, 19 (2003) 211-216.

[2003Was] D.N. Wasnik, G.K. Dey, V. Kain and I. Samajdar, Precipitation stages in a 316L austenitic stainless steel, Scripta Materialia, 49 (2003) 135-141.

[2004Azu] S. Azuma, T. Kudo, H. Miyuki, M. Yamashita and H. Uchida, Effect of nickel alloying on crevice corrosion resistance of stainless steels, Corrosion Science, 46 (2004) 2265-2280.

[2004Ber] J.A. Berrios-Ortiz, J.G. La Barbera-Sosa, D.G. Teer and E.S. Puchi-Cabrera, Fatigue properties of a 316L stainless steel coated with the ZrN deposites, Surface and Coatings Technology, 179 (2004) 145-179.

[2004Chr] T. Christiansen and M.A.J. Somers, On the crystallographic structure of S-phase Scripta Materialia., 50 (2004) 35-37.

[2004Ley] A. Leyland and A. Matthews, Design criteria for wear-resistant nanostructured and glassy-metal coatings, Surface and Coatings Technology, 177-178 (2004) 317-324.

[2004Puc] E.S. Puchi-Cabrera, F. Matinez, I. Herrera, J.A. Berrios, S. Dixit and D. Bhat, On the fatigue behaviour of an AISI 316L stainless steel coated with a PVD TiN deposit, Surface and Coatings Technology, 182 (2004) 276-286.

[2004Som] M. Somers, T. Christiansen and M. Ller Per, Case-hardening of stainless steel, European Patent 1521861 EU (2004).

[2004Tok] K. Tokaji, K. Kohyama and M. Akita, Fatigue behaviour and fracture mechanism of 316 stainless steel hardened by carburising, International Journal of Fatigue, 26 (2004) 543-551.

[2005Chr] T. Christiansen and M.A.J. Somers, Low temperature gaseous nitriding and carbon of stainless steel, Surface Engineering, 21 (2005) 445-455.

[2005Day] R.K. Dayal, N. Parvathavarthini and B. Raj, Influence of metallurgical variables on sensitisation kinetics in austenitic stainless steels, International Materials Review, 50 (2005) 129-155.

[2005Jam] A.S. James, K. Thomas, P. Mann and R. Wall, The role and impacts of surface engineering in environmental design, Materials and Design, 26 (2005) 594-601.

[2005Kra] G. Krauss, Steel – Processing, Structure and Performance, ASM International, Materials Park, OH, USA, (2005) 495-530.

[2005Liu] A. Liu, Mechanics and Mechanism of Fracture, An Introduction, ASM International, Materials Park, OH, USA (2005)

[2005Mat] D.K. Matlock, K.A. Alogab, M.D. Richards and J.G. Speer, Surface processing to improve the fatigue resistance of advanced bar steels for automotive applications, Materials Research, 8 (4) (2005) 453-459.

[2005Sun] Y. Sun, Kinetics of low temperature plasma carburising of austenitic stainless steels, Journal of Materials Processing Technology, 168 (2005) 189-194.

[2005Tsu1] M. Tsujikawa, N. Yamauchi, N. Ueda, T. Sone and Y. Hirose, Behaviour of carbon in low temperature plasma nitriding layer of austenitic stainless steel, Surface and Coatings Technology, 193 (1-3) (2005) 309-313.

[2005Tsu2] M. Tsujikawa, N. Yamauchi, N. Ueda, T. Sone and S. Tanaka, Surface material design of 316 stainless steel by combination of low temperature carburising and nitriding, Surface and Coatings Technology, 200 (2005) 507-511.

[2005Ued] Y. Ueda, N. Kanayama, K. Ichii, T. Oishi and H. Miyake, Metallurgical characteristics of the plasma (ion)-carburised layer of austenitic stainless steel SUS 316L, Surface and Coatings Technology, 193 (2005) 50-54.

[2006Aki] M. Akita and K. Tokaji, Effect of carburising on notch fatigue behaviour in AISI 316 austenitic stainless steel, Surface and Coatings Technology, 200 (2006) 6073-6078.

[2006Ayd] G.H. Aydogdu and M.K. Aydinol, Determination of susceptibility to intergranular corrosion and electrochemical reactivation behaviour of AISI 316L type stainless steel, Corrosion Science, 48 (2006) 3565-3583.

[2006Bha] H.K.D.H. Bhadeshia and R.W.K. Honeycombe, Steels Microstructure and Properties, 3rd Edn., Elsevier Ltd, London, UK (2003).

[2006Chr] T. Christiansen and M. Somers, Characterisation of low temperature surface hardened stainless steel, Struers Journal of Materialography, 9 (2006) 1-17.

[2006Don] H. Dong, P.Y. Qi, X.Y. Li and R.J. Llewellyn, Improving the erosion-corrosion resistance of AISI 316 austenitic stainless steel by low-temperature plasma surface alloying with N and C, Materials Science and Engineering A: Structural Materials: Properties, Microstructure and Processing, 431 (2006) 137-145.

[2006Mic] G.M. Michal, F. Ernst, H. Kahn, Y. Cao, F. Oba, N. Agarwal and A.H. Heuer, Carbon supersaturation due to paraequilibrium carburization: stainless steels with greatly improved mechanical properties, Acta Materialia, 54 (2006) 1597-1606.

[2006Min] N. Mingolo, C.E. Pinedo and A.P. Tschiptschin, On the formation of expanded austenite during plasma nitriding of an AISI 316L austenitic stainless steel, Surface and Coatings Technology, 201 (2006) 4215-4218.

[2006Sha] B.A. Shaw and R.G. Kelly, What is Corrosion, Electrochemical Society Interface 15 (1) (2006) 24-26.

[2006Ter] M. Terada, M. Saiki, I. Costa and A.F. Padilla, Microstructure and intergranular corrosion of the austenitic stainless steel 1.4970, Journal of Nuclear Materials, 358 (2006) 40-46.

[2007Beh] R. Behrisch and W. Eckstein (Eds.) Sputtering by Particle Bombardment. Experiments and computer calculations from threshold to MeV energies, Springer-Verlag, Berlin, Germany (2007).

[2007Buh] J. Buhagiar, H. Bong and T. Bell, Low temperature plasma surface alloying of medical grade austenitic stainless steel with carbon and nitrogen, Surface Engineering, 23 (4) (2007) 313-317.

[2007Cal] W.D. Callister, Jr, Materials Science and Engineering, An Introduction, 7th Edn, John Wiley and Son Inc., New York, USA (2007).

[2007Gan] S. Ganesh Sundara Raman and M. Jayaprakash, Influence of plasma nitriding on plain fatigue and fretting fatigue behaviour of AISI 304 austenitic stainless steel, Surface Coatings and Technology, 201 (2007) 5906-5911.

[2007Hon] S.G. Hong, S.B. Lee and T.S. Byun, Temperature effect on the low-cycle fatigue behaviour of type 316L stainless steel: Cyclic non-stabilization and an invariable fatigue parameter, Materials Science and Engineering A, 457A (2007) 139-147.

[2007Osh] T. Oshima, Y. Habara and K. Kuroda, Efforts to save nickel in austenitic stainless steels, ISIJ International, 47 (3) (2007) 359-364.

[2007Qu] J. Qu, P.J. Blau and B.C. Jolly, Tribological properties of stainless steel treated by colossal carbon supersaturation, Wear, 263 (2007) 719-726.

[2007Tsu] M. Tsujikawa, S. Noguchi, N. Yamauchi, N. Ueda and T. Sone, Effect of molybdenum on hardness of low-temperature plasma carburised austenitic stainless steel, Surface and Coatings Technology, 201 (2007) 5102-5107.

[2008Ces] L. Ceschini and G. Minak, Fatigue behaviour of low temperature carburised AISI 316L austenitic stainless steel, Surface and Coatings Technology, 202 (2008) 1778-1784.

[2008Sto] J. Stokes, Theory and applications of high voltage oxy-fuel (HVOF) thermal spray process, Dublin City University Press, Ireland (2008) 1-14.

[2009Ciu] O. Ciuca, K. Tsuchiya, Y. Yokoyama, Y. Todaka and M. Umemoto, Effect of nanocrystallization and twining on hardness in Ni3Al deformed by high pressure torsion, Materials Transaction, 50(5), (2009) 1123-1127.

[2009Ern] F. Ernst, A. Avishai, H. Kahn, X. Gu, G.M. Michal and A.H. Heuer, Enhanced carbon diffusion in austenitic stainless steel carburised at low

temperature, The Minerals, Metals and Materials Society, Metallurgical and Materials Transactions A, 40A (2009) 1768-1780.

[2009Chr] T.L. Christiansen and M.A.J. Somers, Stress and composition of carbon stabilized expanded austenite on stainless steel, Metallurgical and Materials Transactions A, 40A (2009) 1791-1798.

[2009Gal] S.G. Gallo, Active screen plasma surface engineering of austenitic stainless steel for enhanced tribological and corrosion properties, PhD Thesis, School of Metallurgy and Materials, College of Engineering and Physical Sciences, The University of Birmingham, UK (2009).

[2009Lo] K.H. Lo, C.H. Shek and J.K.L. Lai, Recent development in stainless steels, Material Science and Engineering, 65 (2009) 39-104.

[2009Sou] R.M. Souza, M. Ignat, C.E. Pinedo and A.P. Tschiptschin, Structure and properties of low temperature plasma carburised austenitic stainless steels, Surface and Coatings Technology, 204 (2009) 1102-1105.

[2010Ega] M. Egawa, N. Ueda, K. Nakata, M. Tsujikawa and M. Tanaka, Effect of additive alloying element on plasma nitriding and carburising behaviour of austenitic stainless steels, Surface and Coatings Technology, 205 (2010) 5246-5251.

[2010Mol] J.G. Molleja, L. Nosei, J. Ferron, E. Bemporad, J. Lesage, D. Chicot and J. Feugeas, Characterization of expanded austenite developed on AISI 316L stainless steel by plasma carburization, Surface and Coating Technology, 204 (2010) 3750-3759.

[2010Pin] C.E. Pinedo and A.P. Tschiptchin, Low temperature plasma carburizing of AISI 316L austenitic stainless steel and AISI F51 duplex stainless steel, Proceeding; 10th Brazilian Stainless Steel Conference, Rio de Janeiro, Brazil, September 20th-22nd 2010.

[2010Sun] Y. Sun, Production of nitrogen and carbon S phases in austenitic stainless steels by hybrid plasma surface alloying, Surface Engineering, 26 (1-2) (2010) 114-122.

[2011Chr] T.L. Christiansen, T.S. Hummelshoj and M.A.J. Somers, Gaseous carburising of self-passivating Fe-Cr-Ni alloys in acetylene-hydrogen mixtures, Surface Engineering, 27(8) (2011) 602-608.

[2011Ern] F. Ernst, D. Li, H. Kahn, G.M. Michal and A.H. Heuer, The carbide M_7C_3 in low-temperature-carburised austenitic stainless steel, Acta Materialia, 59 (2011) 2268-2276.

[2011Li] W. Li, X. Li and H. Dong, Effect of tensile stress on the formation of S-phase during low-temperature plasma carburising of 316L foil, Acta Materialia, 59 (2011) 5765-5774.

[2011Log] T.M. Loganathan, J. Purbolaksono, J.I. Inayat-Hussain and N. Wahab, Effects of carburization on expected fatigue life of alloys steel shafts, Journal of Material Design, 32 (2011) 3544-3547.

[2011Mar] N. Maruyama, D. Mori, S. Hiromoto, K. Kanazawa and M. Nakamura, Fatigue strength of 316L-type stainless steel in simulated body fluids, Corrosion Science, 53 (2011) 2222-2227.

[2011Ram] M. Ramesh, H.J. Leber, K.G.F. Janssens, M. Diener and R. Spolenak, Thermomechanical and isothermal fatigue behaviour of 347 and 316L austenitic stainless tube and pipe steels, International Journal of Fatigue, 33 (2011) 683-691.

[2013Ste] D.R. Steinmetz, T. Japel, B. Wietbrock, P. Eisenlohr, I. Gutierrez-Urrutia, A. Saeed-Akbari, T. Hickel, F. Roters and D. Raabe, Revealing the strain-hardening behaviour of twinning-induced plasticity steels: Theory, simulation, experiments, Acta Materialia, 61 (2013) 494-510.

[URLBar] The chemistry of barium oxides. URL: http://www.memidex.com/barium-oxides (Accessed: December 6th, 2012)

[URLCar] Carbon steel microstructures and micro-constituents, URL: http://www.ejsong.com/mdme/memmods/MEM30007A/steel/steel.html. (Accessed: March 20th, 2012).

[URLHar] Hardness correlation, URL: http: //www.mechanicalproperties.com. (Accessed: September, 4th, 2012.).

[URLIs1] International Stainless Steel Forum (ISSF), Stainless steel production (Brussels), URL: http://www.worldstainless.org. (Accessed: December 19th, 2011).

[URLIs2] International Stainless Steel Forum, "New 200-series" steels: An opportunity or a threat to the image of stainless steel? (2005) 1-11 http://www.worldstainless.org/NR/rdonlyres/9BF7E850-7425-4E82-B687-765F33EBF63C/4733/ISSFNew200seriessteelsAnopportunityorathreattothei.pdf. (Accessed: December 22nd, 2011).

[URLMat] Fatigue crack propagation, URL: http://www.materials-news.com/2009/02/b-asically-fatigue-crack-propagation.html. (Accessed: June 29th, 2012)

[URLMic] Microstructural evolution in power plant materials, URL: http://www.le.ac.uk/engineering/svh2/microstructure.htm. (Accessed: August 29th, 2012).

[URLStr] Stress relief and fatigue behaviour of stainless steels URL: http://www.efunda.com/processes/heat_treat/matl_modify/stress_relieving.cfm (Accessed: October 23th, 2012).

APPENDICES

"Great is the art of beginning, but greater is the art of ending".

— Henry Wadsworth Longfellow

APPENDIX A

The presentations and papers during the course of these investigations are:

- D.E. Fiawoyife, L.A. Cornish, C. Polese, L.H. Chown & S. Kwofie, Effect of carburising temperature on the mechanical behaviour of AISI 316L austenitic stainless steel, DST/NRF Centre of Excellence in Strong Material Students Presentation (Poster presentation), Johannesburg, 30th May, 2012.

- D.E. Fiawoyife, L.A. Cornish, C. Polese, L.H. Chown & S. Kwofie, Effect of temperature and carbonaceous environment on the fatigue behaviour of AISI 316L austenitic stainless steel, Proceeding of Ferrous 2012, Ferrous and Base Metals Development Network Conference 2012, Advanced Materials Initiative (AMI), South African Institute of Mining and Metallurgy, Symposium Series S73, 449-460, Magaliesburg, South Africa, 15th-17th, October, 2012.

- D.E. Fiawoyife, L.A. Cornish, C. Polese, L.H. Chown & S. Kwofie, Effect of temperature and carbon content on the mechanical behaviour of AISI 316L stainless steel, Book of Abstract, 4th Cross-faculty Postgraduate Symposium, Showcasing Postgraduate Research (Poster presentation), University of the Witwatersrand, Johannesburg, 19th-22nd, November, 2012.

- D.E. Fiawoyife, L.A. Cornish, C. Polese, L.H. Chown & S. Kwofie, Effect of pack carburising on the mechanical behaviour of AISI 316L stainless steels, Proceedings of the Microscopy Society of Southern Africa (MSSA) conference Vol. 42, 75 Cape Town, 4th-7th December, 2012.